# MATHEMATICAL MODELLING OF CLIMBING FILM EVAPORATORS

by

**Stephen David Peacock**

Submitted in fulfilment of the academic requirements for the degree of Masters of Science in Engineering in the Department of Chemical Engineering, University of Natal.

01 February 2001

# Abstract

Climbing film evaporators are in widespread use in the South African sugar industry, with the vast majority of the local sugar mills currently utilising these evaporators as first effect vessels in multiple effect evaporator sets. However, it is generally considered that the performance of these evaporators has not been maximised, and that improvements could be achieved by proper optimisation of the operating parameters. Unfortunately, very little comprehensive design information has been published in the literature, owing to the complexity of the heat transfer and hydrodynamic interactions in the evaporator tube. Attempts at performance improvement have been hampered by the lack of any theory to explain fully the effects of the operating parameters and physical properties of the feed liquor on the performance of the evaporator.

In this study, a mathematical model of the climbing film evaporator system was developed in order to assess the effects of changing operating conditions on evaporator performance, based on as solid a theoretical foundation as currently possible. The model was tested against experimental data from a pilot plant climbing film evaporator and this experimental data was used to enhance the accuracy of the model by means of process identification.

Because of the complexity of the model and the extensive computational time required for its solution, a simplified evaporator model was also developed, based on linearisation of the system of ordinary differential equations describing the climbing film evaporator system. This simplified model was used to predict trends in evaporator behaviour under various operating conditions.

# Preface

The work published in this thesis is, unless stated to the contrary in the text, my own. No portion of this work has been submitted, either in whole or in part, to any other university. Substantial portions of this work have, however, previously been published by the author in journals relating to the sugar industry.

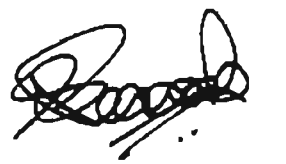

Stephen Peacock

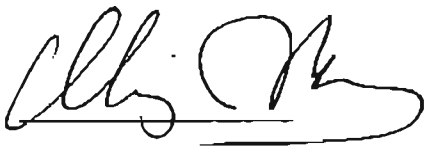

Prof. Maciej Starzak

# Acknowledgements

I would like to gratefully acknowledge the guidance and assistance of the following people and organisations, without whom this work could not have been carried out:

- The Sugar Milling Research Institute and the South African sugar industry - for their financial support of the work, and for permission to publish the results thereof.

- My supervisor, Maciej Starzak, who sacrificed many, many hours in the interests of improving both sugar technology and my capabilities as a chemical engineer.

- Dennis Walthew, Raoul Lionnet, Steve Davis, Brian Purchase and the rest of the staff of the Sugar Milling Research Institute, both past and present, who assisted with the project.

- Rob Whitelaw, Guy Montocchio, Dave Love, Ian Smith, Dave Meadows, Peter Rein and the rest of the staff of the Tongaat-Hulett Sugar group, most notably those at the Felixton sugar mill, who provided assistance and guidance on the project.

# Contents

# List of Tables

# List of Figures

# Chapter 1
# Introduction

The climbing film evaporator was first introduced by Kestner, in 1899, and consists of one or more vertical tubes within a shell, usually heated by condensing steam. Typically, the tubes are six to ten metres in length and 27 to 50 millimetres in diameter. As many as five thousand tubes may commonly be placed within a single shell. The liquor to be evaporated is fed to the bottom of the tubes, where it vapourises and the liquid phase is carried up the tube in a thin film against the tube wall (the 'climbing film'). The difference in density between the liquid phase entering the tube bottom and the evaporating two phase mixture within the tubes results in this natural circulation flow. At the top of the tubes, the vapour is removed from the concentrated liquor in a separator (see Figure 1). As the climbing film evaporator is an upward flow type evaporator, the boiling point of the liquor to be concentrated is greater at the bottom of the tubes than at the top because of the greater hydrostatic pressure at the tube bottom. Thus, in the lower part of the tubes there is no boiling and the temperature increases with increasing height, until the boiling point corresponding to the local pressure in the tube is reached. After this point, the temperature of the liquid falls with increasing height, and vapourisation of the liquor occurs due to both flashing and the further addition of heat. Even though the liquor concentration increases along the length of the tube, resulting in an increased boiling point elevation with increasing height, the effect of the decreasing hydrostatic head is more significant, yielding an overall effect of decreasing boiling point with increasing distance along the tube.

The primary advantage of the climbing film evaporator is its short liquor residence time, typically of the order of thirty seconds to three minutes. High rates of heat transfer can be obtained without the use of high steam temperatures or long liquor contact times, allowing the concentration of heat-sensitive liquors for which such subjective properties as flavour,

colour and aroma are of prime importance. Other advantages include simplicity of construction, cleaning and maintenance, low cost per unit of heat transfer area, small floor space requirements and the ability to handle viscous and foaming liquors. The long tubes make it possible to achieve high evaporation loads in a single pass. Disadvantages of the climbing film evaporator include the need for an external vapour/liquid separation vessel and the potential for the occurrence of transient pulsation phenomena (Gundmundson & Olauson, 1971).

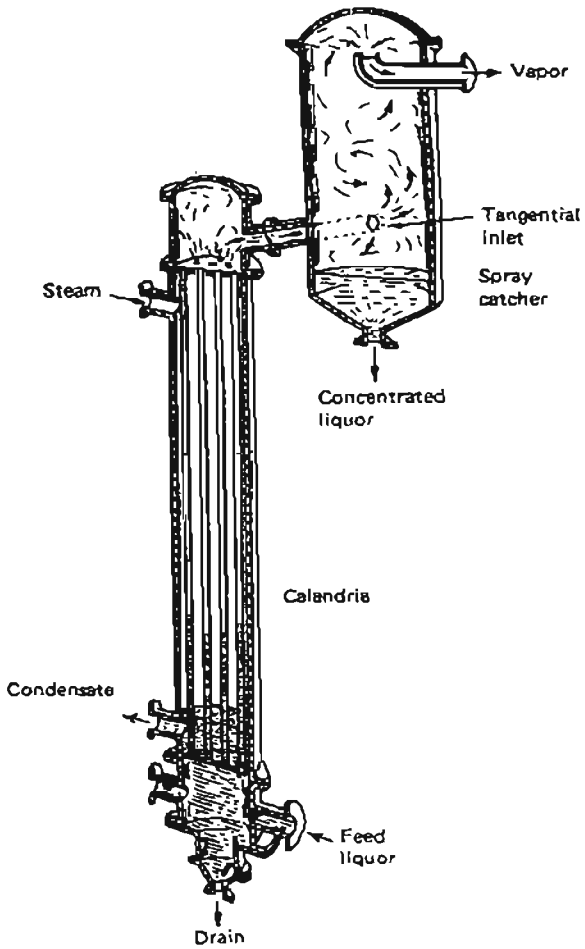


**Figure 1.** Climbing film evaporator with cyclonic separator (Smith, 1983).

Climbing film evaporators are widely used in the South African sugar industry. The first evaporator of this type was installed at the Darnall mill in 1969, with 6,7 metre long tubes. Currently, 13 of the 17 local sugar mills utilise climbing film evaporators as first effect vessels, with tube lengths of up to 7,3 metres (Rein & Love, 1995). The short evaporator residence time, small liquor hold up volume and low temperature of operation minimise the occurrence of browning reactions, either by caramelisation of sugars or the reaction of proteins with sugars. However, it is generally considered that the performance of these evaporators is not optimal and that improvements could be achieved by proper optimisation of the operating parameters. Unfortunately, very little design information is available in the literature, owing to the complexity of the heat transfer and hydrodynamic interactions in the evaporator tube. Attempts at performance improvement have been hampered by the lack of any theory to explain fully the effects of the operating conditions and physical properties of the feed liquor on the performance of the evaporator.

The objective of this study is the production of a mathematical model of the climbing film evaporator system which can be used to assess the effects of changing operating conditions on evaporator performance, based on as solid a theoretical base as currently possible.

# *Part I :*

# *Theory and Model Development*

# Chapter 2
# Literature Review

A thorough review of the literature regarding climbing film evaporators, and two phase heat transfer in general, was performed. The characteristics of the two phase flow and heat transfer phenomena occurring in climbing film evaporators were examined, and the existing models of climbing film evaporators were studied.

## 2.1 TWO PHASE FLOW AND HEAT TRANSFER CHARACTERISTICS

The two phase flow and heat transfer phenomena occurring within the tubes of a climbing film evaporator are complex and very closely related. It is not possible to study these phenomena separately, and any study of the heat transfer occurring in climbing film evaporators must take into account the changing flow patterns within the tubes. This analysis is complicated by the large number of variables involved and the limited nature of the current knowledge in the field of two phase hydrodynamics. Furthermore, there is a strong coupling between the heat transfer phenomena on the boiling and condensation sides of the evaporator tubes which must be accounted for.

### 2.1.1 Flow boiling in vertical tubes

If the liquid to be concentrated enters the bottom of the evaporator tubes at a temperature below its boiling point, then the first section of the tube will act as a single phase heater, raising the temperature of the liquid towards its boiling point. This regime is commonly referred to as the *non boiling zone* and the heat transfer mechanism within this zone is that of single phase liquid convection. As the velocity of the liquid feed entering climbing film

evaporators is generally low, leading to laminar flow of the liquid within the tube, heat transfer in this zone is poor. The length of the non boiling zone is dependent on the temperature of the liquid entering the bottom of the tubes; the lower the entrance temperature, the longer the non boiling zone.

When the tube wall temperature rises above the maximum superheat temperature of the liquid phase in contact with it (the 'critical wall temperature for nucleation'), bubble formation on the tube wall commences, even though the bulk fluid temperature in the tube is below the boiling point temperature at the local pressure. The bubbles formed at the tube wall move out into the subcooled bulk liquid, where they subsequently collapse. This region of the tube is referred to as the *subcooled nucleate boiling zone*. Heat transfer in this zone is more efficient than that in the non boiling zone, due to the disturbance of the liquid boundary layer against the tube wall by the bubbles of vapour. Two mechanisms contribute to the heat transfer occurring in this regime, namely convective heat transfer and nucleate boiling. Convective heat transfer is strongly dependent on the velocity of the two phase mixture within the evaporator tube, as the main resistance to this mechanism of heat transfer results from the liquid phase boundary layer against the tube wall. The nucleate boiling mechanism, however, is largely independent of velocity as the liquid phase boundary layer is destroyed by the action of the bubbles formed at the tube wall. These two heat transfer mechanisms act in parallel within the tube, with convective boiling taking place in the liquid phase surrounding the bubbles formed by nucleate boiling. Initially, the contribution of the nucleate boiling mechanism to the total heat transfer dominates.

As the fluid rises through the evaporator tube, it is heated and the local pressure decreases due to the decrease in hydrostatic head with increase in height. When the bulk liquid reaches its boiling point temperature at the local pressure, the *saturated nucleate boiling zone* commences, with bubbles of vapour dispersed in the continuous liquid phase. Progressive vapourisation of the liquid leads to a variety of two phase flow patterns, as shown in Figure 2, with the rate of heat transfer at any point in the tube dependent on the

relative flow rates of liquid and vapour at that point. As the proportion of vapour in the tube increases, the velocity of the two phase flow increases because of the greater volume occupied by the vapour phase (the mass flow rate remains constant). The pressure gradient in the tube is subsequently increased because of the greater wall drag and the force necessary to accelerate the two phase flow to the higher velocities. While the nucleate boiling mechanism still dominates heat transfer in this regime, the contribution of the convective boiling mechanism increases with increasing two phase velocity through the tube.

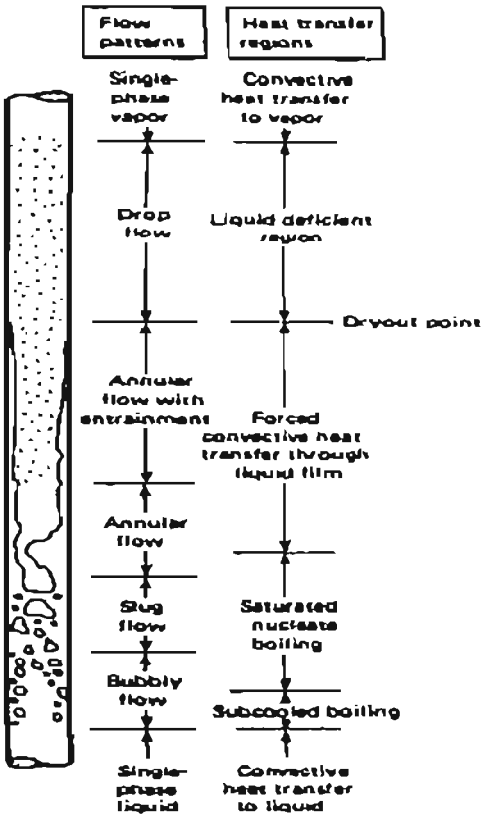


**Figure 2**: Two phase flow patterns in a climbing film evaporator tube (Collier, 1980).

Initially, in the saturated nucleate boiling zone, the vapour bubbles are dispersed in the liquid phase. Further up the tube, the bubbles become more numerous and elongated, and some bubble coalescence occurs. Eventually, slugs of vapour with diameters approaching

that of the tube are formed. This unstable flow pattern quickly breaks down to form the *annular flow regime*, in which vapour forms the central core within the tube with the liquid phase carried up the tube wall in a thin film (the 'climbing film') by the drag induced by the high velocity flow of vapour in the core. The separation of the phases in this manner results from the difference in their densities. In an accelerating flow (the total mass flow rate through the tube is constant, but the average density of the two phase mixture is constantly falling), the pressure gradient is the same for both phases, but the less dense vapour phase is accelerated more than the denser liquid phase and thus travels at a higher velocity through the tube. The vapour phase therefore moves to the centre of the tube in order to minimise the retarding frictional effects on its flow, allowing it to travel at several times the speed of the liquid phase (Winterton, 1981). As the annular flow regime is characterised by very efficient heat transfer, it is usually considered ideal to operate climbing film evaporators so as to utilise the annular flow regime throughout as much of the tube length as possible.

As evaporation proceeds further up the tube, the annular liquid film becomes progressively thinner. As the thickness of the liquid film against the tube wall is decreased by evaporation and its velocity subsequently increases due to the increased drag of the higher velocity vapour phase, the contribution of the convective boiling mechanism to overall heat transfer may exceed that of the nucleate boiling mechanism. In some cases, heat transfer by convection may be so efficient that the tube wall is cooled to below the critical temperature required for nucleate boiling. Under these circumstances, bubble formation ceases and further vapourisation occurs by convective boiling heat transfer alone, with vapourisation occurring at the vapour-liquid interface.

In the final stage of evaporation, if the liquid flow rate through the evaporator is low or the temperature difference driving force for evaporation very high, the thin annular film of liquid breaks down under the high vapour velocities in the tube. The *dispersed flow regime*, with liquid entrainment in a core of vapour and a partially dry tube wall, may occur. Each droplet of liquid is cushioned from impact against the tube wall by the layer

of vapour generated by the droplet as it approaches the tube wall (Rohsenow, 1983; Winterton, 1981). As vapour phase convective heat transfer is considerably less efficient than liquid phase convective heat transfer, the dispersed flow regime is characterised by falling heat transfer coefficients with increasing proportion of vapour in the two phase flow through the tube.

### 2.1.2 Condensation

When a saturated vapour is brought into contact with a surface which is at a temperature below the saturation temperature of the vapour, heat is transferred from the vapour to the surface and condensate is produced. Under normal circumstances, the liquid wets the surface, spreads out and forms a condensate film. If the vapour is condensing on a vertical surface, such as an evaporator tube, the condensate film flows downwards under the influence of gravity, but is retarded by the viscosity of the liquid. This flow will normally be streamline, and further condensation will occur at the vapour-liquid interface (increasing the thickness of the condensate film), with associated heat flow through the liquid film by conduction. Under conditions of relatively long surfaces or high condensation rates, the flow of the condensate film may become turbulent, leading to an increase in the rate of heat transfer through the condensate film due to the disturbance of the fluid boundary layer against the surface by the turbulent flow conditions.

If an incondensible gas, such as air, is present in the vapour to be condensed, the incondensible gas will remain, and accumulate, at the condensing surface following the condensation of the vapour. Further vapour must diffuse through this layer of gas collected in the vicinity of the heat transfer surface before it can condense. Thus, the presence of incondensible gas adjacent to the heat transfer surface acts as a thermal resistance to heat transfer, resulting in a significant reduction in the efficiency of condensation heat transfer.

## 2.2 EXISTING MODELS OF CLIMBING FILM EVAPORATORS

Very few climbing film evaporator models have been published in the literature. Most of those studies which have been performed have focussed on the empirical correlation of a few operating variables, over a very limited range of operating conditions.

In early studies, the climbing film evaporator was considered as a lumped-parameter system and only relationships between process variables averaged over the entire apparatus were discussed. The first distributed-parameter model accounting for the distribution of temperature, pressure and juice composition over the length of the tubes was by Bourgois and Le Maguer (1983a; 1983b; 1984). This model, however, was based on several simplifying assumptions, such as the assumption of a constant rate of evaporation along the tube length, which is its most serious drawback. Zinemanas *et al.* (1984) performed a general study into the simulation of heat exchangers with change of phase, allowing for multicomponent phase equilibria. In principle, the model which was developed in the current study follows the concepts formulated by Zinemanas *et al.*

### 2.2.1 Coulson and Mehta, (1953)

Coulson and Mehta presented information regarding the performance of a small stainless steel climbing film evaporator with one tube 5 ft. 3 in. (1,6 m) long and ½ in. (12,7 mm) outside diameter (20 s.w.g. wall thickness). The heat transfer area based on the mean diameter of the tube was 0,637 sq. ft. (0,0592 $m^2$). A travelling thermocouple moving within the centre of the tube was used to determine the liquor temperature profile up the tube during the evaporation process.

Around two hundred experimental tests were carried out, using distilled water, sucrose solutions of different concentrations (20%, 30% and 40%), Teepol solutions of different concentrations (0,01% and 0,1%) and isopropyl alcohol. The variables selected as being

possible factors affecting evaporator performance were temperature difference (varied between 15 and 62°F [8,3 and 34,4°C]), feed rate (varied between 24 and 180 lb./hr [10,9 and 81,6 kg/hr]), boiling point temperature (varied between 110 and 160°F [43,3 and 71,1°C]), surface tension (varied between 21 and 68 dynes/cm [$2{,}1\times10^{-2}$ and $6{,}8\times10^{-2}$ N/m]) and viscosity (varied between 0,45 and 2 cP [$4{,}5\times10^{-4}$ and $2\times10^{-3}$ Pa.s]). The general approach to experimentation was to vary one of the factors of interest while maintaining all of the others at fixed levels.

For each of the experimental runs, the authors measured an overall heat transfer coefficient. A film coefficient for the boiling liquid was then calculated by eliminating the heat transfer resistance due to the tube wall and the heat transfer resistance on the outside of the tube. These experimentally determined film coefficients were assumed to be related to the variables of interest by a relation of the following form:

$$h_B = K(\Delta T^a . W_f^b . \sigma^c . \mu_L^{\ d} . T_{bp}^{\ e})$$

where K is a constant which was expected to vary with the liquid used in the tests due to the effects of physical property terms not included within the bracketed expression, $\Delta T$ is the difference between the mean temperature on the boiling side and the mean temperature on the heating medium side, $W_f$ is the mass feed rate to the evaporator, $\sigma$ is the surface tension of the boiling liquid, $\mu_L$ is the viscosity of the boiling liquid, $T_{bp}$ is the boiling temperature of the liquid and a, b, c, d and e are constants.

Following the conclusion of the experimental program, only three of the initial five factors were considered to significantly affect the performance of the evaporator, leading to a performance equation as follows:

$$h_B = K'(\Delta t^{0,6} . W_f^{0,25} . \mu_L^{\ -0,49})$$

where K' is a constant term including the effects of all parameters not contained within the bracketed expression and $\Delta t$ is the calculated temperature difference across the boiling

film itself (the difference between the temperature of the inner wall of the tube and the bulk fluid temperature).

### 2.2.2 Piret and Isbin, (1954)

Piret and Isbin measured heat transfer coefficients in an experimental apparatus consisting of a single tube vertical evaporator utilising a 46,5 in. (1,18 m) long, 1 in. (25,4 mm) diameter, electrically heated copper test section. Heat fluxes ranging from 5,89 kW/m$^2$ to 165,62 kW/m$^2$ were supplied by three spirally wound heater coils attached to the outside of the test section.

In total, 94 runs were performed using six different test fluids, namely water, isopropyl alcohol, n-butyl alcohol, carbon tetrachloride and 35% and 50% potassium carbonate solutions. It was found that all of the runs could be fitted by the following empirical relation (developed by extension from the work of Linden and Montillon (1930) in developing log mean velocity correlations for liquid film heat transfer coefficients):

$$\frac{h_{av}\,D}{k_L} = 0{,}0086\left(\frac{D\,u_m\,\rho_L}{\mu_L}\right)^{0,8}\left(\frac{C_{pL}\,\mu_L}{k_L}\right)^{0,6}\left(\frac{\sigma_w}{\sigma}\right)^{0,33} \quad \ldots (1)$$

where $h_{av}$ is the average boiling heat transfer coefficient, D is the inner tube diameter, $k_L$ is the thermal conductivity of the liquid, $u_m$ is the log mean liquid-vapour velocity in the pipe: $u_m = (u_V - u_L)/\ln[u_V/u_L]$, $\rho_L$ is the liquid phase density, $\mu_L$ is the liquid phase viscosity, $C_{pL}$ is the liquid phase heat capacity, $\sigma_w$ is the surface tension of water at its normal boiling point and $\sigma$ is the surface tension of the fluid of interest at its normal boiling point. This relationship was found to fit the data with a mean deviation of only 4%, and with 91,3% of the runs having a deviation of less than 10%. This empirical relationship was further tested by making use of additional data for water and sucrose solutions up to 50%. All of these data showed good agreement with the empirical relationship, as shown in Figure 3.

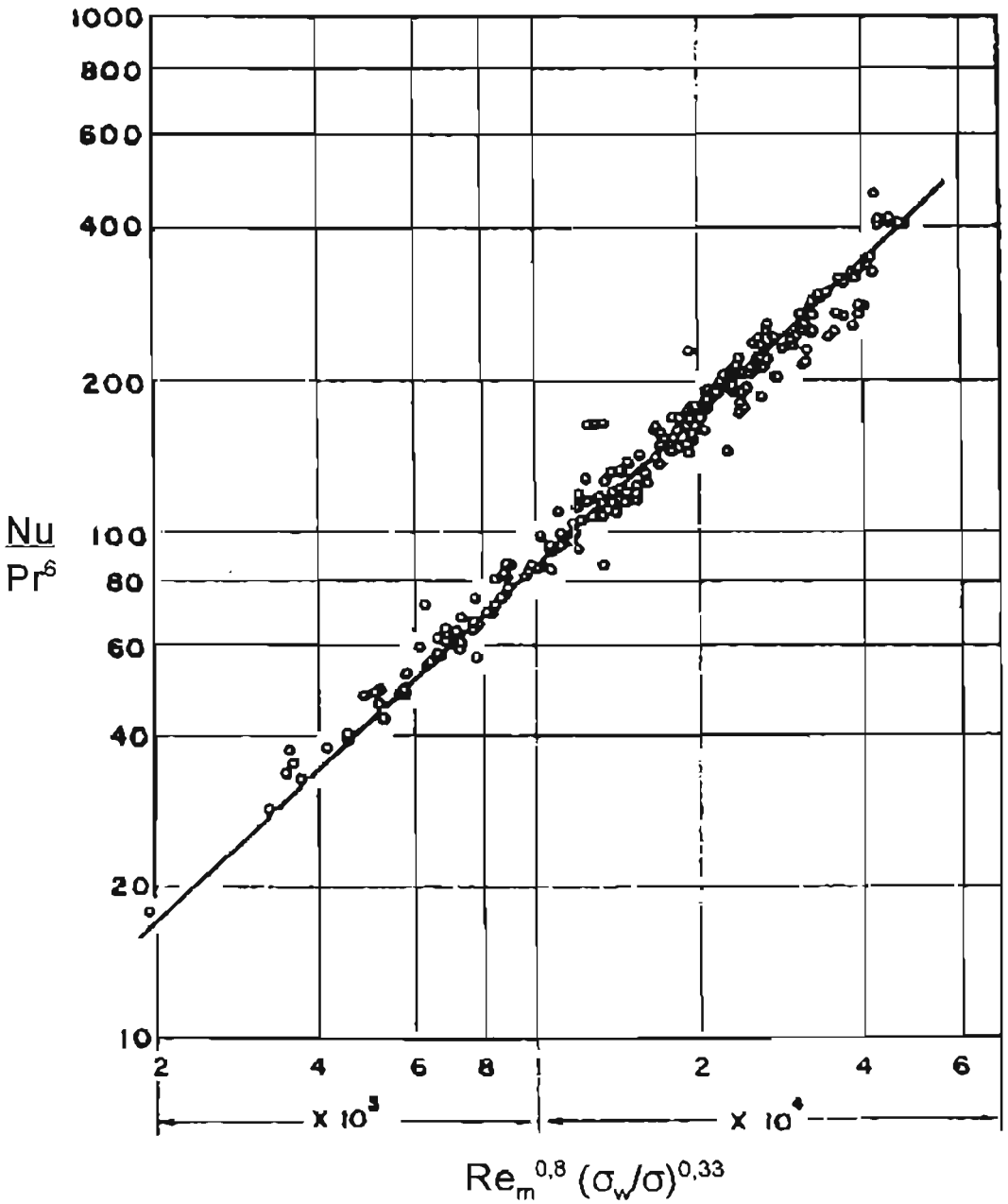


**Figure 3.** Correlation of the data of Piret and Isbin with equation (1). [Piret and Isbin, 1954]

Piret and Isbin also correlated their experimental data using the pool boiling relationship developed by Rohsenow (1953):

$$\frac{C_{pL}T_x}{h_{fg}} = C_{sf}\left[\frac{\{Q/A\}}{\mu_L h_{fg}}\sqrt{\frac{\sigma}{g(\rho_L-\rho_V)}}\right]^{0,33}\left(\frac{C_{pL}\mu_L}{k_L}\right)^{1,7} \quad \text{... (2)}$$

where $T_x$ is the heating surface temperature minus the fluid saturation temperature, $h_{fg}$ is the latent heat of vapourisation, $C_{sf}$ is an empirical constant which depends both on the tube metal and the liquid being evaporated, Q/A is the heat transfer rate per unit area of heating surface, g is the acceleration due to gravity and $\rho_V$ is the density of the vapour phase. The fitted data for the various fluids used in their study are shown in Figure 4.

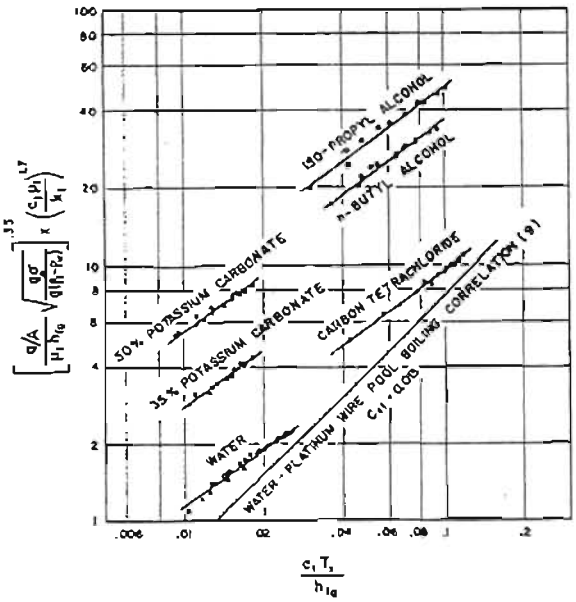


**Figure 4.** Correlation of the data of Piret and Isbin with equation (2). [Piret and Isbin, 1954]

### 2.2.3 Coulson and McNelly, (1956)

Coulson and McNelly extended the work previously published by Coulson and Mehta

(1953), with particular reference to the influence of large temperature differences on the heat transfer coefficient. They also developed a better idea of the mechanism of boiling within the tubes of a climbing film evaporator, and derived a general correlation for use in the design of these evaporators. In order to carry out the experimental work, their previously described equipment was modified to use pressurised hot water as the heating medium and to allow for the use of tubes varying in diameter from ¼ in. (6,35 mm) to 1 in. (25,4 mm).

Some six hundred experimental investigations were carried out using a variety of fluids, namely water, ethanol, carbon tetrachloride, isopropyl alcohol, kerosene, toluene and cyclohexane. Most of the work was carried out with silver tubes, but some tests were also performed with stainless steel and copper tubes. However, the nature of the tube material used in the tests was not found to have any significant effect on the observed heat transfer. For each test, the feed liquid was introduced into the evaporator at its boiling point at the desired pressure of operation. The experimental results were all found to fit the general form shown in Figure 5, with the average boiling heat transfer coefficient as a function of the temperature difference driving force at fixed values of the liquid feed rate, showing three distinct regions AB, BC and CD.

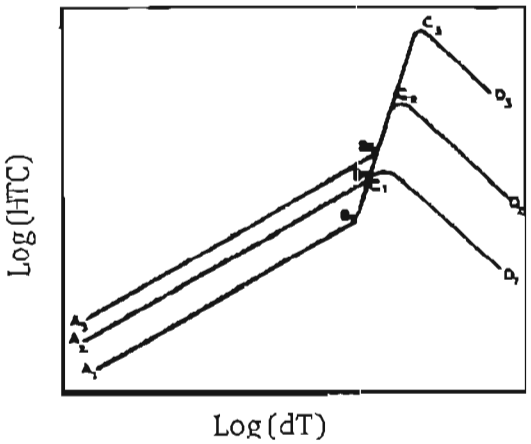


**Figure 5.** General form of the relationship between boiling heat transfer coefficient and temperature difference. [Coulson and McNelly, 1956]

Region AB covers heat transfer at the relatively low values of temperature difference which are industrially the most important and were the only ones previously examined. In this region, the heat transfer coefficient was found to increase with both temperature difference and feed rate (with $A_1B_1$, $A_2B_2$ and $A_3B_3$ for increasing feed rates being parallel). In this region, the forced convective heat transfer mechanism dominates within the tube, and the increased turbulence created by increased flow through the tube results in enhanced heat transfer.

At point B, there is a change in the dominant mechanism of heat transfer to that of nucleate boiling, where the turbulence in the fluid within the tube is largely created by the very rapid formation of bubbles. In the region BC there is a very rapid increase in the heat transfer coefficient with increasing temperature difference, but the flow rate of the fluid has no significant effect, with all of the curves shown in Figure 5 converging to fall on a common line (the nucleate boiling curve for the fluid of interest).

At high rates of evaporation in a climbing film evaporator, a condition may occur where there is no unevaporated liquid leaving the tube, or at least an insufficient amount to completely wet the tube surface. The heat flux then remains at a constant value corresponding to the total evaporation and, as the temperature difference is increased, the average boiling heat transfer coefficient correspondingly decreases (region CD in Figure 5).

In the development of a general expression to express their results in a useful form, Coulson and McNelly ignored region CD, as it was considered to be of no practical value. In region AB, it was assumed that the annular liquid flow and the central vapour flow within the tube were turbulent, leading to the following expression for the heat transfer process:

$$Nu = (1,3+39d)\left\{ Pr_L^{0,9} . Re_L^{0,23} . Re_V^{0,34} . \left(\frac{\rho_L}{\rho_V}\right)^{0,25} . \frac{\mu_V}{\mu_L} \right\}$$

where Nu is the Nusselt number, d is the tube inner diameter in feet, $Pr_L$ is the liquid phase Prandtl number, $Re_L$ is the Reynolds number for the liquid flow in the tube, $Re_V$ is the Reynolds number based on the vapour flow in the tube, $\rho_L$ is the density of the liquid phase, $\rho_V$ is the density of the vapour phase, $\mu_V$ is the viscosity of the vapour phase and $\mu_L$ is the viscosity of the liquid phase. Expanding this relationship gives:

$$\left(\frac{h_B D}{k_L}\right) = (1,3+39d)\left\{ \left(\frac{C_{PL}\mu_L}{k_L}\right)^{0,9} . \left(\frac{4W_f}{D\mu_L}\right)^{0,23} . \left(\frac{QL}{\lambda\mu_V}\right)^{0,34} . \left(\frac{\rho_L}{\rho_V}\right)^{0,25} . \left(\frac{\mu_V}{\mu_L}\right) \right\}$$

where $h_B$ is the average boiling heat transfer coefficient, D is the tube inner diameter, $k_L$ is the thermal conductivity of the liquid phase, $C_{PL}$ is the heat capacity of the liquid phase, $W_f$ is the mass feed rate of the liquor entering the evaporator, Q is the heat flux per unit area through the tube wall, L is the tube length and $\lambda$ is the latent heat of vapourisation of the fluid of interest. Figure 6 shows a comparison of this expression with the experimental data, including some data from other authors.

In the region labelled BC in Figure 5, the heat transfer coefficients measured by Coulson and McNelly were found to be approximately the same as those for submerged nucleate boiling, with the turbulence produced by bubble formation greatly exceeding that arising from the bulk flow of the liquid and vapour phases along the tube. The authors recommended a correlation by McNelly (1953) to evaluate the boiling heat transfer coefficient in this region:

$$\frac{h_B D}{k_L} = 0,225\left[\frac{C_{PL}\mu_L}{k_L}\right]^{0,69} . \left[\frac{QD}{\lambda\mu_L}\right]^{0,69} . \left[\frac{PD}{\sigma}\right]^{0,31} . \left[\frac{\rho_L}{\rho_V} - 1\right]^{0,33}$$

where P is the operating pressure of the evaporator.

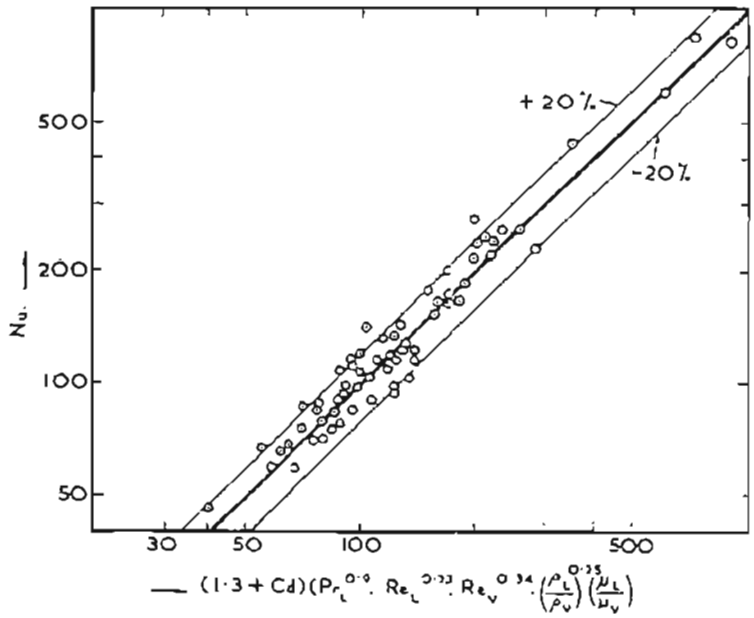


**Figure 6.** Comparison of the expression of Coulson and McNelly for region AB with the experimental data. [Coulson and McNelly, 1956]

Coulson and McNelly found that their developed expressions correlated the experimental data to within about ± 30%.

### 2.2.4 Gupta and Holland, (1966a)

Gupta and Holland studied the concentration of hard water using steam heating in a single tube climbing film evaporator. The evaporator consisted of a jacketed nine foot length of 316 stainless steel 16 BWG tube, of 0,87 in (22,1 mm) inner diameter and 1 in (25,4 mm) outer diameter. The evaporator performance was evaluated by measuring the change in water hardness across the evaporator. Further experiments were performed concentrating 55% sodium isethionate solutions and 35% sodium methyl taurine solutions.

Seventy five experiments were done concentrating hard water. Four steam pressures, namely 76, 96, 118 and 132 psia (524, 662, 814 and 910 kPa(a)) were used. The feed temperature varied between 50 and 180°F (10 and 82,2°C), with the feed water flow rate ranging between 300 and 633 lb/hr (136,1 and 287,1 kg/hr). The heat flux data obtained from the hard water concentration experiments were found to fit the empirical equation:

$$\frac{Q}{A} = \Psi M^{0,6} + 90,3(T_b - T_i)C_P \qquad \text{... (3)}$$

with a standard deviation of 2,6%, where Q is the heat transfer rate in Btu/hr, A is the heat transfer surface area in $ft^2$, M is the liquid feed flow rate in lb/hr, $T_b$ is the boiling point temperature of the water at the pressure of interest in °F, $T_i$ is the feed inlet temperature in °F, $C_p$ is the specific heat capacity of water in Btu/lb/°F and $\Psi$ is a graphically determined function of $\Delta T$, the temperature difference driving force in °F, as shown in Figure 7. The curve in Figure 7 exhibits a maximum point at approximately 125°F. This behaviour can be explained by the theory of vapour blanketing. Initially, the heat transfer rate increases as the temperature difference driving force increases (for a particular feed temperature and flow rate). Eventually, however, a steam pressure is reached at which the temperature difference driving force is sufficient for the formation of a vapour blanket over the heat transfer surface. Any increase in steam pressure beyond this point results in an increase in the degree of vapour blanketing of the heat transfer surface, with a resulting decrease in the heat transfer rate, since the heat transfer coefficient for transfer to a vapour is much lower than the corresponding coefficient for heat transfer to a liquid.

For feed liquid entering the tube at its boiling point, equation **(3)** reduces to:

$$\frac{Q}{A} = \Psi M^{0,6}$$

Utilising the definition of the overall heat transfer coefficient results in the following equation for feed entering the tubes at the boiling point:

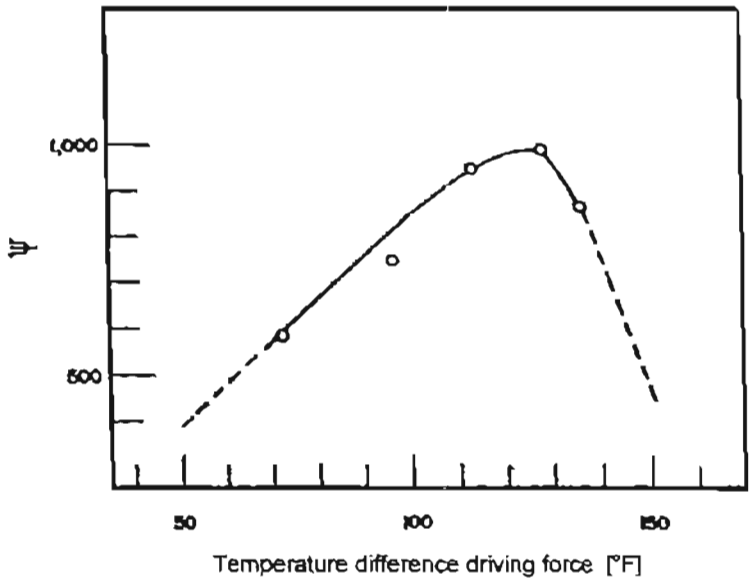


**Figure 7.** Graphical plot of the Ψ function. [Gupta and Holland, 1966a]

$$U = \frac{\Psi M^{0,6}}{\Delta T}$$

where U is the overall boiling heat transfer coefficient in Btu/hr/ft$^2$/°F. The overall boiling heat transfer coefficients from experiment were found to fit this equation with a standard deviation of 2,85%.

Although equation **(3)** was empirically derived from the experimental data for the concentration of hard water only, it was found to fit the heat flux data for sodium methyl taurine solutions with a standard deviation of 16% and the data for sodium isethionate solutions with a standard deviation of 8%. In these experiments, the boiling temperature $T_b$ was taken as the average boiling point temperature of the solutions between their initial and final concentrations.

### 2.2.5 Gupta and Holland, (1966b)

In the continuation of their work on climbing film evaporators, Gupta and Holland defined three regions within the tube of a climbing film evaporator (namely liquid, foam and climbing film) and presented a technique for estimating the lengths of these three regions and the heat transfer coefficients within them. In the development of this technique, data collected during their previous study was used, along with additional data collected using the same experimental apparatus. The results obtained were plotted graphically, and no adjustments or extensions to their previous climbing film evaporator model were proposed.

### 2.2.6 Tang, (1980)

Tang modelled the flow in a climbing film evaporator tube on a theoretical hydrodynamic and thermodynamic basis. The obtained model was used to determine the exit vapour and liquid phase velocities, the mean residence time of the liquor within the evaporator tube and the effective mean temperature difference across the tube wall. The predictions of the model were found to compare favourably, at least in order of magnitude, with the results of experimental tests concentrating a sodium thiocyanide solution in a stainless steel climbing film evaporator (tube diameter 25 mm, wall thickness 1,62 mm, length 3 m). Unfortunately, no attempt was made to correlate heat transfer coefficients using the model.

### 2.2.7 Mayinger and Schult, (1981)

Mayinger and Schult developed a model to predict the dynamic behaviour of a generalised double phase change heat exchanger (a heat exchanger with a condensing fluid as the heating medium and an evaporating fluid as the heated fluid). The primary bases of the

model were the basic laws of conservation of mass, energy and momentum, taking into account the strong coupling between the boiling and condensation sides of the exchanger via the heat fluxes transported and the heat stored. The partial differential equations so obtained are highly nonlinear, and were therefore solved by an appropriate computer program, using numerical methods. In order to simplify the mathematical treatment and avoid long computational times for the numerical analysis of the system, the following assumptions were made:

- The flow on each side of the tube wall was considered one-dimensional
- The vapour and liquid were considered to be in thermodynamic equilibrium
- The tube wall was considered to be very thin, or having a high thermal conductivity, thus allowing it to be effectively neglected in the analysis
- The boiling fluid was considered to enter the tube in a subcooled state
- The condensing vapour was considered saturated

In order to solve the system of differential equations describing the system, constitutive equations describing the following phenomena needed to be developed: subcooled boiling on the evaporating side, two phase flow pressure drop on the evaporating and condensing sides, the slip ratio on the evaporating and condensing sides and heat transfer with boiling and with condensation. The information used to describe these phenomena was taken from the literature in the form of empirical equations. As phenomena such as pressure drop and heat transfer may be strongly dependent on the geometric conditions in the heat exchanger, an experimental programme was used to select those equations from the literature best suited to incorporation in the model. This experimental programme utilised a very simple double phase change heat exchanger, evaporating refrigerant R12 using condensing steam.

Mayinger and Schult found that their model agreed well with the results of their experiments, provided that no two-phase flow instabilities occurred, the frequency of system perturbations was not too high and the system pressure was not changed too much.

### 2.2.8 Bourgois and Le Maguer, (1983a)

Bourgois and Le Maguer performed a literature survey in the field of climbing film evaporator modelling, covering the period from 1970 to 1980. They found that very little work had been done in the area of interest. Due to the large number of variables involved and the limited state of knowledge of heat transfer, the results which had been obtained by various authors for one set of conditions were of little real value in predicting performance under a different set of conditions. They set out to establish relationships for the heat transfer and fluid flow phenomena in the boiling and non-boiling zones within the tube of a climbing film evaporator. The constant coefficients in these relationships could then be empirically established using experimental data.

Theoretical analysis of the heat transfer across the tube wall in a section of tube $\delta z$ within the non-boiling zone led to the following equation:

$$Nu_z = \frac{Pe_i}{4} \frac{d\ln(T^*)}{dZ^*} \qquad \ldots (4)$$

where $Nu_z$ is the local Nusselt number, characteristic of the evaporator length and the heat transfer coefficient at position z in the tube, $Pe_i$ is the Peclet number calculated at the evaporator inlet conditions, $T^*$ is a dimensionless temperature variable:

$$T^* = \frac{(T_s - T_i)}{(T_s - T)}$$

which is a function of position within the tube, $T_s$ is the condensing steam temperature, $T_i$ is the temperature of the subcooled liquid at the inlet of the tube, T is the liquid temperature at a distance z along the tube and $Z^*$ is the dimensionless distance along the tube $Z^* = z/L$, where L is the tube length. Evaluation of equation (4) requires a knowledge of the relationship between $\ln(T^*)$ and $Z^*$, which can be determined experimentally.

Making the following assumptions:

- The vapour phase within the tube is always saturated

- The inertia and acceleration terms within the momentum balance equation are much larger than the frictional terms (which is usually true for rapid evaporation)
- Incompressibility of the liquid phase
- Not much temperature variation within the boiling zone, thus allowing the temperature dependence of the liquid and vapour phase densities to be ignored
- Along the saturation curve of water, the absolute temperature and pressure can be related by $T = cP^n$, where c = 166,766 and n = 0,06978, and the vapour phase behaves as an ideal gas

and carrying out a momentum balance, Bourgois and Le Maguer developed the following relationship for the pressure distribution along the tube of a climbing film evaporator:

$$\frac{dP}{dZ^*} = \frac{-\frac{V_l}{\pi R^2}\left(\rho\frac{(\rho_1 - S\rho_2)}{S\rho_1\rho_2} + S - 1\right)\frac{dW_2}{dZ^*} - g(\alpha\rho_2 + \rho_1(1-\alpha))L}{1 - \rho V_l^2\frac{\alpha}{\rho_2}\frac{(1-n)}{Rc}P^{-n}} \quad \text{... (5)}$$

where P is the pressure at distance z along the tube, $V_l$ is the liquid phase velocity at distance z along the tube, R is the universal gas constant (8314,5 J/kmol/K), $\rho$ is the density of the two phase mixture at distance z along the tube, $\rho_1$ is the liquid phase density at distance z along the tube, S is the slip ratio ($V_2/V_2$ where $V_2$ is the vapour phase velocity at distance z along the tube), $\rho_2$ is the vapour phase density at distance z along the tube, $W_2$ is the vapour phase mass flow rate at distance z along the tube, g is the acceleration due to gravity and $\alpha$ is the volume fraction of the vapour phase at distance z along the tube. The value for $\alpha$ is not known, but was determined by Bourgois and Le Maguer using the modified Darmouth correlation for vertical upward cocurrent annular flow as proposed by Turner (1966):

$$\frac{j_2^*}{1 - 3{,}1(1-\alpha)} - \frac{j_1^*}{3{,}1(1-\alpha)} = 1$$

where $j_1^*$ is the dimensionless volumetric liquid flux at distance z along the tube, as

defined by:

$$j_1^* = \frac{j_1 \sqrt{\rho_1}}{\sqrt{gD(\rho_1 - \rho_2)}}$$

($j_1$ is the volumetric liquid flux at distance z along the tube and D is the inside diameter of the tube). Similarly, $j_2^*$ is the dimensionless volumetric vapour flux at distance z along the tube, as defined by:

$$j_2^* = \frac{j_2 \sqrt{\rho_2}}{\sqrt{gD(\rho_1 - \rho_2)}}$$

where $j_2$ is the volumetric vapour flux at distance z along the tube.

Equation **(5)** can be solved numerically once $dW_2/dZ^*$ is known.

From a steady state heat balance at a distance z along the tube, Bourgois and Le Maguer developed the following relationship for $U_z$, the local heat transfer coefficient, in the boiling zone, at distance z along the tube:

$$U_z = \frac{1}{\pi DL(P_s^n - P^n)}\left[\frac{\lambda}{c}\frac{dW_2}{dZ^*} + (W_1 C_{p1} + W_2 C_{p2})\, nP^{n-1}\frac{dP}{dZ^*}\right] \qquad \ldots (6)$$

where $P_s$ is the pressure of the condensing steam, $\lambda$ is the latent heat of vapourisation of the liquid phase, $W_1$ is the liquid phase mass flow at distance z along the tube, $C_{p1}$ is the heat capacity of the liquid phase and $C_{p2}$ is the heat capacity of the vapour phase.

Assuming a constant mass rate of evaporation along the length of the tube, equation **(6)** can be solved numerically together with equation **(5)** once $dW_2/dZ^*$ is known (or determined by experiment).

### 2.2.9 Bourgois and Le Maguer, (1983b)

In the second publication regarding their climbing film evaporator model, Bourgois and Le Maguer validated their theoretically developed equations using a pilot scale single tube borosilicate glass climbing film evaporator. The glass tube used was 3 metres in length, with a 30 mm inside diameter and a 1,53 mm wall thickness. This tube was exposed to a 2,7 metre long glass steam jacket of diameter 50 mm. Seven thermocouples were located along the axis of the tube in order to determine the temperature profile of the boiling fluid.

To allow for independent study of the separate zones within a climbing film evaporator, the experimental study was divided into three parts:

- Experiments with the liquid phase completely filling the tube, with no evaporation. This allowed the phenomena of the non-boiling zone to be studied.
- Experiments with the liquid phase entering the tube at its boiling point, to enable the phenomena of the boiling zone to be studied.
- Experiments utilising a combination of conditions in the previous two sets of experiments, to permit the study of the performance of the evaporator under normal conditions of use in industry. For these tests, sucrose solutions and tomato juice were used in addition to water.

Results obtained during the first set of tests suggested that, for a given flow rate, $\ln(T^*)$ could be approximated by a second degree polynomial in $Z^*$:

$$\ln(T^*) = A + B.Z^* + C.Z^{*2}$$

leading to the following form for equation (4) describing the heat transfer in the non-boiling zone:

$$Nu_z = \frac{Pe_i}{4}(B + 2CZ^*)$$

where the coefficients B and C were determined by best least squares fit of the

experimental data as:

$$B = -0{,}458 + \frac{9445}{Pe_i} + \frac{5{,}22 \times 10^6}{Pe_i^2}$$

and

$$C = 0{,}238 + \frac{755}{Pe_i} - \frac{135 \times 10^7}{Pe_i^2}$$

In the second series of tests, the boiling zone was studied. For this zone, the equations previously developed by Bourgois and Le Maguer for pressure drop and heat transfer contain the mass flow rates of the liquid and vapour phases within the tube. However, these values can only be determined by experiment at the inlet and outlet of the evaporator tube. For their analysis, the authors assumed a linear increase in vapour quality (and hence vapour mass flow rate) with distance along the tube, yielding:

$$\frac{dW_2}{dZ^*} = W_{2e}$$

where $W_{2e}$ is the mass flow rate of vapour exiting the tube. This allows the differential equation describing the pressure drop (equation **(5)**) to be numerically solved to obtain local values of pressure along the length of the tube. Similarly, equation **(6)** can be numerically evaluated to yield local values of the boiling heat transfer coefficient along the length of the tube. Bourgois and Le Maguer also correlated the heat transfer coefficients obtained in their experiments with the dimensionless distance along the tube, $Z^*$, using a least squares fit for a polynomial equation of order 2:

$$U_z = 615{,}5 - 112\,Z^* + 41{,}55\,Z^{*2}$$

Using this correlation within equation **(6)**, with rearrangement, allows the vapour generation rate $dW_2/dZ^*$ to be determined at any point within the tube:

$$\frac{dW_2}{dZ^*} = \frac{\pi DcLU_z}{\lambda}(P_s^n - P^n) - \frac{(W_1C_{p1} + W_2C_{p2})\, ncP^{n-1}}{\lambda}\frac{dP}{dZ^*}$$

In the third set of experiments, the authors tested their model by using conditions resulting in both the non-boiling and boiling zones being present within the tube. The known variables used as inputs to the model were the initial feed conditions (such as the feed inlet temperature $T_i$ and the mass flow rate of feed W), the system vacuum pressure at the top of the tube $P_v$ and the steam pressure $P_s$. The desired outputs of the model were the distance at which boiling starts $Z_b^*$, the mass flow rate of vapour at the exit of the tube $W_{2c}$ and the temperature at the outlet of the evaporator $T_c$.

The experimental work to test the model was carried out with water, sucrose solutions of different concentrations and tomato juice. Bourgois and Le Maguer found that the differences between the experimental values of the distance at which boiling began and the vapour production rate at the evaporator exit were always within 10% of the calculated values using the model. They considered this to be reasonable, given the measurement errors inherent to their system.

### 2.2.10 Bourgois and Le Maguer, (1984)

In the third paper regarding their climbing film evaporator model, Bourgois and Le Maguer applied the model to an industrial scale climbing film evaporator used to concentrate pineapple juice from 13,5 to 62% (m/m) at a feed flow of approximately 5 t/h. The evaporator was composed of three sections, each section having a greater number of tubes than the previous one to allow for the increased volume of vapour and to ensure a climbing film boiling regime during the entire evaporative process. The tubes in the first

two sections of the evaporator were of length 2,13 m, while those in the third section were of length 2,44 m. All tubes were of stainless steel, with inner diameter 19 mm. The heat transfer information used in the evaporator model was corrected for the change in thermal conductivities to take into account the change in tube material from glass to stainless steel.

As the inlet pressure into the industrial evaporator was unknown, it was necessary for Bourgois and Le Maguer to estimate this quantity before computing the model. This estimate was then iteratively updated following successive model runs, in order to match the outlet pressure to that observed experimentally. The method of calculation of the model was as follows:

- From the estimate of the inlet pressure and the composition and temperature of the feed, a flash calculation was performed to calculate the ratio of vapour to liquid in the feed entering the tubes.
- Assuming that the flow in the industrial evaporator was equally distributed between all of the tubes, the flow to one tube in the evaporator was calculated. The original model was then applied to a single tube.
- Account was taken of the pressure drop between successive sections of the three stage evaporator, based on losses due to hydrostatic head, expansion and contraction.

Bourgois and Le Maguer found that the model was adequate for predicting the behaviour of the industrial climbing film evaporator under study. The measured values for the product concentration and vapour flow rate at the evaporator outlet were found to differ from the calculated values by 2,7% and 0,8%, respectively. The calculated amount of flash vapour generated on entry into the tubes was calculated to be 4% of the feed flow, ensuring immediate two phase flow within the tubes. The initial void fraction was calculated as 0,619, with the local heat transfer coefficient found to decrease with increasing void fraction. The velocities at the top of the tubes were found to be 1,59 m/s for the liquid phase and 59,0 m/s for the vapour core. From the inlet to the outlet, the slip

ratio within the tubes varied by no more than 5%, which was considered to be consistent with theory.

### 2.2.11 Zinemanas *et al.*, (1984)

Zinemanas and his co-workers developed a general algorithm for the simulation of vertical and horizontal shell and tube heat exchangers with change of phase of one or more components. The algorithm calculates local values of the variables of interest along the length of the heat exchanger tubes and was found to yield acceptable accuracy when compared with experimental data for systems of one to three components.

*Model Development*

The design of heat exchangers follows the basic differential equation for heat transfer:

$$\frac{dQ}{dA} = U.\Delta T \qquad \ldots (7)$$

where dQ is the amount of heat transferred, U is the local overall heat transfer coefficient, $\Delta T$ is the temperature difference driving force and dA is the heat transfer area element. Rigorous integration of equation (7) is possible if reliable correlations for the heat transfer coefficients, pressure drop and physical properties are available. In their study, Zinemanas *et al.* utilised simultaneous pointwise integration of both equation (7) and the differential equation describing the hydrodynamics of the system, using the best available correlations in the literature for each flow pattern type within the heat exchanger tube. A vapour-liquid equilibrium correlation was used for systems of more than one component[1]. The assumptions employed in the model development were:

- steady state,

[1] This aspect of the model of Zinemanas *et al.* will not be discussed in detail here, as it is not relevant to the current study.

- adiabatic overall heat exchanger system,
- thermodynamic equilibrium between the phases,
- uniform temperature profiles across any cross-section of the tube.

Rearranging equation **(7)** yields:

$$A = \int_0^{Q_T} \frac{dQ}{U.\Delta T} \qquad \text{... (8)}$$

where U and $\Delta T$ are non-linear, non-explicit functions of Q. Thus numerical integration is needed. Q is obtained from the enthalpy balance of the system

$$dQ = M.dH \qquad \text{... (9)}$$

where M is the mass flow rate and dH is obtained from:

$$dH = \left(x C_{pL} + (1 - x) C_{pV}\right) dT + \lambda\, dx \qquad \text{... (10)}$$

where dT is the differential change in temperature of the stream, x is the steam quality, $C_{pL}$ and $C_{pV}$ are the heat capacities of the liquid and vapour phases and $\lambda$ is the phase change enthalpy, neglecting the pressure change in the differential element.

Equations **(8)**, **(9)** and **(10)** are integrated numerically, together with the pressure drop relationship for the flow pattern identified within the tubes.

The local overall heat transfer coefficient used in the integration is calculated using

$$\frac{1}{U} = \frac{1}{h_i} + R_{fi} + \frac{D_i}{2k_w} \ln\frac{D_o}{D_i} + R_{fo} + \frac{D_i}{h_o D_o}$$

where U is the overall heat transfer coefficient, $D_o$ and $D_i$ are the outer and inner tube diameters, respectively, $R_{fo}$ and $R_{fi}$ are the outer and inner fouling resistances, $k_w$ is the thermal conductivity of the tube wall material and $h_o$ and $h_i$ are the outer and inner local

heat transfer coefficients.

The model calculation is based on numerical integration using steps of constant enthalpy change ($\Delta H_k$). For each integration step (k), the physical properties are a function of the local conditions for that step. The incremental pressure in the current step is that calculated in the previous step. The temperature is calculated from the incremental enthalpy balance, resulting in

$$T_{k+1} = T_k + \frac{\Delta Q}{M C_{pk}}$$

for single phase flow and

$$x_{k+1} = x_k + \frac{\Delta Q_k / M - \left[(1-x)C_{pL} + xC_{pV}\right].\left[T_s(x_{k+1}, P_k) - T_s(x_k, P_{k-1})\right]}{\lambda}$$

for two phase flow, where $T_s(x, P)$ is the saturation temperature. This is a nonlinear equation which needs to be solved (for $x_{k+1}$) simultaneously with the material balance. The flow pattern prevailing within the tubes is identified and the applicable heat transfer correlations are used. The overall local heat transfer coefficient is calculated, together with the heat flux equalities on both sides of the wall, which have to be matched, by an iterative procedure.

The area increment which corresponds to the relevant enthalpy increment step is then calculated

$$\Delta A_k = \frac{\Delta Q_k}{U_k . \Delta T_k}$$

From the corresponding length increment calculated from the geometry of the tubes, the pressure for the next step is calculated:

$$P_{k+1} = P_k + \left(\frac{dP}{dz}\right).\Delta z_k$$

(refer to the next section on *Hydrodynamics and Heat Transfer* for details). The calculation procedure stops when the total heat transferred reaches the total required heat duty for the heat exchanger ($Q_T$).

*Hydrodynamics and Heat Transfer*

A thorough review of the literature was undertaken by Zinemanas *et al.* in order to choose the best available heat transfer and pressure drop correlations for inclusion into the model. Correlations were also chosen for the identification of the flow pattern existing within the tubes.

For single phase flow, the pressure drop is well defined. The local heat transfer coefficient values within the tubes were calculated using Dittus-Boelter type expressions, as recommended by Hughmark (1969).

The pressure drop equations for two phase flow included an acceleration term in addition to the frictional and gravitational terms. The Lockhart-Martinelli (1949) pressure drop correlation was utilised, in the form presented by Collier (1980). For calculation of the two phase local heat transfer coefficients within the tubes, the correlation of Chen (1966) was used.

*Experimental Verification*

Zinemanas *et al.* tested their model using data available in the open literature. In general, the tube lengths calculated by the model agreed well with the experimental lengths. For one of the data sets tested, the average difference for all runs was found to be 22,5%, which shows some limitations in the heat transfer correlations used in the model.

## 2.3 CONCLUSIONS

Not many mathematical models of the climbing film evaporator system exist in the available literature. Early studies considered the evaporator system using lumped-parameter models, utilising average values of the relevant process variables to describe the overall behaviour of the system.

Only two distributed-parameter climbing film evaporator models were found in the author's survey of the literature, the first being due to Bourgois and Le Maguer (1983a, 1983b, 1984). Their model was, however, based on several simplifying assumptions, such as the assumption of a constant mass rate of evaporation along the length of the tube. This assumption may is the major drawback of the model.

The most recent work in the field of climbing film evaporator modelling was the comprehensive study of Zinemanas *et al.* (1984), who studied the simulation of heat exchangers with change of phase. While the model of Zinemanas *et al.* is, in principle, similar to that developed by the author, their work was aimed at providing a generalised model for many types of evaporating heat exchanger, and incorporating multicomponent vapour-liquid equilibrium. The aim of the current study is to provide a mathematical model specific to the climbing film evaporator in the sugar industry, based on experimental data gathered under industrial conditions, and including extension to practical applications.

# Chapter 3
# Model Description

To describe fully the climbing film evaporator system, it is necessary to obtain information about the pressure, component flow rate and temperature distributions along the length of one of the tubes within the apparatus under steady state conditions. For this purpose, a system of ordinary differential equations can be developed from first principles to describe fully the conditions inside and outside an evaporator tube. These strongly-coupled differential equations require solution using a numerical integration procedure.

## 3.1 BASIC MODEL PHILOSOPHY

The system to be modelled is that of a climbing film evaporator in a raw sugar mill, as shown conceptually in Figure 8. Clarified cane juice (known as clear juice) is fed to a preheater, where it is heated to a temperature close to, or slightly above, the normal juice boiling point. The heated juice is then fed to the bottom of the tubes of the climbing film evaporator. For the purposes of modelling, the clear juice is assumed to be a three-component mixture, consisting of water, sucrose and non-sucrose dissolved solids (impurities).

The main purpose of modelling the climbing film evaporator system is to determine the temperature distribution across a single tube of the apparatus as a function of the tube length. This temperature distribution will include:

- the steam temperature, $T_s$
- the outer tube wall temperature, $T_{w1}$
- the inner tube wall temperature, $T_{w2}$
- the liquid temperature, $T_L$, and
- the vapour temperature, $T_v$.

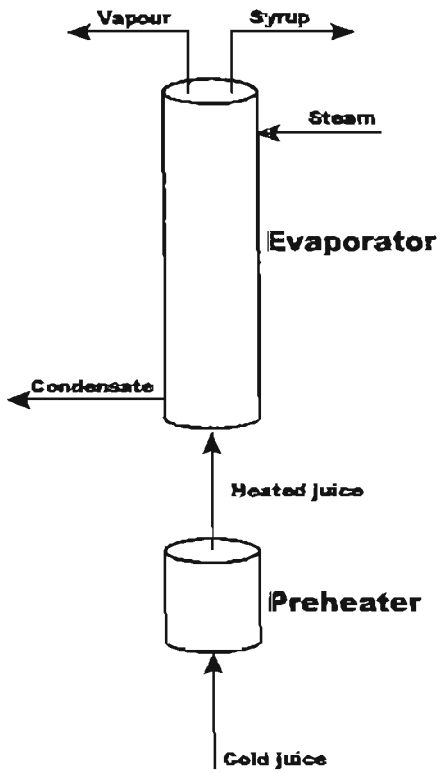


**Figure 8.** A conceptual view of the system to be modelled.

The steam temperature is assumed to be constant and known. The two tube wall temperatures result from the continuity conditions for the steady state heat flux across the tube wall. Under conditions of no boiling within the tube, the liquid temperature results from an enthalpy balance for the liquid. Under boiling conditions, the liquid boiling point temperature is defined by the pressure and the liquid composition. At any cross-section within the tube, the vapour temperature is assumed to be the same as that of the liquid phase. This implies a certain degree of superheating of the vapour phase.

The hydrodynamics of the climbing film evaporator system can be characterised by:

- the mass flow rate of condensate per unit length of the tube perimeter, $\Gamma$
- the mass flow rate of the liquid, L, and
- the mass flow rate of the vapour, V.

The mass flow rate of condensate per unit perimeter length results from an enthalpy

balance, based on the Nusselt theory of condensation. The mass flow rate of liquid is calculated using a total flow (liquid and vapour) mass balance within the tube. The mass flow rate of vapour results from an enthalpy balance within the tube.

The composition of the liquid phase within the tubes can be defined by two mass fractions:

- the mass fraction of sucrose, s, and
- the mass fraction of impurities, r.

The sucrose content of the liquid phase results from a sucrose balance within the tube. Similarly, the impurity content results from an impurity mass balance. The vapour phase is assumed to be pure water, free of both sucrose and impurities.

The total pressure within the tubes is governed by a momentum balance within the tube, containing terms due to:

- the viscous fluid pressure drop
- the weight of the two-phase mixture (hydrostatic head), and
- the flow acceleration affect.

For the purposes of model solution, it is assumed that the following boundary condition quantities are known under a given set of evaporator operating conditions and can be assigned numerical values as system input parameters:

- the mass flow rate of cold juice through the preheater, $F_0$
- the mass fraction sucrose content of the clear juice fed to the preheater, $s_p$
- the mass fraction impurity content of the clear juice fed to the preheater, $r_p$
- the temperature of the heated juice leaving the preheater, $T_{L0}$
- the vapour space pressure at the top of the evaporator tubes, $p_{top}$
- the mass flow rate of condensate per unit tube perimeter at the top of the evaporator tubes, $\Gamma_0$

The mass flow rate of condensate per unit perimeter length at the top of the tubes, $\Gamma_0$, is

taken to be zero, as there is assumed to be no condensate film present at the very top of the tubes.

## 3.2 GENERATION OF THE BALANCE EQUATIONS

Mass, momentum and enthalpy balances can be formulated for the climbing film evaporator system, utilising the following assumptions:

- steady state conditions are assumed to exist in the evaporator system at all times, and
- a plug flow model is assumed for the hydrodynamics of the system (i.e. there is no radial or axial mixing of the fluid being evaporated).

As all the variables of interest vary continuously along the length of the tube, the relevant balance equations were formulated for a differential tube length section, dz. The bottom cross-section of the tube was assumed to be at $z = 0$.

### 3.2.1 Total mass balance of liquid and vapour

A total mass balance can be formulated by considering the differential element, dz, shown in Figure 9.

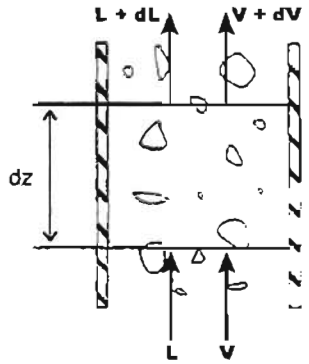


**Figure 9.** The differential element used to formulate the total mass balance.

The resulting balance

$$\frac{d(L+V)}{dz} = 0$$

is trivial and can be analytically integrated to yield

$$L + V = L_0 + V_0 \quad \ldots (11)$$

where $L_0$ and $V_0$ are the mass flow rates of liquid and vapour, respectively, entering the bottom of the tube. Equation (11) can be used to determine the mass flow rate of liquid at position z in the tube, once the mass flow rate of vapour has been calculated using the enthalpy balance within the tube.

### 3.2.2 Sucrose mass balance

Similarly, a sucrose mass balance can be formulated using a differential element of tube height, resulting in the following balance equation:

$$\frac{d(L.s)}{dz} = 0$$

which can be easily analytically integrated to yield

$$L.s = L_0.s_0 \quad \text{... (12)}$$

where $s_0$ is the mass fraction sucrose in the liquid phase entering the bottom of the tubes.

### 3.2.3 Impurity mass balance

An impurity mass balance can be formulated to yield

$$\frac{d(L.r)}{dz} = 0$$

which is trivial and can be analytically integrated to yield

$$L.r = L_0.r_0 \quad \text{... (13)}$$

where $r_0$ is the mass fraction non-sucrose dissolved solids (impurities) in the liquid phase entering the bottom of the tubes.

### 3.2.4 Total enthalpy balance of liquid and vapour

A total enthalpy balance within the tube can be formulated by considering the differential element of tube length, dz, shown in Figure 10.

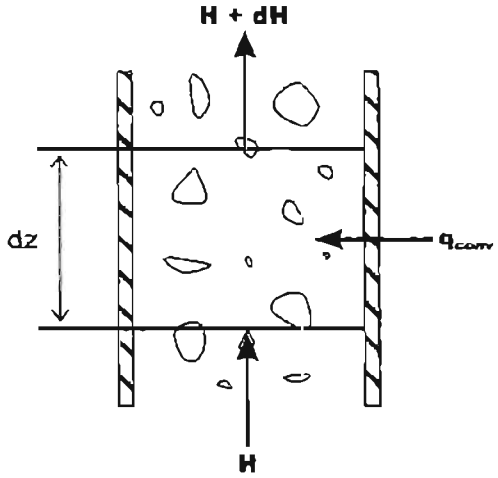


**Figure 10.** The differential element used to formulate the enthalpy balance.

The resulting balance equation is

$$\frac{dH}{dz} = \pi D_2 q_{conv} \quad \text{... (14)}$$

where H is the total enthalpy flow of the liquid and vapour within the tube [W], $D_2$ is the inner wall diameter of the tube and $q_{conv}$ is the heat flux from the tube wall into the fluid, due primarily to convection heat transfer:

$$q_{conv} = \alpha (T_{w2} - T_L)$$

where $\alpha$ is the heat transfer coefficient within the tube, $T_{w2}$ is the inner tube wall temperature and $T_L$ is the bulk liquid temperature within the tube. This heat transfer coefficient is a complicated function of the physical properties of the fluid being evaporated and the hydrodynamics of the system.

### 3.2.5 Analysis of the condensation process

Traditionally, the condensation process is analysed as originally postulated by Nusselt (see Monrad and Badger, 1930), where wholly laminar flow of the condensate film and a constant wall temperature are assumed. However, for this study, the second simplification was considered unrealistic and thus the traditional theory was appropriately modified to allow for a more general approach (based on the approach by Mills, 1992).

The condensation process occurring on the outside tube wall can be analysed by considering a differential element of tube length, dz, as shown in Figure 11.

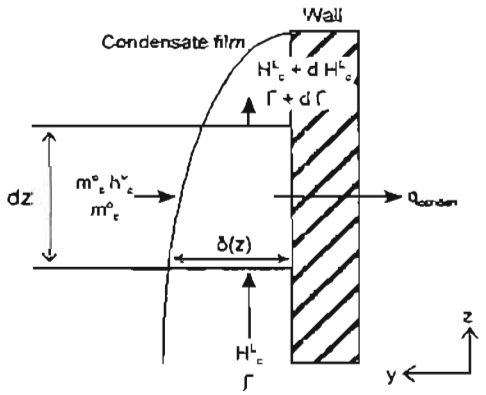


**Figure 11.** The differential element used for the condensation analysis.

There are two assumptions made in analysing the control element shown in Figure 11:

- the film velocity of the flowing condensate is fairly low (laminar flow), and
- temperature gradients in the z direction (along the length of the tube) can be considered negligible.

A mass flow rate of condensate per unit length of tube perimeter ($\Gamma$) can be defined as

$$\Gamma = \int_0^{\delta(z)} \rho \, u \, dy$$

where $\rho$ is the density of the condensate, u is the velocity of the condensate film at position y in the condensate film, $\delta(z)$ is the thickness of the condensate film at position z along the tube length and dy is a differential element of condensate film thickness. It should be noted that this definition for $\Gamma$ is independent of the nature of the flow pattern

assumed to exist within the condensate film.

Further defining a mass flux of condensation, $m^0_c$ in kg/m$^2$.s, and taking a mass balance around the differential element dz shown in the figure yields

$$\frac{d\Gamma}{dz} = - m^0_c \quad \text{... (15)}$$

Similarly, an enthalpy flow rate of condensate per unit length of tube perimeter ($H^L_c$) can be defined as

$$H^L_c = \int_0^{\delta(z)} \rho\, u\, h^L_c \, dy$$

where $h^L_c$ is the specific enthalpy of the condensate at position y in the condensate film.

Taking an enthalpy balance around the differential element shown in Figure 11 yields

$$\frac{dH^L_c}{dz} = q_{conden} - m^0_c\, h^V_c \quad \text{... (16)}$$

where $q_{conden}$ is the heat flux through the tube wall as a result of condensation heat transfer and $h^V_c$ is the specific enthalpy of the condensing vapour phase. This vapour phase enthalpy can be considered constant, as its value depends entirely on the temperature of the condensing steam, which is constant. By contrast, the specific enthalpy of the liquid phase can not be considered to be constant, as a result of the subcooling effect in the condensate film (dependence on z) and the temperature profile across the film of condensate (dependence on y).

Combining equations **(15)** and **(16)** (the mass and enthalpy balances) results in

$$\frac{dH^L_c}{dz} = q_{conden} + \frac{d\Gamma}{dz} h^V_c \quad \text{... (17)}$$

Since $h^V_c$ can be considered constant and independent of the position along the length of

the tube (z), equation (17) can be written as

$$\frac{dH_c^L}{dz} = q_{conden} + \frac{d}{dz}\left(\Gamma h_c^V\right)$$

which can be rearranged to yield

$$\frac{d\left(\Gamma h_c^V - H_c^L\right)}{dz} = -q_{conden}$$

By appropriately defining a condensation and subcooling enthalpy flow rate for the condensate film ($H_c$ in W/m) as

$$H_c = \Gamma h_c^V - H_c^L$$

the mass and enthalpy balances for the condensate film can be reduced to one simple differential equation:

$$\frac{dH_c}{dz} = -q_{conden} \quad \text{... (18)}$$

### 3.2.6 Momentum balance within the tube

Considering the differential element of tube length, dz, shown in Figure 12, a two phase momentum balance within the tube can be formulated (Holland and Bragg, 1995) to yield

$$\frac{dp}{dz} = -\left(\frac{1}{A_x}\frac{dF}{dz}\right) - \left[\frac{1}{A_x}\frac{d}{dz}\left(L u_L + V u_v\right)\right] - \left(\frac{A_{xv}}{A_x}\rho_v + \frac{A_{xL}}{A_x}\rho_L\right) g$$

where p is the pressure at height z within the tube, $A_x$ is the cross-sectional area for flow within the tube, F is the frictional drag force of the tube wall, L is the mass flow rate of the liquid phase, V is the vapour phase flow rate, $u_L$ is the liquid phase velocity, $u_v$ is the vapour phase velocity, $A_{xv}$ and $A_{xl}$ are the cross-sectional areas for flow of the vapour and

liquid phases within the tube, respectively and $\rho_v$ and $\rho_L$ are the vapour and liquid phase densities, respectively.

Assuming the homogenous flow model of two-phase fluid flow within the tube, which implies no slip between the liquid and vapour phase flows, the following simplification results:

$$\frac{dp}{dz} = -\frac{1}{A}\frac{dF}{dz} - \frac{d}{dz}\left(m' u\right) - \rho_m g \quad \text{... (19)}$$

where m' is the total mass flux of the two phase fluid flowing through the tube, u is the average velocity of the two phase fluid at point z in the tube, $\rho_m$ is the density of the two phase fluid and g is the acceleration due to gravity.

Making use of the following definition:

$$u = \frac{m'}{\rho_m}$$

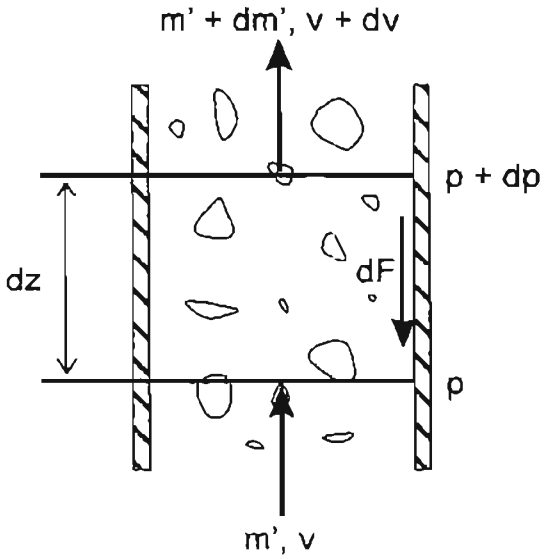


**Figure 12.** The differential element used to formulate the momentum balance.

equation **(19)** can be rewritten as

$$\frac{dp}{dz} = \left(\frac{dp}{dz}\right)_{friction} - m'^2 \frac{dv}{dz} - \rho_m g$$

where v is the specific volume of the fluid ($1/\rho_m$) and the frictional pressure drop term can be written as

$$\left(\frac{dp}{dz}\right)_{friction} = \Phi_{lo}^2 \left(\frac{dp}{dz}\right)_{fr\,lo}$$

where $\phi^2_{lo}$ is the two phase pressure drop enhancement factor and $(dp/dz)_{fr\,lo}$ is the pressure drop due to friction for single phase liquid flow in the tube. The momentum balance equation thus consists of three contributory terms, namely a viscous / frictional pressure drop term, an accelerational term due to the increase in the specific volume of the fluid during its flow through the tube (as a result of vapour production) and a hydrostatic head

term.

It is numerically convenient to combine the two derivatives in the equation into one term. Thus, defining a modified pressure term, the following ordinary differential equation results:

$$\frac{d\bar{p}}{dz} = \left(\frac{dp}{dz}\right)_{friction} - \rho_m g \quad \text{... (20)}$$

where

$$\bar{p} = p + \frac{m'^2}{\rho_m}$$

### 3.2.7 The balance equations

To summarise, the following balance equations can be formulated for the climbing film evaporator system:

$$L + V = L_0 + V_0 \quad \text{... (11)}$$

$$L.s = L_0.s_0 \quad \text{... (12)}$$

$$L.r = L_0.r_0 \quad \text{... (13)}$$

$$\frac{dH}{dz} = \pi D_2 q_{conv} \quad \text{... (14)}$$

$$\frac{dH_c}{dz} = -q_{conden} \quad \text{... (18)}$$

and

$$\frac{d\bar{p}}{dz} = \left(\frac{dp}{dz}\right)_{friction} - \rho_m g \quad \text{... (20)}$$

where

$$\bar{p} = p + \frac{m'^2}{\rho_m}$$

Thus the system is described fully by a set of six ordinary differential equations, three of which can be analytically integrated.

### 3.2.8 Heat flux continuity across the tube wall

In the climbing film evaporator system, heat flows from the condensing steam to the boiling juice through the tube wall. Under steady state conditions, continuity of this heat flow requires that the product of heat flux and surface area remain constant for each of the heat transfer mechanisms involved in the system. This concept is represented by the following conditions:

$$q_{conden} D_1 = q_{conduct} D_1 = q_{conv} D_2 \quad \text{... (21)}$$

where $q_{conduct}$ is the heat flux transmitted through the tube wall material by conduction and $D_1$ and $D_2$ are the outer and inner tube diameters, respectively.

### 3.2.9 Overall heat balance for the system

Considering heat flow continuity between the condensing steam and the boiling juice, it can be seen that the enthalpy balance for the condensing steam and the enthalpy balance for the liquid and vapour within the tube are mutually dependent. Writing these two enthalpy balances, and the continuity condition:

$$\frac{dH}{dz} = \pi D_2 q_{conv} \quad \text{... (14)}$$

$$\frac{dH_c}{dz} = - q_{conden} \quad \text{... (18)}$$

$$q_{conden} D_1 = q_{conv} D_2 \quad \text{... (22)}$$

equations **(14)** and **(22)** can be combined to yield

$$\frac{dH}{dz} = \pi D_1 q_{conden}$$

This relationship can, in turn, be combined with equation **(18)**, resulting in

$$\frac{dH}{dz} = - \pi D_1 \frac{dH_c}{dz}$$

which can be easily integrated to yield a simple linear relationship between the enthalpy of the fluid being boiled and the enthalpy of the condensate:

$$H - H(0) = \pi D_1 (H_c - H_c(0)) \quad \text{... (23)}$$

Equation **(23)** represents, in fact, an overall enthalpy balance involving the bottom of the tube (position z = 0) and an arbitrary cross-section. Using this simple relationship in the model allows the enthalpy of condensate, and hence the flow rate of condensate per unit perimeter length, to be easily calculated once the enthalpy of the boiling fluid is known. This result allows solution of one of the ordinary differential equations on the list of balance equations, leaving only two ordinary differential equations requiring numerical solution. The final system of six ordinary differential equations describing the climbing film evaporator system is thus:

$$L + V = L_0 + V_0 \quad \text{... (11)}$$

$$L.s = L_0.s_0 \quad \text{... (12)}$$

$$L.r = L_0.r_0 \quad \text{... (13)}$$

$$\frac{dH}{dz} = \pi D_2 q_{conv} \quad \ldots (14)$$

$$H - H(0) = \pi D_1 (H_c - H_c(0)) \quad \ldots (23)$$

and

$$\frac{d\bar{p}}{dz} = \left(\frac{dp}{dz}\right)_{friction} - \rho_m g \quad \ldots (20)$$

where

$$\bar{p} = p + \frac{m'^2}{\rho_m}$$

with only equations (14) and (20) requiring numerical solution.

## 3.3 EVALUATION OF THE DIFFERENTIAL EQUATIONS

Solution of the system of ordinary differential equations making up the climbing film evaporator model requires evaluation of the rate terms on the right hand sides of these equations.

### 3.3.1 Heat flux through the tube wall by convection

In equation (14), the heat flux through the tube wall by convection, $q_{conv}$ results from

$$q_{conv} = \alpha (T_{w2} - T_L)$$

where $\alpha$ is the heat transfer coefficient within the tube, a complicated function of the physical properties of the fluid being evaporated and the hydrodynamics of the system.

Under conditions within the tube where the liquid phase temperature is below its boiling point at the prevailing pressure, and the inner tube wall temperature is below that required for nucleation and bubble formation to occur, single phase convective heat transfer can be considered to occur. Under these conditions, the heat transfer coefficient within the tube results from liquid phase convective heat transfer alone ($\alpha = \alpha_L$) and can be evaluated using the Engineering Sciences Data Unit correlation (Engineering Sciences Data Unit, 1967; Engineering Sciences Data Unit, 1968):

*For laminar flow ($Re_L < 2100$)*

$$Nu_L = 1{,}86\left(Re_L\, Pr_L \frac{D_2}{Z}\right)^{1/3}\left(\frac{\mu_L}{\mu_{Lw}}\right)^{0{,}14} \quad \text{... (24)}$$

*For transitional flow ($2100 < Re_L < 4000$)*

$$Nu_L = 0{,}116\,(Re_L - 125)\,Pr_L^{1/3}\left(\frac{\mu_L}{\mu_{Lw}}\right)^{0{,}14}\left[1 + \left(\frac{D_2}{Z}\right)^{2/3}\right] \quad \text{... (25)}$$

*For turbulent flow ($4000 < Re_L < 1 \times 10^5$)*

$$Nu_L = 0{,}02246\, Re_L^{0.795}\, Pr_L^{(0.495 - 0.0255 \log Pr_L)}\left(\frac{\mu_L}{\mu_{Lw}}\right)^{0.18}\left[1 + \left(\frac{D_2}{Z}\right)^{0.7}\right] \quad \text{... (26)}$$

where $Nu_L$ is the single phase liquid Nusselt number, defined as

$$Nu_L = \frac{\alpha_L D_2}{k_L} \quad \text{... (27)}$$

(where $k_L$ is the thermal conductivity of the liquid phase within the tube), $Re_L$ is the single

phase liquid Reynolds number, defined as

$$Re_L = \frac{4L}{\pi D_2 \mu_L} \quad \text{... (28)}$$

(where L is the liquid phase mass flow rate through the tube), $Pr_L$ is the single phase liquid Prandtl number, defined as

$$Pr_L = \frac{\mu_L C_{pL}}{k_L} \quad \text{... (29)}$$

(where $C_{pL}$ is the specific heat capacity of the fluid within the tube), Z is the total length of the tube, $\mu_L$ is the viscosity of the liquid phase in the tube at the bulk liquid phase temperature and $\mu_{Lw}$ is the viscosity of the fluid at the temperature of the inner tube wall, $T_{w2}$.

Bubbles do not form on a heated surface until the degree of superheat is sufficient for the pressure inside a nucleation site to overcome the surface tension force tending to prevent bubble growth (Smith, 1986). Thereafter bubbles will form, become detached and pass into the bulk of the liquid phase. If the temperature of this bulk liquid phase is below its boiling point, these bubbles will subsequently collapse. When the inner tube wall temperature, $T_{w2}$ rises above a certain critical value for nucleation, $T^*$, subcooled nucleate boiling can be considered to occur. The critical wall temperature for nucleation can be calculated according to the method developed by Davis and Anderson (1966), as described by Smith (1986):

$$T^* = T_{bp} + \sqrt{\frac{8\sigma q_{crit nb} T_{bp}}{k\lambda\rho_v}} \quad \text{... (30)}$$

where $T_{bp}$ is the boiling point of the fluid in the tube at the prevailing pressure, $\sigma$ is the surface tension of the fluid within the tube, $q_{crit nb}$ is the critical heat flux for the initiation of nucleate boiling, $\lambda$ is the latent heat of vapourisation and $\rho_v$ is the density of the vapour

phase). However, $q_{crit\,nb}$ is a function of the critical wall temperature for nucleation

$$T^* = \frac{q_{crit\,nb}}{\alpha_L} + T_L$$

(where $T_L$ is the temperature of the liquid phase within the tube and $q_{crit\,nb}$ is the critical heat flux for initiation of nucleate boiling) and thus equation **(30)** is a quadratic equation in the square root of $T^*$, which can be solved algebraically to yield:

$$q_{crit\,nb} = \left( \frac{c_1 + \sqrt{\Delta}}{2} \right)^2$$

where

$$\Delta = c_1^2 + 4c_2$$

$$c_1 = \alpha_L \cdot \sqrt{\frac{8\sigma\,(T_{bp} + 273{,}15)}{k_L \lambda \rho_v}}$$

and

$$c_2 = \alpha_L (T_{bp} - T_L)$$

Once the fluid temperature within the tube rises above the local boiling point temperature at the prevailing pressure, fully developed / saturated nucleate boiling can be considered to occur. For both the subcooled and saturated nucleate boiling regimes, the heat transfer within the tube can be described by a correlation developed by Chen (1966), although it is assumed that no vapour phase is present during subcooled nucleate boiling. The basic premise assumed by Chen is that, since both convective heat transfer and nucleate boiling heat transfer contribute to the overall transfer of heat during boiling, the heat transfer coefficients for these two mechanisms can be additively superimposed to yield the overall boiling heat transfer coefficient, $\alpha$:

$$\alpha = F\alpha_L + S\alpha_{nb} \quad \text{... (31)}$$

where $\alpha_L$ is the liquid phase convective heat transfer coefficient calculated using equations **(24), (25)** and **(26)** and $\alpha_{nb}$ is the nucleate boiling heat transfer coefficient, calculated using a nucleate pool boiling correlation adapted from Foster and Zuber (1955):

$$\alpha_{nb} = 0{,}00122 \frac{k_L^{0,79} C_{pL}^{0.45} \rho_L^{0,49} (T_{w2} - T_L)^{0,24} \Delta p^{0,75}}{\sigma^{0,5} \mu_L^{0,29} \lambda^{0,24} \rho_v^{0,24}}$$

where $\Delta p$ is the difference in vapour pressures corresponding to the temperature difference between the inner tube wall and the boiling fluid, $T_{w2} - T_L$.

The terms F and S in equation **(31)** are empirical factors developed by Chen to account for the interfering effects of the two heat transfer mechanisms on each other. The convective heat transfer enhancement factor, F, reflects the fact that nucleate boiling enhances the effectiveness of convective heat transfer by disturbing the boundary layer of fluid against the tube wall in which the convection is taking place. F was found by Chen to be a function of the Martinelli factor, $X_{tt}$, devised by Lockhart and Martinelli (1949) for correlating data on two phase pressure drops:

$$X_{tt} = \left(\frac{1 - x_v}{x_v}\right)^{0,9} \left(\frac{\rho_v}{\rho_L}\right)^{0.5} \left(\frac{\mu_v}{\mu_L}\right)^{0,1}$$

where $x_v$ is the mass fraction vapour in the tube, $\rho_v$ is the density of the vapour phase, $\rho_L$ is the density of the liquid phase, $\mu_v$ is the viscosity of the vapour phase and $\mu_L$ is the viscosity of the liquid phase within the tube. The F parameter may be described by the following equations:

*For $1/X_{tt} < 0,1$*

$$F = 1$$

*For $0,1 < 1/X_{tt} < 0,7$*

$$F = 2,2709\left(\frac{1}{X_{tt}}\right)^{0,3562}$$

*For $1/X_{tt} > 0,7$*

$$F = 2,608\left(\frac{1}{X_{tt}}\right)^{0,7434}$$

It can be seen from these equations that, for the subcooled nucleate boiling zone, with no vapour phase present, the Chen F factor will have a value of 1.

The nucleate boiling suppression factor, S, accounts for the shear stress at the tube wall due to flow, which renders the temperature difference less effective for nucleate boiling:

$$S = \frac{1}{1 + 2,53 \times 10^{-6} Re_{tp}^{1,17}}$$

where $Re_{tp}$ is the two phase Reynolds number, calculated from the liquid phase Reynolds number (equation **(28)**):

$$Re_{tp} = Re_L . F^{1,25}$$

At a certain stage in the evaporative process in a vertical tube, fully developed film boiling may take place. Under these conditions, the convective heat transfer mechanism becomes dominant and nucleate boiling no longer occurs, with heat being rapidly transferred across the thin film of liquid against the tube wall and vapourisation occurring at the surface of the liquid film only. Klimenko (1988) provided a scheme for evaluation of the heat transfer coefficient within the tube under these conditions. The first step is to evaluate the Klimenko parameter $\Phi$ to determine whether fully developed film boiling is occurring:

$$\Phi = \frac{4(L+V)\lambda}{\pi D_2^2 q_{conv}} \left[1 + x_v \left(\frac{\rho_L}{\rho_v} - 1\right)\right] \left(\frac{\rho_v}{\rho_L}\right)^{1/3}$$

Fully developed film boiling can be considered to be the dominating heat transfer mechanism if $\Phi > 1{,}6 \times 10^4$, in which case the heat transfer coefficient within the tube can be calculated as a combination of the single phase convective heat transfer coefficient, $\alpha_L$, and the film boiling heat transfer coefficient, $\alpha_F$:

$$\alpha = \left(\alpha_L^3 + \alpha_F^3\right)^{1/3}$$

The film heat transfer coefficient results from

$$Nu = 0{,}087\, Re_k^{0,6}\, Pr_L^{1/6} \left(\frac{\rho_v}{\rho_L}\right)^{0,2} \left(\frac{k_{Lw}}{k_L}\right)^{0,09}$$

where Nu is the Nusselt number, given by

$$Nu = \frac{\alpha_F L_c}{k_L}$$

$L_c$ is a physical property parameter:

$$L_c = \sqrt{\frac{\sigma}{g(\rho_L - \rho_v)}}$$

$Re_k$ is a modified Reynolds number, given by

$$Re_k = \frac{4(L + V)L_c}{\pi D_2^2 \mu_L} \left[1 + x_v \left(\frac{\rho_L}{\rho_v} - 1\right)\right]$$

and $k_{Lw}$ is the thermal conductivity of the liquid phase at the inner tube wall temperature, $T_{w2}$.

Should the evaporative process continue until most of the liquid phase in the tube has been vapourised, dry-out will occur. At this point, there will be insufficient liquid phase in the tube to properly wet the tube surface. The rate of heat transfer will fall dramatically, as the primary heat transfer mechanism in this regime will be single phase convective heat transfer to the vapour phase.

Dry-out can consider to have occurred if the dimensionless volumetric vapour flux, $j^*$, rises above a value of 2,5 (Bourgois and Le Maguer, 1987, after Wallis, 1969):

$$j^* = \frac{4(L + V)x_v}{\pi^2 D_2^4 (\rho_L - \rho_v)\sqrt{\rho_L g D_2}}$$

The heat transfer coefficient for post-dry-out heat transfer can be calculated using a Dittus-Boelter type expression for turbulent single phase heat transfer:

$$\alpha = 0{,}023\,Re^{0,8}\,Pr^{0.4} \quad \text{... (32)}$$

where the physical properties used to calculate the Reynolds and Prandtl numbers in equation **(32)** are those obtained by taking mass fraction-weighted average values for the liquid and vapour phases in the tube.

### 3.3.2 Viscous pressure drop within the tube

For conditions of single phase flow within the tube (before the development of saturated nucleate boiling), the viscous frictional pressure drop term in the momentum balance, equation **(20)**, can be evaluated using the Churchill correlation for single phase pressure drop (Churchill, 1977):

$$\left(\frac{dp}{dz}\right)_{fr\,lo} = \frac{32\,f_L\,L^2}{\rho_L\,\pi^2\,D_2^5} \quad \text{... (33)}$$

where $f_L$ is the Fanning friction factor for the liquid phase, calculated from:

$$f_L = 2.\left[\left(\frac{8}{Re_L}\right)^{12} + (A + B)^{-1.5}\right]^{1/12} \quad \text{... (34)}$$

where

$$A = \left(-2{,}457.\log\left[\left(\frac{7}{Re_L}\right)^{0.9} + 0{,}27\frac{\varepsilon}{D_2}\right]\right)^{16} \quad \text{... (35)}$$

(where $Re_L$ is the Reynolds number calculated assuming that the entire flow in the tube is in the liquid phase and using physical properties for the liquid phase, and $\varepsilon$ is the absolute roughness of the tube surface in metres), and

$$B = \left(\frac{37530}{Re_L}\right)^{16} \quad \text{... (36)}$$

In this single phase region of the tube, $(dp/dz)_{friction} = (dp/dz)_{fr\,lo}$. For those regions of the tube in which two phase flow exists, the pressure drop is described by:

$$\left(\frac{dp}{dz}\right)_{friction} = \Phi^2_{lo}\left(\frac{dp}{dz}\right)_{fr\,lo}$$

where $\phi^2_{lo}$ is the two phase pressure drop enhancement factor and $(dp/dz)_{fr\,lo}$ is the pressure drop due to friction for single phase liquid flow in the tube as calculated using equation **(33)** (Lockhart and Martinelli, 1949, as described in Smith, 1986). The two phase pressure drop enhancement factor can be calculated using the method of Friedel (1979):

$$\Phi^2 = E + \frac{3{,}24\,F.H}{Fr_{tp}^{0.045}\,We_{tp}^{0.035}}$$

where

$$E = (1 - x_v)^2 + x_v^2\frac{\rho_L f_v}{\rho_v f_L}$$

(where $f_v$ is the Fanning friction factor for the vapour phase, calculated from equations **(34)**, **(35)** and **(36)**, using a vapour phase Reynolds number calculated assuming that the entire flow in the tube is in the vapour phase and using physical properties for the vapour phase,)

$$F = x_v^{0,78}(1 - x_v)^{0,24}$$

$$H = \left(\frac{\rho_L}{\rho_v}\right)^{0.91}\left(\frac{\mu_v}{\mu_L}\right)^{0.19}\left(1 - \frac{\mu_v}{\mu_L}\right)^{0,7}$$

$$Fr_{tp} = \frac{16(L + V)^2}{\pi^2 g D_2^6 \rho_{tp}^2}$$

and

$$We_{tp} = \frac{16(L + V)^2}{\pi^2 D_2^3 \sigma \rho_{tp}}$$

where $\rho_{tp}$ is the two phase density, calculated assuming homogenous flow within the tube:

$$\rho_{tp} = \frac{1}{\left(\frac{x_v}{\rho_v} + \frac{(1 - x_v)}{\rho_L}\right)} \quad \text{... (37)}$$

For post-dry-out conditions within the evaporator tube, the single phase vapour pressure drop is calculated using equations **(33)** through **(36)**, but assuming the entire flow through the tube to be in the vapour phase and using physical properties for the vapour phase.

### 3.3.3 Two phase density of the boiling fluid

In the momentum balance within the tube, equation **(20)**, the two phase density of the boiling fluid, $\rho_m$, is given by

$$\rho_m = \rho_L (1 - \varepsilon_v) + \rho_v \varepsilon_v \quad \text{... (38)}$$

where $\varepsilon_v$ is the volumetric void fraction of vapour within the tube. This void fraction depends on the local ratio of the volumetric flow rate of vapour to that of the liquid, $V_r$:

$$V_r = \frac{x_v}{1 - x_v} \frac{\rho_L}{\rho_v} \quad \text{... (39)}$$

and the slip ratio, $u_r$:

$$u_r = \frac{u_v}{u_L} \quad \text{... (40)}$$

where $u_v$ is the mean velocity of the vapour phase and $u_L$ is the mean velocity of the liquid phase within the tube. The local volumetric void fraction is given by

$$\varepsilon_v = \frac{V_r}{V_r + u_r} \quad \text{... (41)}$$

If homogenous flow is assumed (*i.e.* no slip is assumed to occur between the vapour and liquid phases; both phases are assumed to travel at the same mean velocity through the tube), then $u_r = 1$, and the above equations simplify to equation **(37)**.

For upward vertical flow in a pipe, it is not appropriate to assume homogenous flow (Smith, 1986), and it is necessary to estimate the two phase density using equations **(38)** through **(41)**, estimating the slip ratio, $u_r$, using the correlation of Premoli *et al.* (1970), as recommended by Hewitt in Hetsroni (1982):

$$u_r = 1 + C_3 \sqrt{C_2}$$

where

$$C_3 = 1{,}578\,Re_L^{-0{,}19}\left(\frac{\rho_L}{\rho_v}\right)^{0{,}22}$$

(where $Re_L$ is the Reynolds number calculated assuming that all the flow in the tube is in the liquid phase and using physical properties for the liquid phase), and

$$C_2 = \frac{V_r}{1 + V_r C_1} - V_r C_1$$

where

$$C_1 = 0{,}0273\,We_L\,Re_L^{-0{,}51}\left(\frac{\rho_L}{\rho_v}\right)^{-0{,}08}$$

and $We_L$ is the Weber number calculated assuming all of the flow within the tube is in the liquid phase and using physical properties for the liquid phase:

$$We_L = \frac{16(L + V)^2}{\pi^2 D_2^3 \sigma \rho_L}$$

If the parameter $C_2 \leq 0$, then homogenous flow should be assumed to exist, and the slip velocity $u_r = 1$.

### 3.3.4 Physical properties

A literature survey on the physical properties of cane juices was carried out, in order to evaluate the most appropriate physical property correlations for use in the climbing film evaporator model (Peacock, 1995a; Peacock, 1995b).

*Boiling point elevation*

A series of attempts has been made over the years to correlate the boiling point elevation of sucrose solutions with sucrose concentration. All of these studies were, however, based on a severely limited number of data points provided by the individual authors. Moreover, only a few were based on sound thermodynamic principles, utilising the concept of the activity coefficient. None of these correlations was thus considered to be ideally suited for use in the climbing film evaporator model. Thus, in order to improve the reliability of boiling point elevation prediction, Starzak and Peacock (1997) collected boiling point temperature, vapour pressure, equilibrium relative humidity and other closely related data for aqueous sucrose solutions from 56 studies published over more than a century. These data were processed to derive a thermodynamically rigorous and statistically sound equation for the water activity coefficient, which can be used to predict the boiling point elevation (in °C) of sucrose solutions over the full range of sucrose concentrations and at different system pressures:

$$BPE = \left[ \frac{1 - \frac{Q}{RB} x_s^2 \left(1 + a x_s + b x_s^2\right) \frac{T_0 + C}{T_0 + 273{,}15}}{1 + \frac{T_0 + C}{B} \ln\left(1 - x_s\right)} - 1 \right] \left(T_0 + C\right)$$

where Q = -17 638 J/mole, R = 8,3143 J/mole.K, B = 3797,06°C, C = 226,28°C, a = -1,0038, b = -0,24653, $T_0$ is the boiling point temperature of water at the pressure of interest in °C and $x_s$ is the mole fraction sucrose in the solution under consideration, given by:

$$x_s = \frac{1}{19/s - 18}$$

where s is the mass fraction sucrose in the solution.

This boiling point elevation prediction correlation was compared with twenty other well known prediction methods available in the literature and shown to be the most accurate and reliable of all the methods tested, with a mean deviation of about 2% (Starzak and Peacock, 1998) .

*Density of condensate*

The density of condensate (in kg/dm$^3$) was calculated using the correlation of Aggarwal (1989) for the specific volume of saturated water:

$$\upsilon_c = A_1 + A_2 t_c^{1/3} + A_3 t_c^{5/6} + A_4 t_c^{7/8} + \sum_{n=5}^{9} A_n t_c^{n-4}$$

where $v_c$ is the specific volume of condensate, $t_c$ is the condensate temperature in degrees Kelvin and the coefficients $A_1$ through $A_9$ are given by

*For $t_c \leq 373.2$ K*

$A_1$ = 0.31060619e+01;
$A_2$ = -0.90267563e+01;
$A_3$ = 0.51853027e+02;
$A_4$ = -0.39588600e+02;
$A_5$ = 0.39760528e+01;
$A_6$ = -0.51528862e+02;
$A_7$ = 0.12148573e+03;
$A_8$ = -0.14039282e+03;
$A_9$ = 0.65221863e+02;

*For 373.2 K < $t_c \leq$ 600 K*

$A_1$ = 0.31060000e+01;
$A_2$ = -0.56161909e+01;
$A_3$ = 0.13398111e+02;
$A_4$ = 0.58633842e+01;

$A_5$ = -0.18599625e+02;

$A_6$ = 0.64106083e+01;

$A_7$ = -0.87578869e+01;

$A_8$ = 0.88766804e+01;

$A_9$ = -0.37156558e+01;

*For $t_c$ > 600 K*

$A_1$ = 0.31060000e+01;

$A_2$ = -0.54649353e+01;

$A_3$ = -0.72486047e+03;

$A_4$ = 0.12055044e+04;

$A_5$ = -0.57213086e+03;

$A_6$ = 0.72626416e+03;

$A_7$ = -0.65027012e+04;

$A_8$ = 0.41431125e+05;

$A_9$ = -0.11816734e+06;

*Density of sugar cane juice*

The density of sugar cane juice (in kg/m$^3$) was calculated using the correlation of Kadlec *et. al.* (1983):

$$\rho_L = a + bT_L + cT_L^2 + dT_L^3$$

where the coefficients a, b, c and d are given by:

$$a = a_0 + a_1 Bx + a_2 Bx^2 + a_3 Bx^3$$

$$b = b_0 + b_1 Bx + b_2 Bx^2 + b_3 Bx^3$$

$$c = c_0 + c_1 Bx + c_2 Bx^2 + c_3 Bx^3$$

$$d = d_0 + d_1 Bx + d_2 Bx^2 + d_3 Bx^3$$

where Bx is the dry solids content (sucrose and impurities) of the sugar cane juice on a mass percent basis, and the coefficients are given in Table 1.

**Table 1.** Coefficients for the Kadlec *et. al.* density correlation.

| Concentration range | i = | 1 | 2 | 3 | 4 |
|---|---|---|---|---|---|
| Bx ≤ 69 % | a | 1000,45 | 3,94325 | 0,0146409 | $2,69936 \times 10^{-5}$ |
| | b | $-6,01137 \times 10^{-3}$ | $-6,85707 \times 10^{-3}$ | $-2,63869 \times 10^{-6}$ | $-1,54649 \times 10^{-8}$ |
| | c | $-5,44367 \times 10^{-3}$ | $7,64646 \times 10^{-5}$ | $-6,50649 \times 10^{-7}$ | $8,44748 \times 10^{-9}$ |
| | d | $1,31672 \times 10^{-5}$ | $-3,55879 \times 10^{-7}$ | $6,36639 \times 10^{-9}$ | $-7,25049 \times 10^{-11}$ |
| Bx > 69 % | a | 1316,33 | -6,61119 | 0,130327 | $-3,91182 \times 10^{-4}$ |
| | b | -1,7077 | 0,0299153 | $-1,46234 \times 10^{-4}$ | $-4,69390 \times 10^{-7}$ |
| | c | $6,51225 \times 10^{-3}$ | $-1,65477 \times 10^{-4}$ | $2,15744 \times 10^{-7}$ | $8,36737 \times 10^{-9}$ |
| | d | 0 | 0 | 0 | 0 |

*Density of vapour and steam*

The density of vapour was calculated using the ideal gas equation.

*Enthalpy of saturated liquid water*

The specific enthalpy of saturated liquid water (in kJ/kg) was calculated using the correlation of Aggarwal (1989):

$$h_w = A_1 + A_2 t_w^{1/3} + A_3 t_w^{5/6} + A_4 t_w^{7/8} + \sum_{n=5}^{9} A_n t_w^{n-4}$$

where $h_w$ is the specific enthalpy, $t_w$ is the temperature in degrees Kelvin and the coefficients $A_1$ through $A_9$ are given by

*For $t_w \leq 287,2$ K*

$A_1 = 0.23649149e-02;$

$A_2 = 0.10918589e+04;$

$A_3 = -0.92032929e+04;$

$A_4 = 0.22190031e+05;$

$A_5 = -0.78623057e+04;$

$A_6 = -0.32543672e+05;$

$A_7 = 0.40901742e+05;$

$A_8 = -0.36393298e+03;$

$A_9 = -0.19495543e+05;$

*For $t_w > 287,2$ K*

$A_1 = 0.20860000e+04;$

$A_2 = -0.10864822e+04;$

$A_3 = 0.30911332e+05;$

$A_4 = -0.44055891e+05;$

$A_5 = 0.11541795e+05;$

$A_6 = 0.48651314e+02;$

$A_7 = -0.18603667e+04;$

$A_8 = 0.24305122e+04;$

$A_9 = -0.13371470e+04;$

*Enthalpy of saturated water vapour*

The specific enthalpy of saturated water vapour (in kJ/kg) was calculated using the correlation of Aggarwal (1989):

$$h_v = A_1 + A_2 t_v^{1/3} + A_3 t_v^{5/6} + A_4 t_v^{7/8} + \sum_{n=5}^{9} A_n t_v^{n-4}$$

where $h_v$ is the specific enthalpy, $t_v$ is the temperature in degrees Kelvin and the coefficients $A_1$ through $A_9$ are given by

*For $t_w \leq 591,2$ K*

$A_1 = 0.20860000e+04;$

$A_2 = 0.13530557e+04;$

$A_3 = -0.33616219e+05;$

$A_4 = 0.53989891e+05;$

$A_5 = -0.22623269e+05;$

$A_6 = 0.14442905e+04;$

$A_7 = -0.34480552e+04;$

$A_8 = 0.47304248e+04;$

$A_9 = -0.17240913e+04;$

*For $t_w < 591,2$ K*

$A_1 = 0.20860000e+04;$

$A_2 = 0.86537622e+03;$

$A_3 = 0.46032137e+06;$

$A_4 = -0.72641812e+06;$

$A_5 = 0.31508275e+06;$

$A_6 = -0.39173969e+06;$

$A_7 = 0.37372265e+07;$

$A_8 = -0.25566604e+08;$

$A_9 = 0.77743632e+08;$

*Enthalpy of sugar cane juice*

The specific enthalpy of sugar cane juice (in kJ/kg) was calculated using the correlation by Lyle (1950):

$$h_L = 2{,}326\left\{\left(\frac{Bx}{10}\right)\left(\frac{100 + Bx}{900 - 8\,Bx}\right) + 1{,}8\,T_L\left[1 - \left(\frac{Bx}{100}\right)(0{,}6 - 0{,}0009\,T_L)\right]\right\}$$

where Bx is the dry solids content (sucrose and impurities) of the sugar cane juice on a mass percent basis and $T_L$ is the juice temperature in °C.

*Saturation pressure of water*

The absolute vapour pressure of saturated boiling water (in bar) at a given boiling point temperature, $T_s$ in degrees Kelvin, was calculated using the Wagner equation (Wagner, 1973):

$$P_s = A_6 \exp\left[\frac{A_1 \Psi + A_2 \Psi^{1,5} + A_3 \Psi^3 + A_4 \Psi^6}{1 - \Psi}\right]$$

where

$$\Psi = 1 - \frac{T_s}{A_5}$$

and the coefficients are given by

*For 273,2 ≤ $T_s$ ≤ 323,2 K*

$A_1$ = -8,10988775;

$A_2$ = 2,17464254;

$A_3$ = -3,51897089;

$A_4$ = -0,50283681;

$A_5$ = 647,126;

$A_6$ = 220,55;

*For 323,2 < $T_s$ ≤ 423,2 K*

$A_1$ = -7,81340301;

$A_2$ = 1,55097861;

$A_3$ = -2,84616200;

$A_4$ = -1,26127042;

$A_5$ = 647,126;

$A_6$ = 220,55;

*For 423,2 < $T_s$ ≤ 523,2 K*

$A_1$ = -7,74037537;

$A_2$ = 1,38109682;

$A_3$ = -2,60773347;

$A_4$ = -1,57952429;

$A_5$ = 647,126;

$A_6$ = 220,55;

*For $T_s$ > 523,2 K*

$A_1$ = -7,82843137;

$A_2$ = 1,69248424;

$A_3$ = -4,27203456;

$A_4$ = 49,12068163;

$A_5$ = 647,126;

$A_6$ = 220,55;

*Saturation temperature of water*

The boiling point temperature of pure water (in degrees Kelvin) at a given absolute pressure was calculated using the correlation of Aggarwal (1989):

$$T_s = A_1 + \frac{A_2}{\log P_s + A_3}$$

where $P_s$ is the absolute pressure in Mpa and the coefficients are given as:

*For $P_s$ ≤ 0,085 MPa*

$A_1$ = 0.39612064e+02;

$A_2$ = -0.39839608e+04;

$A_3$ = -0.96562826e+01;

*For 0,085 < $P_s$ ≤ 2,625 MPa*

$A_1$ = 0.45864958e+02;

$A_2$ = -0.38175562e+04;

$A_3$ = -0.93753290e+01;

*For 2,625 < $P_s$ ≤ 11,25 MPa*

$A_1$ = -0.43211877e+01;

$A_2$ = -0.46978731e+04;

$A_3$ = -0.10285592e+02;

*For $P_s$ > 11,25 MPa*

$A_1$ = -0.31177350e+03;

$A_2$ = -0.10757354e+05;

$A_3$ = -0.14310894e+02;

*Specific heat capacity of condensate*

The specific heat capacity of pure water (in kJ/kg.°C) was calculated using an empirical correlation:

$$C_{pw} = 4{,}204 - 1{,}0514 \times 10^{-3} T_c + 1{,}171 \times 10^{-5} T_c^2$$

where $T_c$ is the temperature of the condensate in °C.

*Specific heat capacity of sugar cane juice*

The specific heat capacity of sugar cane juice (in kJ/kg.°C) was calculated using the correlation developed by Watson (1989):

$$C_{pL} = 4{,}1253 - 0{,}024804\,Bx + 6{,}7 \times 10^{-5}\,Bx.T_L + 1{,}8691 \times 10^{-3} T_L - 9{,}271 \times 10^{-6} T_L^2$$

where $T_L$ is the juice temperature and Bx is the dry solids content (sucrose and impurities) of the sugar cane juice on a mass percent basis.

*Specific heat capacity of water vapour*

The specific heat capacity of water vapour (in kJ/kg.°C) was calculated using an empirical correlation:

$$C_{pv} = 0{,}2323418\left(8{,}10 - 0{,}72\times 10^{-3}\, t_v + 3{,}63\times 10^{-6}\, t_v^2 - 1{,}16\times 10^{-9}\, t_v^3\right)$$

where $t_v$ is the vapour temperature in degrees Kelvin.

*Surface tension*

The surface tension at the liquid / vapour interface in sugar cane juice (in N/m) was calculated using the correlation of Watson (1989):

$$\sigma = 0{,}07575 - 1{,}4518\times 10^{-4}\, T_L - 2{,}3922\times 10^{-7}\, T_L^2 + 1{,}10\times 10^{-4}\, Bx$$

where $T_L$ is the temperature of the juice in °C and Bx is the dry solids content (sucrose and impurities) of the sugar cane juice on a mass percent basis.

*Thermal conductivity of condensate*

The thermal conductivity of pure water (in W/m.°C) was calculated using an empirical correlation:

$$k_w = 0{,}574 + 1{,}699\times 10^{-3}\, T_c - 6{,}308\times 10^{-6}\, T_c^2$$

where $T_c$ is the temperature of the condensate in °C.

*Thermal conductivity of sugar cane juice*

The thermal conductivity of sugar cane juice (in W/m.°C) was calculated using the correlation of Riedel (1949):

$$k_L = 1{,}162222\times 10^{-3}\left(486 + 1{,}55\,T_L - 0{,}005\,T_L^2\right)\left(1 - 0{,}0054\,Bx\right)$$

where $T_L$ is the temperature of the juice in °C and Bx is the dry solids content (sucrose and impurities) of the sugar cane juice on a mass percent basis.

*Thermal conductivity of water vapour*

The thermal conductivity of water vapour (in W/m.°C) was calculated using an empirical correlation:

$$k_v = 4{,}1868 \times 10^{-4} \left(17{,}53 - 2{,}42 \times 10^{-2}\, t_v + 4{,}3 \times 10^{-4}\, t_v^2 - 21{,}73 \times 10^{-8}\, t_v^3\right)$$

where $t_v$ is the vapour temperature in degrees Kelvin.

*Viscosity of condensate*

The viscosity of pure water (in kg/m.s) was calculated using an empirical correlation:

$$\mu_w = 2{,}73 \times 10^{-3} + 2{,}88 \times 10^{-6}\, T_c - 5{,}95 \times 10^{-4} \log T_c$$

where $T_c$ is the temperature of the condensate in °C.

*Viscosity of sugar cane juice*

The viscosity of sugar cane juice (in cP, where 1 cP = 1000 kg/m.s) was calculated using the correlation of Genotelle (1978):

$$\log \mu_L = 22{,}46\, N - 0{,}114 + \left(30 - T_L\right)\left(\frac{1{,}1 + 43{,}1\, N^{1{,}25}}{91 + T_L}\right)$$

where $T_L$ is the juice temperature in °C and

$$N = \frac{Bx}{1900 - 18\, Bx}$$

where Bx is the dry solids content (sucrose and impurities) of the sugar cane juice on a mass percent basis.

*Viscosity of water vapour*

The viscosity of water vapour (in kg/m.s) was calculated using an empirical correlation:

$$\mu_v = -3{,}189 \times 10^{-6} + 41{,}45 \times 10^{-9}\, t_v - 8{,}272 \times 10^{-13}\, t_v^2$$

where $t_v$ is the vapour temperature in degrees Kelvin.

## 3.4 NUMERICAL SOLUTION OF THE MODEL

Numerical solution of ordinary differential equations is fairly routine, provided that all the required boundary conditions are known at one of the boundaries of integration. This is known as an initial value problem. However, the system under consideration in this study has boundary conditions at both boundaries of integration, namely the top and the bottom of the evaporator tubes, and thus requires more advanced solution techniques.

The following boundary values are known under a given set of evaporator operating conditions and can be assigned numerical values:

- the mass flow rate of cold juice through the preheater, $F_0$
- the mass fraction sucrose content of the clear juice fed to the preheater, $s_p$
- the mass fraction impurity content of the clear juice fed to the preheater, $r_p$
- the temperature of the heated juice leaving the preheater, $T_{L0}$
- the vapour space pressure at the top of the evaporator tubes, $p_{top}$
- the mass flow rate of condensate per unit tube perimeter at the top of the evaporator tubes, $\Gamma_0$

The mass flow rate of condensate per unit perimeter length at the top of the tubes, $\Gamma_0$, is taken to be zero, as there is assumed to be no condensate film present at the very top of the tubes.

While the starting point of integration is the bottom of the evaporator tube, two of these

boundary conditions, namely the system vapour pressure and the mass flow rate of condensate per unit length of tube perimeter, are only known at the top of the tube. This is known as a two-point boundary value problem. There are several available numerical methods for solving boundary value problems of this type (Davis, 1984; Na, 1979). For this study, a shooting method based on the Newton-Raphson technique was used.

The two-point boundary value problem is solved by successive approximation of the unknown boundary value conditions at the bottom of the evaporator tube. At each step in the iteration procedure, an initial value problem is solved, using the most recent approximation of the unknown boundary conditions. The solution procedure is as follows:

- An estimate is made of the unknown system pressure and condensate flow rate per unit perimeter length at the bottom of the evaporator tube.
- The system of ordinary differential equations comprising the evaporator model is numerically integrated up the length of the tube, as if the problem were an initial value problem.
- The resulting values of the system pressure and condensate flow rate per unit perimeter length at the tube of the tube are compared to the known values of these quantities (i.e. zero in the latter case). If the values are found to differ, a more refined guess, utilising the Newton-Raphson technique, is made of these quantities at the bottom of the evaporator tube and the sequence is repeated.

A fourth order Runge-Kutta method with an automatically controlled step size was used to perform the numerical integration.

An additional degree of complexity is introduced into the model by the presence of the preheater in the system to be modelled. While it is known that the cane juice entering the preheater is entirely in the liquid phase, with a known composition, it is possible for the temperature of the juice exiting the preheater (under pressure) to be at a temperature above the boiling point of the juice at the pressure prevailing at the bottom of the evaporator tubes. Under these circumstances, the feed juice entering the tubes will flash, and the juice

entering the tubes will need to be considered as a juice / vapour mixture. In order to fully account for this phenomenon, it is necessary for the model to perform a flash calculation on the incoming juice to determine the quantity of vapour present in the feed stream, and hence the liquid phase composition, based on the temperature of the hot juice exiting the preheater and the most recent estimate of the prevailing pressure at the bottom of the tubes. The flash calculation is, in essence, an enthalpy balance. If the temperature of the juice exiting the preheater is below the boiling point of the juice at the prevailing pressure at the bottom of the tube, flashing does not occur and no flash calculation is performed. If flashing does occur, then the following enthalpy balance equation is solved for the mass fraction vapour in the juice entering the bottom of the evaporator tube, $x_v$:

$$h_{L1} = (1 - x_v) h_{L2} + x_v h_{v2}$$

where $h_{L1}$ is the specific enthalpy of the hot juice exiting the preheater, assumed to be entirely in the liquid phase, $h_{L2}$ is the specific enthalpy of the liquid phase at the boiling point prevailing at the bottom of the evaporator tube and $h_{v2}$ is the corresponding specific enthalpy of the vapour phase.

# *Part II :*

# *Results and Discussion*

# Chapter 4

# Model Identification

## 4.1 EVAPORATOR SIMULATION PROGRAM

The climbing film evaporator model, as described in Chapter 3, was used to develop an evaporator simulation program in the MATLAB programming language. It should be noted that the program makes provision for the optional inclusion of a fouling layer on the inner wall of the tube as a further barrier to heat transfer. This feature is not discussed as part of this study as, in practice, it was never utilised.

The inputs required for simulation of a climbing film evaporator system using this program are:

- the physical parameters of the evaporator system to be modelled, such as
  - the number of tubes,
  - the inner and outer tube diameters,
  - the length of the evaporator tubes,
  - the surface roughness of the tube material and
  - the thermal conductivity of the tube material.

- and the operational parameters of the evaporator system, such as
  - the mass flow rate of cold sugar cane juice fed to the preheater,
  - the composition of the cold juice fed to the preheater (in terms of sucrose and impurities content),
  - the temperature of the hot juice exiting the preheater,
  - the vapour space pressure at the top of the evaporator tubes and
  - the pressure of the condensing steam within the shell of the vessel.

The outputs provided by the simulation program are profiles of the following quantities as they vary along the length of the tube:

- the two state variables involved in the numerical integration of the ordinary differential equations, namely the enthalpy flow of the boiling fluid within the tube (equation **(14)**) and the modified pressure term contained in equation **(20)**,
- the mass flow rate of condensate per unit length of the tube perimeter,
- the temperatures of the condensing steam, outer and inner tube walls and boiling juice,
- the composition of the boiling liquid phase,
- the local heat transfer coefficients for condensation on the outer wall of the tube and for boiling heat transfer within the tube,
- a local overall heat transfer coefficient for the evaporator system,
- the mass flow rates of the liquid and vapour phases within the tube,
- the absolute pressure within the tube,
- the two phase mixture quality (mass fraction vapour) and
- the heat flux through the tube wall.

The results of a typical simulation are shown in Figure 13. The input parameters for this simulation were partially based on industrial conditions in one of the first effect climbing film evaporators at the Felixton sugar mill, as given in Table 2. The average overall heat transfer coefficient for this evaporator system was calculated to be 1,09 $kW/m^2.°C$.

The graphical results in Figure 13 show the typical behaviour of a climbing film evaporator. Due to the small effect of the acceleration term in the momentum balance, the modified pressure plot shows, in effect, the decrease in absolute pressure with increasing height in the evaporator tube. The point at which boiling starts is clearly visible at a point approximately 1,8 metres up the tube, with the two phase mixture having a lower pressure drop per metre of tube length than the single phase liquid. The enthalpy flow shows a low

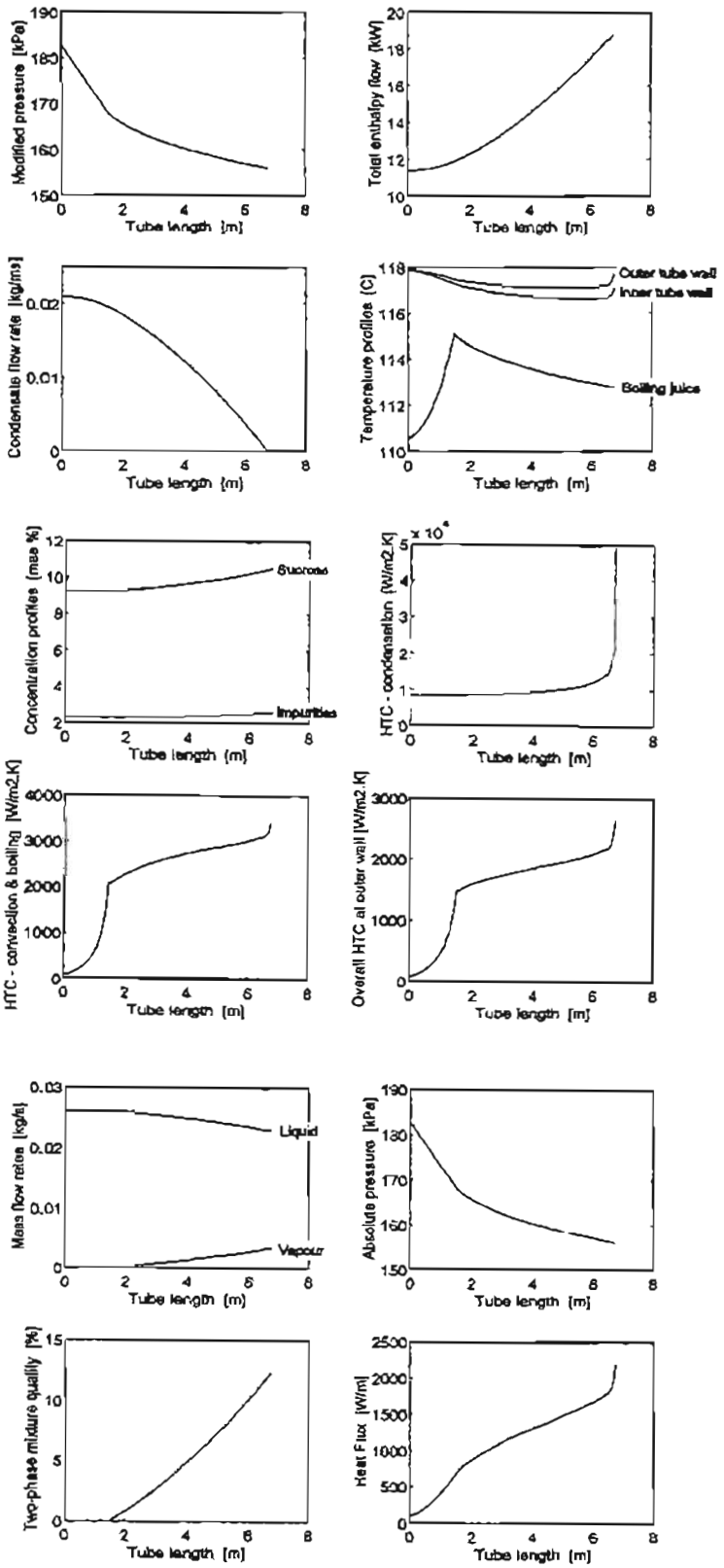


**Figure 13.** Typical simulation results.

rate of enthalpy increase (as a result of the low heat transfer coefficient) in the non-boiling single phase liquid section of the tube, with more effective heat transfer once boiling starts.

**Table 2.** Simulation program parameters.

| | |
|---|---|
| Number of tubes | 5 000 |
| Inner tube diameter | 48,36 mm |
| Outer tube diameter | 50,80 mm |
| Tube length | 6,73 m |
| Tube material surface roughness | 0,25 mm |
| Thermal conductivity of tube material | 25,9 W/m.°C |
| Mass flow rate of cold sugar cane juice | 470 t/h |
| Mass fraction sucrose in cold juice | 0,092 |
| Mass fraction impurities in cold juice | 0,023 |
| Temperature of hot juice | 110,52 °C |
| Vapour space pressure | 156,14 kPa(a) |
| Steam pressure | 186,2 kPa(a) |

The condensate flow rate per unit perimeter length decreases with increase in height up the tube, decreasing to the boundary condition value of zero at the top of the tube. The temperature profile for the boiling juice within the tube clearly shows the point at which boiling begins. From this point upwards, the boiling temperature of the juice falls as the pressure within the tube decreases with increasing height. The concentration profiles for sucrose and the impurities remain constant until boiling begins and then rise. The concentration change in this simulation was found to be small.

The heat transfer coefficient for condensation heat transfer shows the approach to a value of infinity at the top of the tube, where the thickness of the condensate reduces to zero. The other two heat transfer coefficient profiles in the figure show the less efficient heat

transfer taking place in the single phase zone, with enhanced heat transfer once boiling begins.

The liquid and vapour mass flow rates clearly show the production of vapour within the tube once boiling begins to occur. This is also reflected in the plot for the two phase mixture quality.

The last plot shows the heat flux transferred from the condensing steam to the boiling juice through the tube wall.

An overall average heat transfer coefficient for the modelled evaporator can be calculated from the results of the simulation, based on the heat transfer across the tube wall required to heat the juice to its boiling point and vapourise a portion of the liquid phase:

$$U = \frac{L_0 C_{pLm} \left(T_{L0} - T^v_{bp}\right) + V_e \lambda}{A \left(T_s - T_{ve}\right)}$$

where $L_0$ is the flow rate of liquid entering the bottom of the evaporator tube, $C_{pLm}$ is the average specific heat capacity of the liquid phase in the non-boiling zone of the evaporator tube, $T_{L0}$ is the temperature of the feed liquid entering the bottom of the evaporator tube, $T^v_{bp}$ is the boiling point of the liquid phase at the vapour pressure prevailing at the top of the evaporator tube, $V_e$ is the vapour phase flow rate exiting the top of the evaporator tube, $\lambda$ is the average latent heat of vapourisation within the tube, A is the surface area for heat transfer within the tube, $T_s$ is the temperature of the heating steam and $T_{ve}$ is the temperature of the vapour phase exiting the top of the evaporator tube.

This approximate overall average heat transfer coefficient was also used in analysis of the experimental climbing film evaporator data collected by the southern African sugar industry, as described in the next section.

## 4.2 EXPERIMENTAL DATA COLLECTION

From 1994 to 1997, the Sugar Milling Research Institute operated a pilot plant climbing film evaporator at the Felixton sugar mill. The pilot plant evaporator was designed to investigate the effects of both mechanical and operational parameters on climbing film evaporator performance through the measurement of an approximate overall average heat transfer coefficient (Walthew *et al.*, 1995; Walthew and Whitelaw, 1996). A schematic diagram of the pilot plant evaporator is shown in Figure 14.

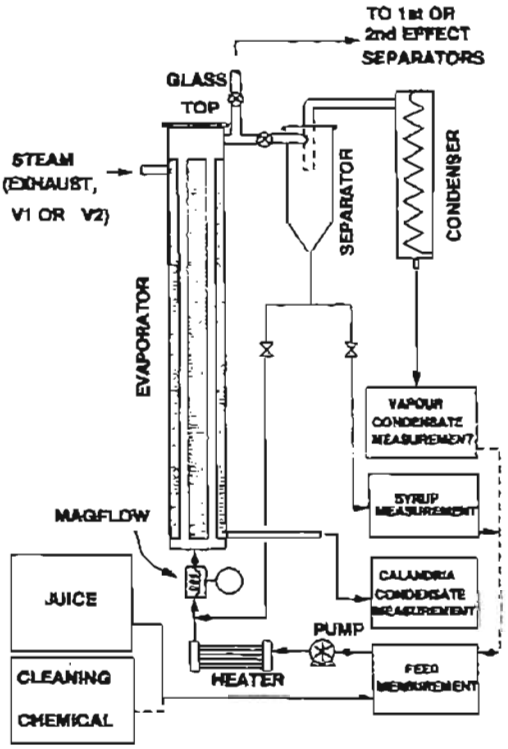


**Figure 14.** Schematic diagram of the pilot plant climbing film evaporator.

The pilot plant evaporator consists of three stainless steel tubes of two inch nominal diameter and of length 7,0 metres, within a mild steel shell. Feed juice from the factory is fed to a galvanised steel drum, suspended from a load cell to enable the mass flow rate of juice to be determined. From the feed drum, the juice is pumped by a variable speed

fixed displacement pump, through a preheater, to the bottom saucer of the evaporator. The concentrated juice / vapour mixture exiting the top of the evaporator tubes is separated in a cyclonic separator and the vapour stream is condensed. Both products of the evaporation process are cooled and then stored in further galvanised drums, suspended from load cells to allow for flow rate measurement.

The pilot plant is thoroughly instrumented, allowing for the measurement of the feed liquor, product syrup, steam condensate and vapour condensate flow rates, steam and vapour pressures, feed juice temperature and the pressure drop over the length of the tube. The juice concentrations before and after evaporation were determined by the mill laboratory at the Felixton mill, using refractive index measurements.

During the 1995 season, the Felixton pilot plant climbing film evaporator was used to investigate the effects of selected operating conditions on first effect evaporator performance, using a factorial experimental design (Walthew and Whitelaw, 1996). The dependent variable in this study was the average overall heat transfer coefficient, while the independent variables (or factors) which were selected for study were:

- the temperature difference driving force for evaporation,
- the feed juice flow rate,
- the feed juice temperature, and
- the feed juice concentration.

The independent variables and their low and high values in the factorial experiment were chosen based on the prevailing operating conditions of first effect climbing film evaporators in the South African sugar industry. The levels of the factors are shown in Table 3. All the experiments were carried out using clean tubes, and the test solutions for evaporation were synthetic solutions made up using high purity refined sugar and water. Thus, no fouling of the tube surfaces occurred during the experimental runs. The results of the factorial experiment are discussed by Walthew and Whitelaw (1996).

**Table 3.** The factorial experimental design.

| Variable type | Variable name | Units | Low level value | High level value |
|---|---|---|---|---|
| Dependent | Overall average heat transfer coefficient | $kW/m^2.°C$ | - | - |
| Independent | Temperature difference | °C | 4 | 7,5 |
| | Feed flow rate | kg/min | 2,5 | 4,5 |
| | Feed temperature | °C | 102 | 110 |
| | Feed concentration | % (m/m) | 8 | 13 |

The raw data from this factorial experiment were collected and used for validation of the climbing film evaporator model, following statistical data reconciliation.

## 4.3 STATISTICAL DATA RECONCILIATION

Initial attempts at model validation using the data collected during the first effect factorial experiment showed the presence of some inconsistencies in the experimental data. It was found that, in many cases, the mass and enthalpy balances around the pilot plant evaporator were not satisfied during the experimental runs. While the errors in the overall mass balance and the sucrose balance were found to be evenly distributed around zero, the error in the enthalpy balance was found to be consistently positive. That is, more steam was condensed in the calandria than was accounted for in the observed heat transfer. It was thus decided to statistically reconcile the experimental data so as to satisfy the mass and enthalpy balances (Peacock, 1995c).

Additionally, an estimate was made by the author of the convective heat transfer losses from the external surfaces of the pilot plant evaporator, so as to account for some of the excess calandria condensation observed during the factorial experiment. This heat loss

estimate was based on tests carried out on the pilot evaporator with no feed flow (i.e., with no evaporation taking place, with all the observed steam condensation being due to convective heat losses) and a confirmatory theoretical estimate based on published convective heat transfer coefficient correlations in the literature.

Statistical data reconciliation involves the manipulation of the experimentally measured variables so as to satisfy the mass and enthalpy balances for the system, while changing the experimental data as little as possible. For the purposes of this analysis, each experimental variable was assigned a variance, representing the range of experimental error expected for that variable. These variances were determined by statistically analysing the fluctuations in the individual variables during continuous steady state operation of the pilot plant evaporator. An optimisation index was then defined as:

$$\text{Index} = \sum_{j=1}^{n} \frac{\left(x_j - \chi_j\right)^2}{\text{var}_j}$$

where $x_j$ is the optimised / altered value of the $j^{th}$ variable, $\chi_j$ is the experimentally measured value of the $j^{th}$ variable and $\text{var}_j$ is the variance of the $j^{th}$ variable. The reconciliation algorithm satisfies the mass and enthalpy balances while minimising the optimisation index (i.e., minimising the effect on the experimental data). Thus, the experimental data are weighted by the inverses of their variances. The more accurately measured variables will be affected less during the reconciliation procedure than those measured less accurately (with higher variances). The variables subject to reconciliation were:

- the juice feed flow rate,
- the juice feed concentration,
- the steam pressure,
- the vapour space pressure,
- the juice feed temperature,
- the steam condensate flow rate,
- the vapour condensate flow rate,

- the concentrated juice product flow rate, and
- the concentrated juice product concentration.

The data reconciliation algorithm was implemented by means of a MATLAB computer program. Seven of the original 27 experiments were discarded due to gross errors in the data from these tests. The results of data reconciliation of the remaining 20 tests are discussed by Peacock (1995c), which is included as Appendix A. The modified data from the statistical reconciliation procedure were used for model validation.

## 4.4 MODEL IDENTIFICATION

Preliminary model verification, by comparing the results of model simulation with the results of experimentation using the pilot plant climbing film evaporator, showed that the model results did not agree with those obtained by experiment. In general, it was found that the simulation program consistently under-predicted the actual heat transfer occurring in the pilot plant evaporator. That is, the simulation program predicted lower heat transfer coefficients, steam condensate flow rates, concentrated juice product concentrations, vapour condensate flow rates, heat fluxes and two phase mixture qualities than had been observed for the experimental data.

Analysis of the heat transfer components of the climbing film evaporator model showed that the most probable cause of the erroneous model results was the boiling heat transfer portion of the Chen correlation for flow boiling in vertical tubes. While the convective heat transfer term in this correlation (the Engineering Sciences Data Unit correlation for single phase convective heat transfer, as given by equations **(24)** through **(26)**) was considered to be accurate, it was felt that the modified Forster-Zuber pool boiling equation (Forster and Zuber, 1955) was inaccurate:

$$\alpha_{nb} = 0{,}00122 \frac{k_L^{0,79} C_{pL}^{0,45} \rho_L^{0,49} (T_{w2} - T_L)^{0,24} \Delta p^{0,75}}{\sigma^{0,5} \mu_L^{0,29} \lambda^{0,24} \rho_v^{0,24}} \quad \text{... (42)}$$

An attempt was made to replace this outdated, inaccurate correlation with a more modern equation of greater accuracy. A literature survey was carried out on the topic of flow boiling in vertical tubes. However, it was found that none of the available correlations (Cooper, 1989; Dhir, 1991; Gorenflo, 1994; Gungor and Winterton, 1986; Kenning and Cooper, 1989; Shah, 1982; Steiner and Taborek, 1992; Webb and Gupte, 1992) could be applied to the conditions normally encountered in climbing film evaporators in the South African sugar industry, due to the extremely low juice flow rates commonly used. Some of the more promising correlations were tested for possible incorporation into the evaporator model, but were found to be unsuitable. It was thus found to be impossible to replace the Forster-Zuber equation with a more accurate alternative correlation.

The Forster-Zuber equation as modified for use in the Chen correlation, equation **(42)**, contains the constant parameter $k_{FZ}$.

$$\alpha_{nb} = k_{FZ} \frac{k_L^{0,79} C_{pL}^{0,45} \rho_L^{0,49} (T_{w2} - T_L)^{0,24} \Delta p^{0,75}}{\sigma^{0,5} \mu_L^{0,29} \lambda^{0,24} \rho_v^{0,24}}$$

The original value of $k_{FZ}$ reported by Forster and Zuber (1955) was 0,0015, later reduced by Chen (1966) to a value of 0,00122. This value is accepted by many authors as being applicable to a wide range of fluids and heating surfaces. By contrast, the value of a similar coefficient in the correlation of Rohsenow (1952) varies greatly, depending on the nature of the fluid being boiled and the surface on which this boiling takes place, as shown in Table 4 (Mills, 1992). According to this correlation:

$$Nu = \frac{Ja^2}{C_{nb}^3 Pr_L^m}$$

**Table 4.** Values of the nucleate boiling constant and exponent for the Rohsenow correlation.

| Liquid | Surface | $C_{nb}$ | m |
|---|---|---|---|
| Water | Copper, scored | 0,0068 | 2,0 |
| Water | Copper, polished | 0,013 | 2,0 |
| Water | Stainless steel, chemically etched | 0,013 | 2,0 |
| Water | Stainless steel, mechanically polished | 0,013 | 2,0 |
| Water | Stainless steel, ground and polished | 0,008 | 2,0 |
| Water | Brass | 0,006 | 2,0 |
| Water | Nickel | 0,006 | 2,0 |
| Water | Platinum | 0,013 | 2,0 |
| Carbon tetrachloride | Copper | 0,013 | 4,1 |
| Benzene | Chromium | 0,010 | 4,1 |
| n-Pentane | Chromium | 0,015 | 4,1 |
| Ethanol | Chromium | 0,0027 | 4,1 |
| Isopropyl alcohol | Copper | 0,0023 | 4,1 |
| n-Butyl alcohol | Copper | 0,0030 | 4,1 |
| 35% $K_2CO_3$ | Copper | 0,0027 | 4,1 |

where Ja is the Jakob number

$$Ja = \frac{C_{pL}\left(T_{w2} - T_{bp}\right)}{\lambda}$$

(where $C_{pL}$ is the specific heat capacity of the liquid being boiled, $T_{w2}$ is the inner tube wall temperature, $T_{bp}$ is the temperature of the boiling liquid and $\lambda$ is the latent heat of vapourisation of the liquid), $C_{nb}$ is the nucleate boiling coefficient (similar to $k_{FZ}$), $Pr_L$ is the Prandtl number for the liquid (as defined in equation **(29)**), m is the nucleate boiling exponent (as given in Table 4). The Nusselt number, Nu, is given by

$$Nu = \frac{\alpha L_c}{k_L}$$

where $\alpha$ is the boiling heat transfer coefficient, $k_L$ is the thermal conductivity of the liquid being boiled and $L_c$ is a characteristic length, given as

$$L_c = \sqrt{\frac{\sigma}{(\rho_L - \rho_v)g}}$$

where $\sigma$ is the surface tension of the boiling liquid, $\rho_L$ is the liquid phase density, $\rho_v$ is the vapour phase density and g is the acceleration due to gravity.

Consequently, it may be inferred from the variation in the parameters in Table 4 that the nature of the boiling fluid and the surface characteristics may greatly influence $k_{FZ}$. It was thus decided to utilise the Forster-Zuber coefficient, $k_{FZ}$, being the most uncertain parameter in the evaporator model, as the parameter to be optimised in order to improve the accuracy of the model predictions. It was felt that this approach was justified, for the following reasons:

- There is a large degree of variability present in the data published in the literature on the topic of nucleate boiling (Winterton, personal communication, 1995). Heat transfer coefficient predictions for the nucleate boiling regime, using published correlations, may vary by up to 1900% (Hewitt *et al.*, 1994).
- Most nucleate boiling correlations are inapplicable to the conditions normally encountered in climbing film evaporators in the South African sugar industry, due to the low juice flow rates normally employed (Müller-Steinhagen, personal communication, 1995; Steiner, personal communication, 1995; Stephan, personal communication, 1995; Winterton, personal communication, 1995).

A least-squares optimisation algorithm was used for the improvement of the model accuracy, by identification of a new value of $k_{FZ}$, minimising a specially defined performance index (or objective function) to give a better fit to the experimental data

under study. The performance index consisted of a weighted deviation of the model predictions from the corresponding experimental output values. As experimental values of the measured quantities are only available at the ends of the evaporator tubes, it was the end-of-tube model predictions which were used for comparison. As for the statistical data reconciliation, the weights used in optimisation of the performance index were the inverses of the variances of the individual variables of interest. The more accurately measured variables were more important during the optimisation procedure than those measured less accurately (with higher variances).

Ten experimental tests were selected for the optimisation procedure. The evaporator operating conditions used during these tests are shown in Table 5. The performance index was optimised separately for each of the tests, using the Marquardt-Levenberg optimisation routine (Marquardt, 1963; Levenberg, 1944), yielding a different value of $k_{FZ}$ for each test. Some of the results of the extensive computations are shown in Table 6.

**Table 5.** Operating conditions used during the optimisation.

| Run number | Feed juice flow rate [kg/s] | Feed juice concentration [%(m/m)] | Feed juice temperature [°C] | Vapour space pressure [kPa(a)] | Steam pressure [kPa(a)] |
|---|---|---|---|---|---|
| 1 | 0,0175 | 8,0 | 96,3 | 151,3 | 173,5 |
| 2 | 0,0183 | 13,0 | 105,7 | 151,3 | 196,3 |
| 3 | 0,0252 | 12,9 | 102,5 | 151,3 | 196,3 |
| 4 | 0,0142 | 8,0 | 100,7 | 151,4 | 173,5 |
| 5 | 0,0147 | 12,9 | 108,4 | 151,4 | 195,5 |
| 6 | 0,0233 | 13,0 | 108,7 | 151,3 | 196,3 |
| 7 | 0,0237 | 13,0 | 107,0 | 151,4 | 194,9 |
| 8 | 0,0236 | 8,0 | 109,3 | 151,3 | 173,3 |
| 9 | 0,0252 | 8,0 | 106,9 | 151,4 | 191,8 |
| 10 | 0,0148 | 8,0 | 102,0 | 151,3 | 183,8 |

**Table 6.** Final simulation results after optimisation of $k_{FZ}$.

| Run number | Steam condensate flow rate [kg/s] | | Product juice concentration [%(m/m)] | | Vapour product flow rate [kg/s] | | Product juice flow rate [kg/s] | | Forster-Zuber constant (× 1000) |
|---|---|---|---|---|---|---|---|---|---|
| | Exptl. | Calc. | Exptl. | Calc. | Exptl. | Calc. | Exptl | Calc. | |
| 1 | 0,0031 | 0,0030 | 9,5 | 9,5 | 0,0028 | 0,0025 | 0,0147 | 0,0150 | 8,94 |
| 2 | 0,0092 | 0,0097 | 32,1 | 31,6 | 0,0109 | 0,0094 | 0,0074 | 0,0077 | 5,63 |
| 3 | 0,0092 | 0,0095 | 22,1 | 21,6 | 0,0105 | 0,0090 | 0,0147 | 0,0157 | 4,43 |
| 4 | 0,0028 | 0,0026 | 9,9 | 9,7 | 0,0027 | 0,0023 | 0,0115 | 0,0119 | 8,92 |
| 5 | 0,0084 | 0,0090 | 40,0 | 39,7 | 0,0099 | 0,0089 | 0,0048 | 0,0049 | 3,15 |
| 6 | 0,0104 | 0,0108 | 27,7 | 27,0 | 0,0124 | 0,0107 | 0,0109 | 0,0120 | 4,20 |
| 7 | 0,0105 | 0,0109 | 27,3 | 26,7 | 0,0124 | 0,0107 | 0,0113 | 0,0123 | 4,12 |
| 8 | 0,0043 | 0,0041 | 10,2 | 9,9 | 0,0048 | 0,0039 | 0,0188 | 0,0199 | 6,75 |
| 9 | 0,0090 | 0,0090 | 13,7 | 13,3 | 0,0105 | 0,0087 | 0,0147 | 0,0163 | 5,10 |
| 10 | 0,0079 | 0,0078 | 20,9 | 19,9 | 0,0092 | 0,0074 | 0,0057 | 0,0070 | 5,75 |

It was found that the calculated optimal values of the Forster-Zuber constant were several times higher than Chen's original value of 0,00122, ranging from 0,003 to 0,009. Typically, it was observed that lower values of $k_{FZ}$ (between 0,003 and 0,005) occurred for experimental runs characterised by a large change in the juice concentration over the evaporator (of the order of 15%(m/m) to 30%(m/m)). Experimental runs yielding only a slight increase in juice concentration (of the order of 3%(m/m) to 5%(m/m)) resulted in higher values of $k_{FZ}$ (between 0,007 and 0,009). This behaviour was found to be strongly correlated with the average heat flux across the evaporator tube, as shown in Figure 15. However, the hypothesis of a relationship between $k_{FZ}$ and the average heat flux needs further confirmatory investigation.

A comparison between the model predictions and experimental data for run 2 is shown in

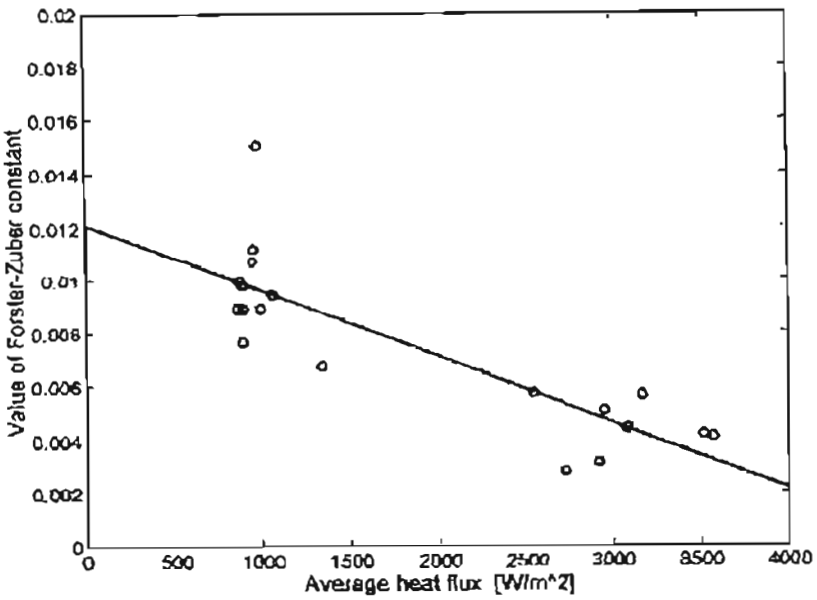


**Figure 15.** Variation of the calculated Forster-Zuber constant with the average heat flux.

Figure 16, with the model predictions shown as solid lines (profiles over the length of the tube) and the experimental results shown as circles. All of the key output variables (such as product juice concentration, product juice flow rate, vapour product flow rate, steam condensate flow rate and vapour space pressure) could be predicted to within ±5% relative error. Additionally, the distribution of the local overall heat transfer coefficient along the length of the tube (the solid line in the last graph of the figure) was found to be in good agreement with the average overall experimental heat transfer coefficient (dashed line) calculated for the pilot plant during this run (see Walthew and Whitelaw, 1996, for details of the technique used in the calculation of the experimental average overall heat transfer coefficient).

Figure 17 shows the difference in the profiles of the heat transfer parameters (such as temperature profiles, product juice concentration and overall heat transfer coefficient) as they vary along the length of the tube, depending on the operating conditions of the climbing film evaporator. The lines on the temperature profile plots refer (from top down) to the steam temperature (constant), the temperature of the outer wall of the tube, the temperature of the inner wall of the tube and the temperature of the fluid within the tube.

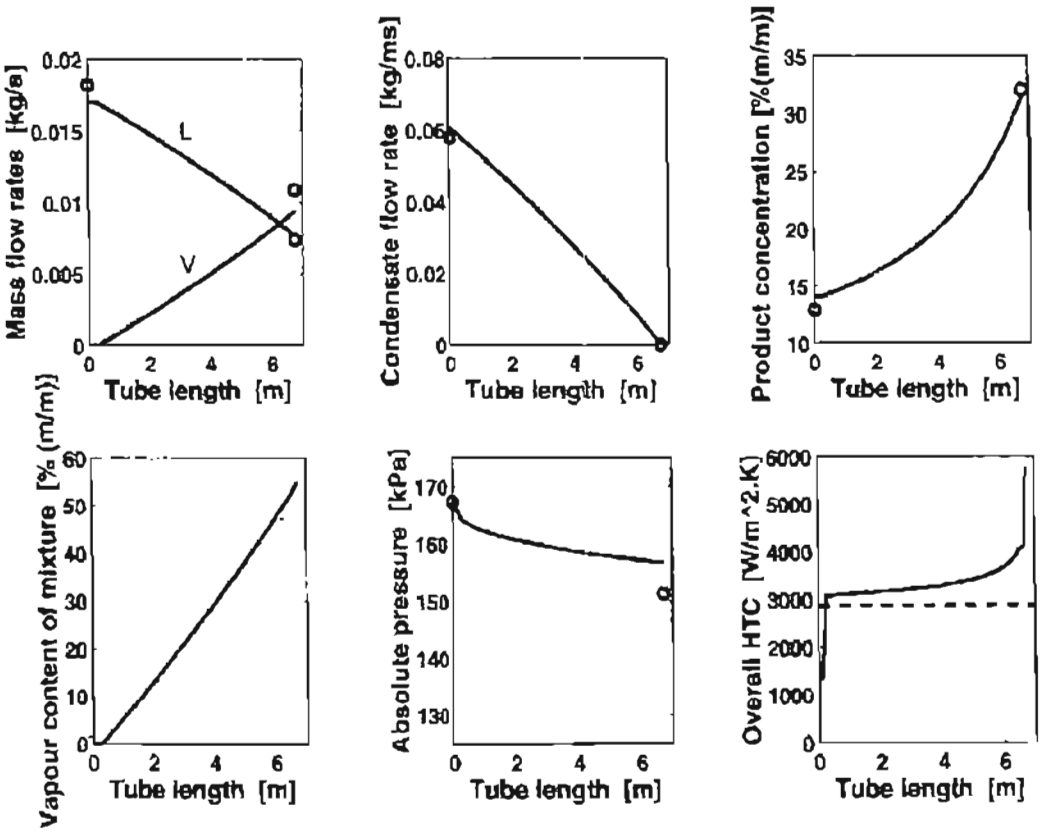


**Figure 16.** Simulation results for experimental run number 2.

Plots (a), (b) and (c) in the figure show the results for experimental run number 4, characterised by a low steam temperature. It can be seen that, over almost half of the length of the tube, the evaporator functions as a juice heater, with only single phase liquid convective heat transfer taking place. Low local overall heat transfer coefficient values occur in this region of the tube, mostly due to the laminar flow nature of the single phase flow as a result of the low juice flow rate. Obviously, these conditions result in a very poor final product concentration.

By contrast, the results for experimental run number 10 are shown in plots (d), (e) and (f) in Figure 17. This experimental run is characterised by a high steam temperature, resulting in a high overall heat transfer coefficient being observed over almost the entire length of the tube. Both heat transfer profiles shown in the figure exhibit two characteristic

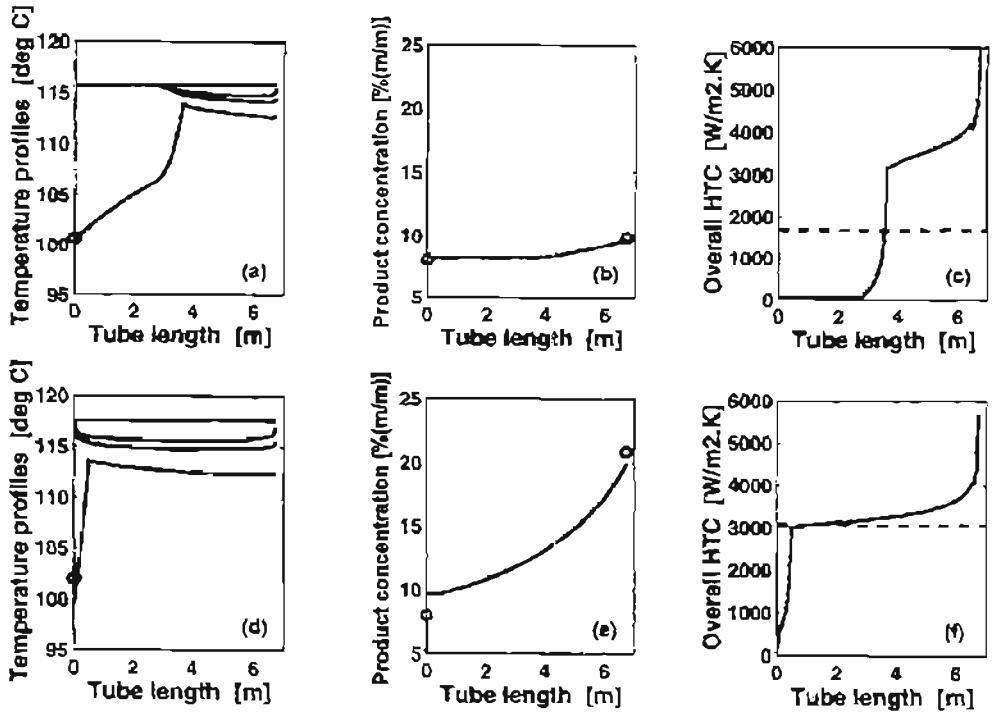


**Figure 17.** Comparison of the simulation results for experimental runs 4 and 10.

discontinuities of slope. The first occurs at the transition from single phase convective heat transfer to subcooled nucleate boiling, as at approximately 2,75 metres along the length of the tube in plot (c). The second occurs at the transition from subcooled nucleate boiling to fully developed saturated nucleate boiling, as at approximately 3,75 metres along the length of the tube in plot (c). The dramatic increase in the overall heat transfer coefficient which occurs at the very end of the evaporator tube can be explained by the extremely high condensation heat transfer coefficient which occurs at the end of the tube due to the absence of a condensate film at this point.

## 4.5 CONCLUSIONS

The climbing film evaporator model, as described in Chapter 3, was used to develop an evaporator simulation program in the MATLAB programming language. This simulation program can be used to simulate climbing film evaporator performance under various

operating conditions. Apart from changes in traditional operating parameters, such as steam pressure, feed juice flow rate and feed juice temperature, etc., the program can also be used to predict the effect on system performance of changes which are inconvenient to evaluate in practice, such as those of tube size and tube material.

A series of experiments was carried out on a pilot plant climbing film evaporator at the Felixton sugar mill to investigate the efficiency of heat transfer under varying operating conditions. The factorial experiment involving changes in feed juice flow rate, feed juice temperature, feed juice concentration and temperature difference driving force resulted in a set of experimental data which was used to evaluate the performance of the simulation program, and then to improve the performance of the model using process identification. The initial model was modified by varying the Forster-Zuber coefficient in the Chen correlation for boiling heat transfer. The identification of this constant led to a great improvement in the model performance, giving 5% relative error between the model predictions and the experimental measurements. A variation in the value of the Forster-Zuber coefficient was observed, which could be correlated with heat flux.

# Chapter 5
# Simplified Model

The original system of ordinary differential equations describing the steady-state operation of a climbing film evaporator was strongly coupled and nonlinear. Moreover, the nonlinearity was strengthened by the fact that the mechanism of heat transfer within the tube changed dramatically when moving through the various zones within the tube, such as

- the non-boiling, single phase convective heat transfer zone,
- the subcooled nucleate boiling zone, and
- the saturated nucleate boiling zone.

As a result, obtaining an analytical solution to the system of ordinary differential equations was impossible and numerical integration techniques had to be used, requiring extensive computational time. This limited the usefulness of the model for practical application.

A simplified model of the climbing film evaporator system was thus developed, based on linearisation of the original ordinary differential equations, which could be analytically integrated. This simplified model was found to be an acceptable approximation of the complex model, giving similar solutions under all of the process conditions tested.

## 5.1 DEVELOPMENT OF THE SIMPLIFIED MODEL

Of the six ordinary differential equations describing the climbing film evaporator system, the two strongly coupled, nonlinear equations requiring numerical solution were those resulting from the overall enthalpy balance, equation **(14)**, and the momentum balance, equation **(20)**. These equations can be represented in the following general mathematical form:

$$\frac{dH}{dz} = F\left(z, H, \bar{p}\right) \qquad \frac{d\bar{p}}{dz} = G\left(z, H, \bar{p}\right)$$

The complex functions F and G depend not only on the enthalpy and pressure terms, but also on the independent variable of the model, the distance along the evaporator tube, z. This is a result of the changes in the two phase flow and heat transfer characteristics which take place as the fluid being boiled moves upwards through the tube. Moreover, as different heat transfer correlations are used in each of the individual heat transfer regimes within the tube, some of the changes in F and G at the transition points between these zones are discontinuous. Thus the characteristics of F and G change dramatically as the tube is traversed.

It was decided to emphasise the discontinuities in these functions by using piecewise representations for F and G, with individual function segments being valid in each of the heat transfer zones within the tube. In other words, each of the two nonlinear functions is represented by three "sub-functions", each being applicable in only one of the three major heat transfer zones, and independent of the distance along the tube, z. This concept can be expressed mathematically as:

$$F\left(z, H, \bar{p}\right) = \begin{cases} F_1\left(H, \bar{p}\right), & 0 \le z \le z_{12}, \quad \text{non-boiling zone} \\ F_2\left(H, \bar{p}\right), & z_{12} \le z \le z_{23}, \quad \text{subcoooled boilingzone} \\ F_3\left(H, \bar{p}\right), & z_{23} \le z \le L, \quad \text{saturated boiling zone} \end{cases}$$

where $F_1$, $F_2$ and $F_3$ are the three "sub-functions" making up the nonlinear function F, $z_{12}$ is the transition point between the non-boiling and subcooled boiling zones, $z_{23}$ is the transition point between the subcooled nucleate boiling and saturated nucleate boiling zones and L is the length of the evaporator tube. A similar representation can be given to the nonlinear function G. Obviously, this piecewise representation of the two governing ordinary differential equations complicates the process of their linearisation, with each of the three heat transfer zones requiring separate treatment.

### 5.1.1 The non-boiling zone

With the application of some generally acceptable simplifying assumptions, such as:

- negligible heat transfer resistance on the condensation side of the tube,
- negligible heat transfer resistance due to the tube wall,
- a constant wall temperature in this zone, being the same temperature as the condensing steam (this is, in fact, a direct result of the first two simplifying assumptions),
- a negligible acceleration term in the momentum balance, and
- constant physical properties of the juice,

the two functions characterising the non-boiling zone, $F_1$ and $G_1$, become linear without the need for any specialised linearisation technique. The enthalpy and momentum balance equations simplify as follows:

$$L_0 C_{pL} \frac{dT_L^1}{dz} = \pi D_2 \alpha_L \left(T_s - T_L^1\right) \quad \text{with } T_L^1(z=0) = T_{L0} \quad \text{... (43)}$$

and

$$\frac{dp^1}{dz} = \left[\frac{dp}{dz}\right]_{friction} - \rho_L g \quad \text{with } p^1(z=0) = p_0 \quad \text{... (44)}$$

where $L_0$ is the feed juice flow rate, $C_{pL}$ is the heat capacity of the liquid within the tube, $T^1_L(z)$ is the local juice temperature at position z in zone 1 (the non-boiling zone), $D_2$ is the inner tube diameter, $\alpha_L$ is the liquid phase convective heat transfer coefficient in the non-boiling zone, calculated using the Engineering Sciences Data Unit correlation (equations **(24)** through **(26)**), $T_s$ is the steam temperature, $T_{L0}$ is the temperature of the juice entering the bottom of the tube (at $z = 0$), $p^1(z)$ is the local pressure at point z within the tube, $\rho_L$ is the density of the liquid within the tube, g is the acceleration due to gravity, $p_0$ is the pressure at the bottom of the tube (at $z = 0$), and $[dp/dz]_{friction}$ is the frictional pressure drop per unit tube length of tube for liquid phase flow only, calculated using the Churchill equation for single phase pressure drop, equation **(33)**.

Equations **(43)** and **(44)** can then be independently analytically integrated to give an exponential distribution for the local juice temperature:

$$T_L^1(z) = T_s - (T_s - T_{L0}) \exp\left(-\frac{\pi D_2 \alpha_L}{L_0 C_{pL}} \cdot z\right)$$

and a linear distribution of the local pressure:

$$p^1(z) = p_0 - \left(\rho_L g - \left[\frac{dp}{dz}\right]_{friction}\right).z$$

The enthalpy flow profile in the non-boiling zone is given by:

$$H^1(z) = L_0 C_{pL} T_L^1(z)$$

assuming a constant heat capacity. These three distributions are only valid for the non-boiling zone within the tube (i.e. for $z \in [0, z_{12}]$).

### 5.1.2 Transition to the subcooled nucleate boiling zone

When the temperature of the heated tube wall rises above the critical wall temperature for bubble nucleation, boiling will begin to occur at some nucleation sites on the wall surface. If the bulk liquid temperature within the tube is below the local boiling point, this situation is known as subcooled nucleate boiling.

The critical wall temperature for nucleation can be calculated using the method developed by Davis and Anderson (1966), as given by equation **(30)**. As the wall temperature is assumed to be constant and equal to the temperature of the condensing steam, $T_s$, this equation actually defines the critical bulk liquid temperature at which nucleation begins:

$$T_L^* = T_s - \frac{\lambda \rho_v k_L}{8 \sigma T_{bp} \alpha_L}\left(T_s - T_{bp}\right)^2$$

where $T^*_L$ is the critical bulk liquid temperature for nucleation, $\lambda$ is the latent enthalpy of vapourisation of the liquid being boiled, $\rho_v$ is the density of the vapour phase, $k_L$ is the thermal conductivity of the liquid phase, $\sigma$ is the surface tension of the liquid and $T_{bp}$ is the local boiling point of the liquid within the tube. Note that the critical bulk temperature for nucleation is a function of distance along the length of the tube, z. This is because $T^*_L(z)$ is a function of the juice boiling point, $T_{bp}$, which is determined by the local pressure, $p^j(z)$.

The first transition point in the simplified climbing film evaporator model, $z_{12}$, can be defined as the distance, measured from the bottom of the evaporator tube, at which the local bulk temperature of the juice, resulting from the non-boiling zone model, approaches the critical bulk temperature for nucleation. Mathematically, this condition is defined as:

$$T^1_L(z) - T^*_L(z) = 0 \quad \text{... (45)}$$

Since the functions for calculating both of these temperatures are nonlinear, numerical techniques are required to solve equation (45) for the transition point, $z_{12}$.

### 5.1.3 The boiling zones

The F and G functions for the two nucleate boiling zones (the subcooled and saturated nucleate boiling zones) are much more complex than those for the non-boiling zone, and simple physical arguments like those used in section 5.1.1 above are insufficient to linearise them. A purely formal linearisation technique, such as a truncated Taylor expansion around an arbitrarily chosen point ($H^*$, $\bar{p}^*$) could be used. Alternatively, as F and G are functions of two variables, linearisation could be performed by approximating some actual known values of the F and G functions with planar (two-dimensional linear) representations over a certain range of H and $\bar{p}$ values. In this study, the second method of linearisation was considered more suitable, as it provides more realistic values of the linearised functions over the whole (H, $\bar{p}$) domain of interest, rather than around an

arbitrary point.

Using the general equation of a plane in three-dimensional space to approximate both $F_i$ and $G_i$ results in:

$$F_i^{Lin}(H,\bar{p}) = a_{10} + a_{11} H + a_{12} \bar{p}$$

$$G_i^{Lin}(H,\bar{p}) = a_{20} + a_{21} H + a_{22} \bar{p} \quad \text{... (46)}$$

(for clarity, the "i" indices on the a coefficients have been omitted on the right hand sides of the equations) where the unknown coefficients $a_{jk}$ can be determined by minimising the distance between the actual surfaces, $F_i$ and $G_i$, and their linearised counterparts, $F_i^{Lin}$ and $G_i^{Lin}$, respectively. In general, the method of least squares was used for these calculations. However, the approach differed slightly, depending on the actual shape of the F and G functions in three-dimensional space.

Examples of the F and G surfaces for the subcooled and saturated nucleate boiling zones have been numerically generated and are shown in Figures 18 and 19, respectively. The surfaces $F_2(H, \bar{p})$ and $G_2(H, \bar{p})$, characterising the subcooled nucleate boiling zone, are fairly planar and can be easily linearised, with the additional requirement that the linearised planar representation pass through the F and G function values prevailing at the first transition point, $z_{12}$. In other words, the linearised planar representation is constrained to pass through $(H_{12}, \bar{p}_{12}, F_{12})$ and $(H_{12}, \bar{p}_{12}, G_{12})$. This produces a very reliable approximation around the point of transition between the non-boiling zone and the subcooled nucleate boiling zone, which is critical to accurate model performance in both of these heat transfer zones. Moreover, this can be achieved without significantly sacrificing model accuracy at $(H, \bar{p})$ points lying far from the transition point, due to the fairly planar nature of the actual F and G curves.

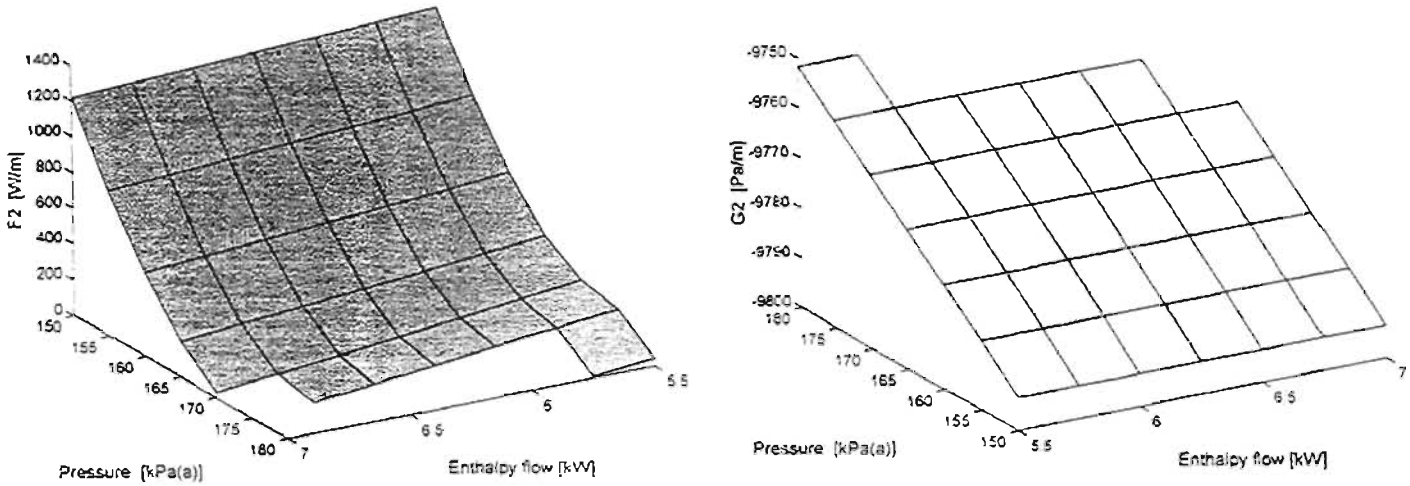


**Figure 18.** Examples of the $F_2$ and $G_2$ surfaces for the subcooled nucleate boiling zone.

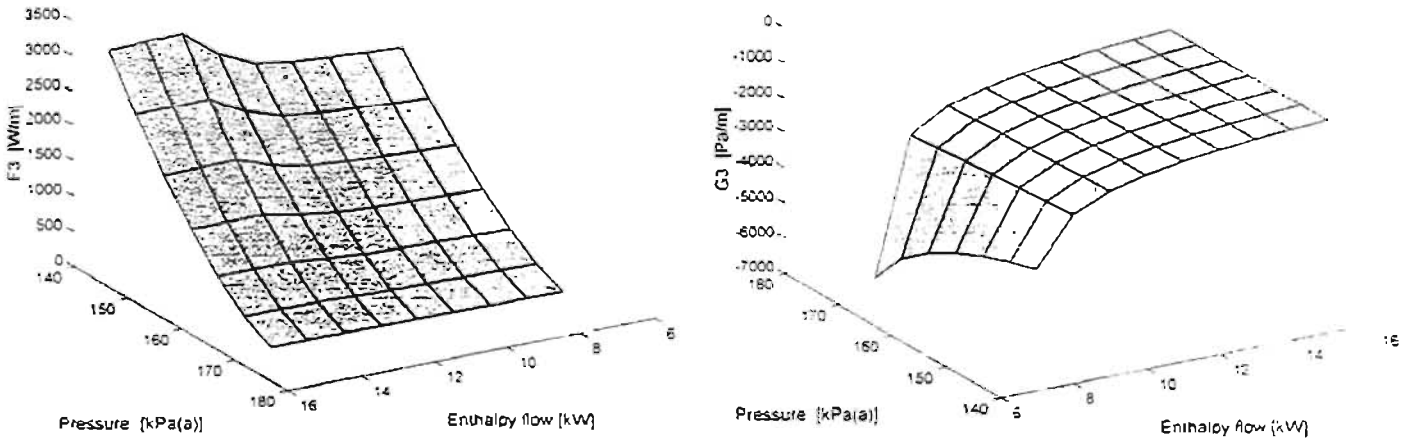


**Figure 19.** Examples of the $F_3$ and $G_3$ surfaces for the saturated nucleate boiling zone.

By contrast, inspection of the $F_3$ and $G_3$ surfaces for the saturated nucleate boiling zone, shown in Figure 19, shows that surface $G_3$ in particular is highly nonlinear over a certain region of enthalpies and pressures. This surface exhibits a large inflection in the region of the graph representing the transition from subcooled nucleate boiling to saturated nucleate boiling. However, numerical investigation of the phenomenon showed that this initial phase of the saturated nucleate boiling zone had a negligible effect on the overall heat transfer behaviour of the evaporator. Consequently, it was decided not to include the requirement that the planar representations of the $F_3$ and $G_3$ surfaces pass through the transition point, $z_{23}$.

### 5.1.4 The subcooled nucleate boiling zone

As discussed previously, the approximating planes for $F_2$ and $G_2$ are constrained to pass through the corresponding conditions at the first transition point, $z_{12}$, namely ($h_{12}$, $\bar{p}_{12}$, $F_{12}$) and ($h_{12}$, $\bar{p}_{12}$, $G_{12}$). This additional requirement converts the equations for these planes, equation **(46)**, into a more specific form:

$$F_2^{Lin}(H,\bar{p}) = F_{2,12} + a_{11}\left(H - H_{12}\right) + a_{12}\left(\bar{p} - \bar{p}_{12}\right)$$

$$G_2^{Lin}(H,\bar{p}) = G_{2,12} + a_{21}\left(H - H_{12}\right) + a_{22}\left(\bar{p} - \bar{p}_{12}\right) \quad \text{... (47)}$$

where $F_{2,12}$ is the value of the function $F_2$ at $z_{12}$ and, similarly, $G_{2,12}$ is the value of the function $G_2$ at $z_{12}$. The four unknown coefficients $a_{11}$, $a_{12}$, $a_{21}$ and $a_{22}$ can be determined using the classic least squares regression, the objective being the minimisation of the sum:

$$I = \sum_{i=1}^{N_F}\left[F_2^{Lin}(H_i,\bar{p}_i) - F^*_{2,i}\right]^2 + \sum_{i=1}^{N_G}\left[G_2^{Lin}(H_i,\bar{p}_i) - G^*_{2,i}\right]^2$$

with respect to the coefficients $a_{jk}$, where $F_2^{Lin}$ and $G_2^{Lin}$ are given by equation **(47)** and $F^*_{2,i}$ and $G^*_{2,i}$ are values determined from the original complex model (i.e. the values making up the original $F_2$ and $G_2$ surfaces). $N_F$ and $N_G$ are the numbers of ($H_i$, $\bar{p}_i$) points making up the F and G surfaces, respectively. This procedure represents the process of fitting the equation of a plane to a selected set of $F_2$ and $G_2$ data.

Once the coefficients $a_{jk}$ have been determined by least squares regression, it becomes possible to solve the linearised system of ordinary differential equations for the subcooled nucleate boiling zone. These equations can be written in a matrix-vector form as:

$$\frac{d}{dz}\begin{bmatrix} H^2 - H_{12} \\ \bar{p}^2 - \bar{p}_{12} \end{bmatrix} = \begin{bmatrix} F^{Lin}_{2,12} \\ G^{Lin}_{2,12} \end{bmatrix} + \mathbf{A}\begin{bmatrix} H^2 - H_{12} \\ \bar{p}^2 - \bar{p}_{12} \end{bmatrix} \quad \text{... (48)}$$

where $H^2$ and $\overline{p}^2$ are the enthalpy and modified pressure values of interest in zone 2 (the subcooled nucleate boiling zone), with **A** being the matrix of $a_{jk}$ coefficients. The initial conditions are $H^2(z_{12}) = H_{12}$ and $\overline{p}^2(z_{12}) = \overline{p}_{12}$. Since equation **(48)** represents a system of two linear ordinary differential equations with constant coefficients, it can be integrated analytically. The solution of this system can be expressed in terms of the matrix exponential and, in the case where **A** is nonsingular, is given by:

$$\begin{bmatrix} H^2(z) \\ \overline{p}^2(z) \end{bmatrix} = \left[\exp\left(\mathbf{A}(z-z_{12})\right) - E_{2\times 2}\right]\mathbf{A}^{-1}\begin{bmatrix} F^{Lin}_{2,12} \\ G^{Lin}_{2,12} \end{bmatrix} + \begin{bmatrix} H_{12} \\ \overline{p}_{12} \end{bmatrix} \quad \text{... (49)}$$

where $E_{2\times 2}$ is the 2×2 identity matrix.

Equation **(49)** only applies to the subcooled nucleate boiling zone, that is for $z \in [z_{12}, z_{23}]$. In this heat transfer zone, the bulk liquid is subcooled and thus the enthalpy, $H^2(z)$ uniquely defines the liquid temperature, $T^2_L$, in this zone.

### 5.1.5 Transition to the saturated nucleate boiling zone

As the temperature of the juice within the tube approaches its local saturation temperature, $T_{bp}$, the mechanism of heat transfer changes from subcooled nucleate boiling to saturated nucleate boiling heat transfer. The second transition point in the simplified evaporator model, $z_{23}$, is defined as the distance, measured from the bottom of the evaporator tube, at which the local bulk temperature of the juice, resulting from the subcooled nucleate boiling zone model, approaches the local boiling point temperature. Mathematically, this condition can be expressed as:

$$T^2_L(z) - T_{bp}(z) = 0 \quad \text{... (50)}$$

The bulk temperature of the juice in the subcooled nucleate boiling zone is a nonlinear

function with respect to the distance along the tube, z. Furthermore, the local boiling point temperature of the juice is a nonlinear function of the local pressure within the tube, $\bar{p}^2(z)$. Thus, numerical techniques are required to solve equation **(50)** for the transition point, $z_{23}$.

### 5.1.6 The saturated nucleate boiling zone

The $F_3$ and $G_3$ functions for the saturated nucleate boiling zone can be approximated by a planar representation. This is achieved by fitting two equations for planes

$$F_3^{Lin}(H,\bar{p}) = b_{10} + b_{11} H + b_{12} \bar{p}$$
$$G_3^{Lin}(H,\bar{p}) = b_{20} + b_{21} H + b_{22} \bar{p} \quad \text{... (51)}$$

to available $F^*_3$ and $G^*_3$ data. The six unknown $b_{jk}$ coefficients can be determined using a least squares regression technique, as for the subcooled nucleate boiling zone.

Once the $b_{jk}$ coefficients have been determined, equation **(51)** constitutes the right hand sides of the linearised enthalpy and momentum balances for the saturated nucleate boiling zone. This system of two linear ordinary differential equations can be written in matrix-vector form as:

$$\frac{d}{dz}\begin{bmatrix} H^3 \\ \bar{p}^3 \end{bmatrix} = \begin{bmatrix} b_{10} \\ b_{20} \end{bmatrix} + \mathbf{B}\begin{bmatrix} H^3 \\ \bar{p}^3 \end{bmatrix} \quad \text{... (52)}$$

where $H^3$ and $\bar{p}^3$ are the enthalpy and modified pressure values of interest in zone 3 (the saturated nucleate boiling zone), with the matrix **B** being the matrix of $b_{jk}$ coefficients. The initial conditions $H^3(z_{23}) = H_{23}$ and $\bar{p}^3(z_{23}) = \bar{p}_{23}$ result from the linearised model for the subcooled nucleate boiling zone at the second transition point, $z_{23}$. Equation **(52)** is a linear system of equations, and as such is analytically integrable. For a nonsingular matrix **B**, which was found to be true in practice, the solution is:

$$\begin{bmatrix} H^3(z) \\ \bar{p}^3(z) \end{bmatrix} = \left[\exp\left(\mathbf{B}(z-z_{23})\right) - E_{2\times 2}\right]\left(\mathbf{B}^{-1}\begin{bmatrix} b_{10} \\ b_{20} \end{bmatrix} + \begin{bmatrix} H_{23} \\ \bar{p}_{23} \end{bmatrix}\right) + \begin{bmatrix} H_{23} \\ \bar{p}_{23} \end{bmatrix} \quad \text{... (53)}$$

Equation (53) is valid only for the saturated nucleate boiling zone, that is for $z \in [z_{23}, L]$. In this heat transfer zone, the enthalpy within the tube, $H^3(z)$ uniquely defines the flow rate of vapour, rather than the juice temperature, as the temperature of the boiling juice is determined thermodynamically as the boiling point of the juice at the given local pressure and juice composition.

## 5.2 NUMERICAL SOLUTION OF THE SIMPLIFIED MODEL

In practical operation, the operating conditions of a climbing film evaporator are specified in such a way that the juice characteristics, such as temperature and composition, are specified at the bottom of the evaporator tube, while certain operating parameters, such as the vapour space pressure and flow rate of condensate per unit length of tube perimeter, are only available at the top of the evaporator tube. A problem of this nature is classified as a two point boundary value problem, and requires solution using numerical techniques.

The simulation of the original system of ordinary differential equations (the complex model) constitutes a two point boundary value problem of the form:

$$\frac{dH}{dz} = F\left(z, H, \bar{p}; \Gamma(0)\right) \quad H(0) = H_0$$

$$\frac{dp}{dz} = G\left(z, H, \bar{p}\right) \qquad p(L) = p_{top}$$

Note that the two ordinary differential equations utilise boundary conditions known at both ends of the evaporator tube. The above boundary value problem can be solved by numerically finding the root $[\Gamma(0), p(0)]$ of the following system of two algebraic

equations:

$$\begin{aligned} p(L) - p_{top} &= 0 \\ \Gamma(L) &= 0 \end{aligned} \qquad \text{... (54)}$$

where the flow rate of condensate per unit length of tube perimeter, $\Gamma$, results from a combination of the condensate and juice enthalpy balances:

$$\Gamma(z) = \Gamma(0) - \frac{H(z) - H(0)}{\pi D_2 \lambda_c} \qquad \text{... (55)}$$

where $D_2$ is the diameter of the inner tube wall and $\lambda_c$ is the latent enthalpy of condensation for the condensing steam. The process of solution of these algebraic equations is iterative and involves the Newton-Raphson technique. This is particularly time-consuming, in that the integration of successive initial value problems is required, in order to evaluate the right hand side of equation **(54)**, at each iteration step of the Newton-Raphson procedure.

In principle, the simplified, linearised climbing film evaporator model also constitutes a two point boundary value problem. However, as a full analytical solution of the simplified model is available, finding the root of the system of algebraic equations in equation **(54)** no longer requires time-consuming numerical integration of a system of differential equations. The root can be found utilising the same Newton-Raphson solver as for the complex model, and the required solution can be evaluated *via* the following sequence of calculations at each iteration step:

- The first transition point, $z_{12}$ is determined from equation **(45)**, using Newton's method for solution.
- The enthalpy and pressure values at the transition point, $H_{12}$ and $\bar{p}_{12}$, are determined from the equations of the non-boiling zone model.
- The approximating planes for the subcooled boiling zone, $F_2^{Lin}$ and $G_2^{Lin}$, are determined by generating a set of sample points, at which actual values from the $F_2$

and $G_2$ surfaces, $F_{2i}^*$ and $G_{2i}^*$, can be evaluated, and evaluating the matrix of coefficients, **A**.

- The second transition point, $z_{23}$, is determined from equation **(50)**, using Newton's method for solution.
- The enthalpy and pressure values at the transition point, $H_{23}$ and $\bar{p}_{23}$,are determined from the equations of the subcooled nucleate boiling zone approximating planes.
- The approximating planes for the saturated boiling zone, $F_3^{Lin}$ and $G_3^{Lin}$, are determined by generating a set of sample points, at which actual values from the $F_3$ and $G_3$ surfaces, $F_{3i}^*$ and $G_{3i}^*$, can be evaluated, and evaluating the matrix of coefficients, **B**.
- The enthalpy and pressure values at the end of the evaporator tube, $H_L$ and $\bar{p}_L$ are determined from the equations of the saturated nucleate boiling zone approximating planes. $\Gamma(L)$ is calculated using equation **(55)**.
- The right hand side of equation **(54)** is evaluated.

## 5.3 COMPARISON WITH THE COMPLEX MODEL

The simplified climbing film evaporator model was validated by comparing the results of several simulations under different operating conditions against the results obtained using the complex model simulation program under the same conditions. Selected graphical results from two such comparative tests are displayed in Figures 20 and 21, with the results from the complex model being shown as the solid lines in the figures and the results from the simplified model being shown as the dotted lines.

The plots labeled (a) in the figures show the juice temperature profile as the evaporator tube is traversed. Under the conditions used in these two examples, the juice reaches its boiling point fairly rapidly upon entering the tubes (as would typically occur in an industrial situation). Once saturated nucleate boiling has been initiated, the juice temperature remains reasonably constant, decreasing slightly as the tube is traversed due

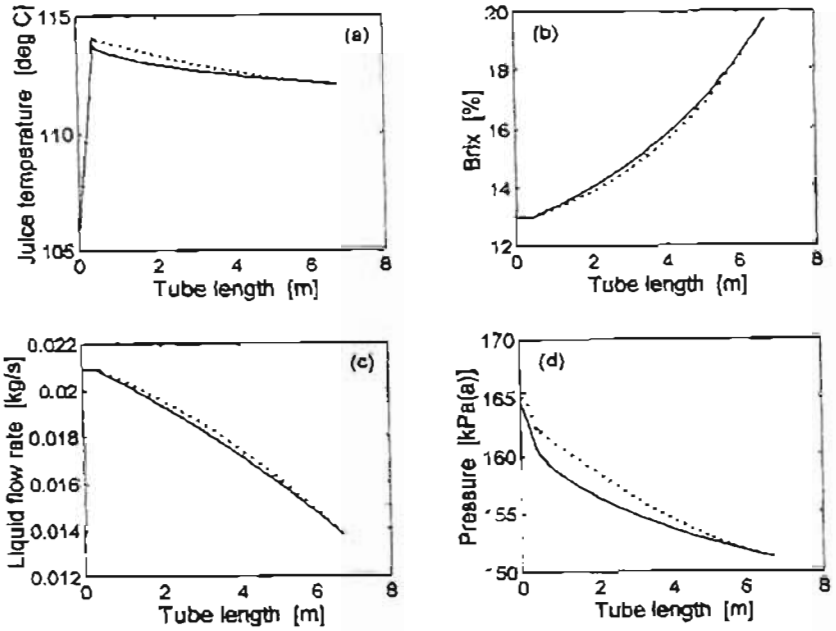


**Figure 20.** Selected graphical results from model simulations.

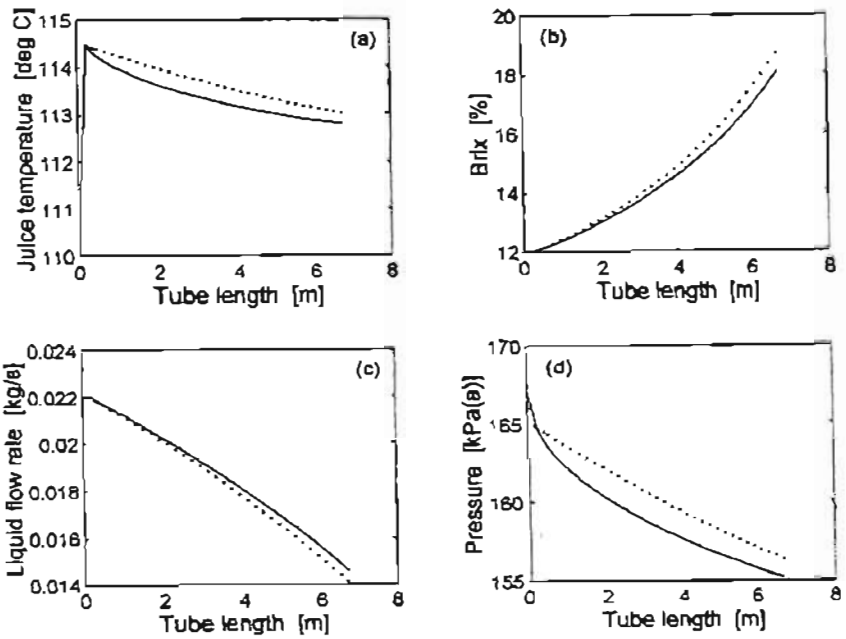


**Figure 21.** Selected graphical results from model simulations.

to the reduction of hydrostatic head with height up the tube.

The plots labeled (b) in Figures 20 and 21 show the concentration profile of the juice as it moves through the evaporator tube. It can be clearly seen that the simplified model better approximated the complex model under the conditions prevailing for the example in Figure 20. A slight error in the prediction of juice concentration is evident in Figure 21(b).

The plots labeled (c) in the figures display the liquid phase flow rate through the evaporator tube. As vapour is formed, the liquid phase flow rate drops proportionately. As the liquid phase flow rate and juice concentration are intimately related, the error evident in Figure 21(b) is also evident in Figure 21(c).

The plots labeled (d) in the figures show the local pressure profiles along the evaporator tube. Once again, it is clear that the example in Figure 20 was more accurately approximated by the simplified model than the example in Figure 21.

While minor differences between the results are apparent, it is evident that the simplified evaporator model is a reasonably good representation of the more exact complex model.

# Chapter 6

# Application of the Simplified Model

The simplified climbing film evaporator model was used to develop an evaporator simulation program in the MATLAB programming language.

The simplified climbing film evaporator model was applied to the study of three important applications in the sugar industry. For these studies, the original value of the Forster-Zuber coefficient, $k_{FZ}$ = 0,00122, as specified by Chen, was used.

## 6.1 THE EFFECT OF JUICE FLOW RATE

The feed juice flow rate to climbing film evaporators is of critical importance to their efficient operation. Tests were carried out using the Felixton mill pilot plant evaporator to determine the effect of feed juice flow rate on evaporator performance, with the other experimental operating parameters held constant (Walthew and Whitelaw, 1996). The results of some of these experimental tests are shown in Figure 22, where the average overall heat transfer coefficient for the evaporator is displayed as a function of the feed juice flow rate.

In order to confirm these experimental observations, the simplified evaporator model was used to study the effect of feed juice flow rate on the average overall heat transfer coefficient of a climbing film evaporator. The operating conditions used in the study, shown in Table 7, were similar to those used for the first effect climbing film evaporators at the Felixton sugar mill. Three different tube diameters (38,40 mm, 48, 36 mm and 71,60 mm) were assumed, with feed juice flow rates varying between 0,5 and 3 kg/min/tube. The results of the model simulations are shown in Figure 23.

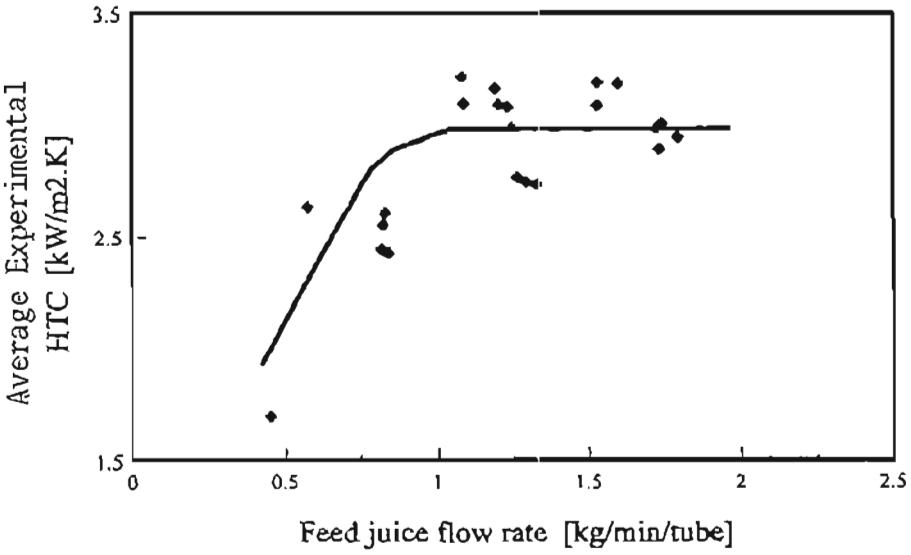


**Figure 22.** The effect of juice flow rate on evaporator performance for a 48,36mm diameter tube. [Walthew and Whitelaw, 1996]

**Table 7.** Operating conditions for the model study of feed juice flow rate.

| | |
|---|---|
| Number of tubes | 5000 |
| Tube length [m] | 6,73 |
| Feed juice sucrose concentration [%(m/m)] | 10,2 |
| Feed juice impurity concentration [%(m/m)] | 1,8 |
| Feed juice temperature [°C] | 110 |
| Steam pressure [kPa(a)] | 200 |
| Vapour pressure [kPa(a)] | 155 |

Figure 23 confirms the general trend of the experimental data, which was obtained using 48,36 mm inner diameter tubes. However, the feed juice flow rate at which the substantial increase in overall average heat transfer coefficient occurs, as predicted by the model, is different to that obtained experimentally. The reason for this difference is not yet known,

and further work would be required to identify the cause.

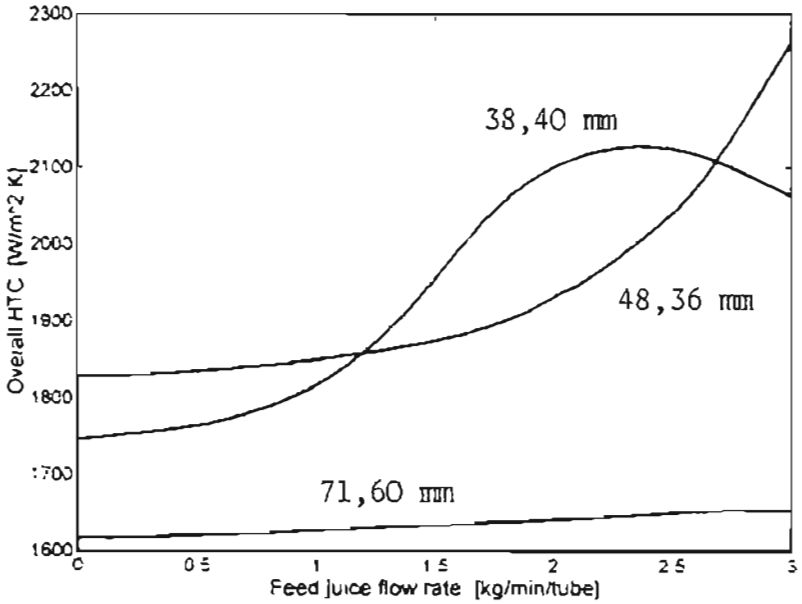


**Figure 23.** The effect of juice flow rate on evaporator performance.

As expected, the flow rate at which the substantial change occurs increases with increasing tube diameter. This is due to the increase in cross-sectional area for flow within the tube with increasing tube diameter. In a small diameter tube, a lower flow rate is required for thorough wetting of the tube wall surface than in a larger diameter tube. The substantial change in heat transfer coefficient is not visible on the curve for the 71,60 mm internal diameter tube, as it probably at a flow rate higher than those studied here.

Using the simplified evaporator model to evaluate the effect of tube diameter on evaporator performance showed that, for each feed juice flow rate, on optimal tube diameter exists which maximises the overall average heat transfer coefficient. At the juice flow rates typically encountered in the South African sugar industry, tubes of inner diameter 48,36 mm (the most common tube size in the industry) would appear to be a reasonable choice.

Walthew and Whitelaw (1996) showed that a low feed juice flow rate limits the maximum

attainable heat transfer coefficient by limiting the water available for evaporation. They also showed that the degree of fouling within evaporator tubes in the sugar industry decreased with increasing feed juice flow rate. These factors, along with the experimental data from the pilot plant climbing film evaporator and the results of this theoretical study, indicate that climbing film evaporators should be ideally be operated so as to achieve a consistently high feed flow rate.

## 6.2 THE EFFECT OF JUICE RECYCLE

The process of heat transfer in a climbing film evaporator is subject to conflicting effects with regard to feed juice flow rate. On the one hand, a relatively low flow rate is desirable to ensure a reasonable juice residence time within the evaporator. This allows for a high degree of evaporation to take place. By contrast, low juice flow rates (and hence low juice velocities within the tubes) result in laminar flow conditions within the evaporator tubes, leading to poor convective heat transfer coefficients[2].

In the subcooled nucleate boiling and saturated nucleate boiling zones, the nucleate boiling heat transfer mechanism dominates, with very little contribution to the overall heat transfer coming from the convective heat transfer mechanism. As nucleate boiling heat transfer is fairly insensitive to the flow rate within the tube, the effect of low juice flow rates on heat transfer within these zones is small. However, laminar flow conditions dramatically affect the length of the non-boiling zone, where single phase convective heat transfer dominates. Any increase in the length of the non-boiling zone results in a shortening of the length of tube available for the more efficient boiling heat transfer zones, negatively impacting on overall heat transfer and, hence, on the amount of water evaporated.

---

[2] Very low juice feed flow rates to climbing film evaporators can also result in partial tube dry-out at the top ends of the tubes, with the consequences of a significant decrease in overall heat transfer and a greatly accelerated rate of fouling.

Two techniques can be used to ensure good heat transfer in a climbing film evaporator. The first of these is adequate feed juice preheating to ensure the onset of nucleate boiling as soon as possible after the juice enters the evaporator tubes, thus effectively eliminating the non-boiling zone. A theoretical study of the effect of feed juice preheating on the length of the non-boiling zone has been performed (Peacock, 1996; Peacock, 1998). The second technique involves recycling a portion of the concentrated liquid phase leaving the evaporator back to the feed juice inlet to improve the system hydrodynamics.

While increasing the juice flow rate per tube results in more efficient convective heat transfer, the overall effect of recycling on evaporator performance is more complex. As a result of the addition of high concentration material from the evaporator outlet, some of the physical properties of the feed juice stream, such as the density and viscosity, will increase, negatively affecting overall evaporator performance. The combined result of these conflicting effects can not be intuitively determined for any given system. It was thus decided to apply the simplified evaporator model to study the effect of recycling on evaporator performance more closely.

### 6.2.1 Recycling for process stability

Recycling of juice during evaporation results in more than just enhanced convective heat transfer, with benefits also realised in terms of process stability. The damping effect of recycling enables minor feed juice flow fluctuations to be eliminated easily, resulting in more steady evaporator operation. The benefits of steady operation, in terms of the elimination of the possibility of tube dry-out and the mitigation of evaporator fouling, are significant. It is predominantly for these reasons that some South African sugar mills have installed recycle lines in their climbing film evaporators, not for the enhancement of convective heat transfer. Nonetheless, it is important to be able to evaluate the effect of recycling on evaporator performance, regardless of the reasons for its use.

### 6.2.2 Model application and results

For this study, the operation of a specific evaporator was simulated under a given set of operating conditions, at several values of the recycle fraction (defined as the fraction of the concentrated liquid phase product from the outlet of the evaporator which is returned to the inlet). The operating conditions used for the study are shown in Table 8. A schematic diagram of this system is shown in Figure 24. The outlet concentration of the product juice was used as the measure of evaporator performance. The results of the model simulations are shown in Figure 25.

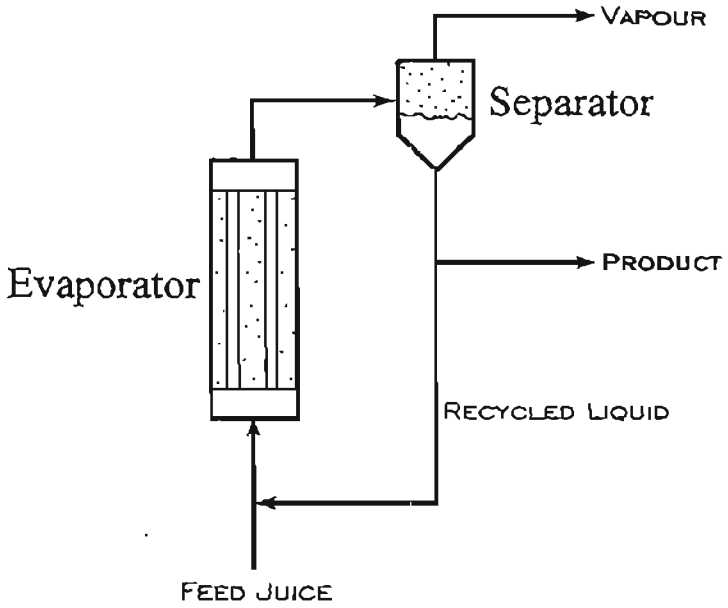


**Figure 24.** Schematic diagram of the evaporator system for the study of juice recycling.

It can be seen that the optimisation of the recycle fraction *per sé* is not possible. As predicted, the effect of juice recycling on product concentration is a complex combination of the enhanced system hydrodynamics and the negative effects of the higher average density and viscosity of the juice within the tubes. At low recycle fractions, the negative

**Table 8.** The operating conditions used for the study of juice recycling.

| | |
|---|---|
| Tube inner diameter [mm] | 48,36 |
| Tube outer diameter [mm] | 50,80 |
| Number of tubes | 5 000 |
| Tube length [m] | 6,73 |
| Juice feed flow rate [$m^3/h$] | 400 |
| Feed juice sucrose concentration [%(m/m)] | 10,2 |
| Feed juice impurity concentration [%(m/m)] | 1,8 |
| Feed juice temperature [°C] | 110 |
| Steam pressure [kPa(a)] | 200 |
| Vapour pressure [kPa(a)] | 155 |

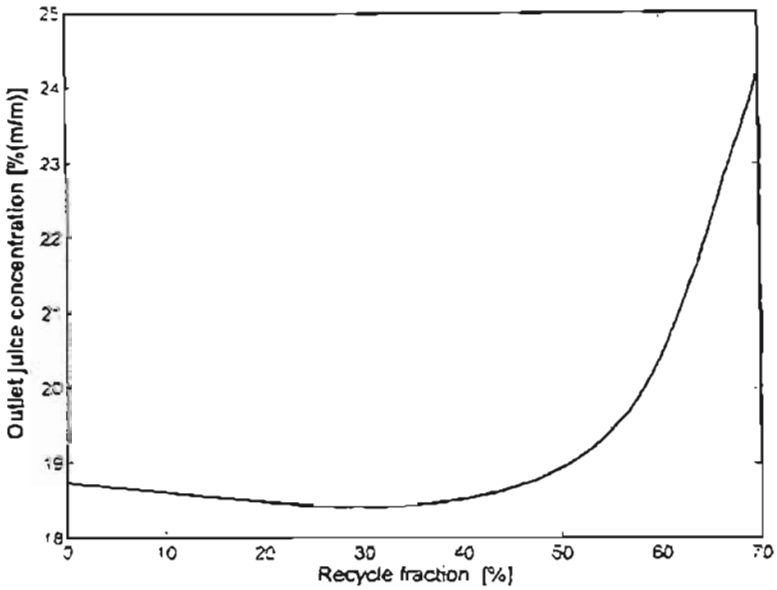


**Figure 25.** The effect of juice recycling on product juice concentration.

physical property effects and the positive hydrodynamic effects appear to balance each other, with no significant effect on evaporator performance being observed as a result of the recycling. At higher recycle fractions, the hydrodynamic advantages of the recycling

start to influence the evaporator performance, improving the product juice concentration substantially. It should be noted, however, that the recycle fractions required to achieve this performance enhancement are high (of the order of 60 to 70% of the product liquid), and some experimental work should be carried out to confirm this result.

The results of this study confirm the conventional wisdom of the sugar industry, in that recycling in climbing film evaporators should be carried out for process stability and fouling control reasons, not for heat transfer performance enhancement. It is clear that recycle fractions of less than 50% will have no significant effect on evaporator performance (excluding considerations of tube dry-out under some conditions). At higher recycle fractions, some performance benefits may be obtained, but at the expense of recycling large quantities of liquid. It should be noted, though, that no significant increase in residence time will result from the increased recycle of liquid, as the liquid inventory of the evaporator vessel is approximately constant.

## 6.3 TUBE CONFIGURATION OPTIMISATION

In the design of climbing film evaporators, it is desirable to know the required surface area for the performance of a specific heat transfer duty under a given set of operating conditions. A problem of particular current interest to the South African sugar industry is the effect of different tube diameters to those commonly used on evaporator performance. The simplified climbing film evaporator model was thus used to evaluate the effects of different tube diameters and numbers of tubes on the required surface area for the achievement of a specific heat transfer duty. In fact, with a fixed tube diameter and number of tubes, evaluating the required surface area for heat transfer reduces to the problem of evaluating the required evaporator tube length, as this is the only surface area parameter not already specified.

The operating conditions used in this study are shown in Table 9. Three different tube

diameters were evaluated (namely 38,40 mm, 48,36 mm and 71,60 mm inner diameters), with numbers of tubes ranging from 3000 to 8500 tubes per evaporator. A summary of the model results is displayed in Figure 26. With a fixed volumetric juice throughput for the vessel, as in this case, specifying the tube diameter and number of tubes uniquely fixes the juice flow rate per tube. As the juice flow velocity through the tube allows for more meaningful comparisons between tubes of varying diameters, compared to the use of numbers of tubes, this parameter is used along the x-axis of the figure.

**Table 9.** Operating conditions for the study of tube diameter effects.

| | |
|---|---|
| Juice flow rate for entire vessel [m3/h] | 400 |
| Feed juice sucrose concentration [%(m/m)] | 10,2 |
| Feed juice impurity concentration [%(m/m)] | 1,8 |
| Required product sucrose concentration [%(m/m)] | 21,3 |
| Feed juice temperature [°C] | 110 |
| Steam pressure [kPa(a)] | 200 |
| Vapour pressure [kPa(a)] | 155 |

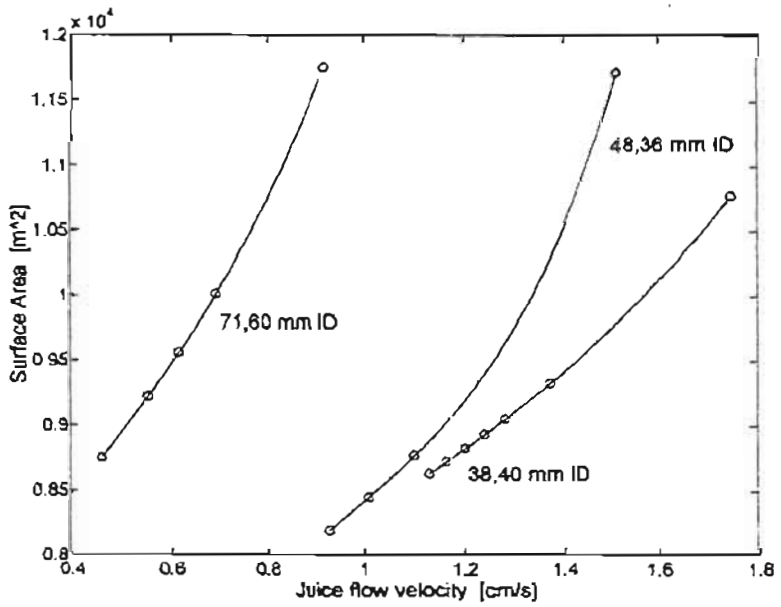


**Figure 26.** Required evaporator surface area for a given heat transfer duty as a function of tube size and number of tubes.

Detailed results are shown in Table 10, where the average HTC is the overall average heat transfer coefficient for the evaporator. When interpreting the results of this study, it must be noted that the product concentration remains fixed in each case, with the tube length being varied to obtain this desired product concentration. This makes comparison of the results quite difficult.

**Table 10.** Detailed results of the model simulations.

| Input Data | | | | Model Results | | |
|---|---|---|---|---|---|---|
| Inner tube diameter [mm] | Outer tube diameter [mm] | Number of tubes | Juice flow velocity [cm/s] | Required surface area [$m^2$] | Average HTC [$kW/m^2.°C$] | Tube length [m] |
| 38,40 | 42,40 | 5 500 | 1,74 | 10 762 | 1,33 | 16,2 |
| | | 7 000 | 1,37 | 9 322 | 1,54 | 11,0 |
| | | 7 500 | 1,28 | 9 048 | 1,59 | 10,0 |
| | | 7 750 | 1,24 | 8 928 | 1,61 | 9,6 |
| | | 8 000 | 1,20 | 8 819 | 1,63 | 9,1 |
| | | 8 250 | 1,16 | 8 719 | 1,64 | 8,8 |
| | | 8 500 | 1,13 | 8 627 | 1,66 | 8,4 |
| 48,36 | 50,80 | 4 000 | 1,51 | 11 713 | 1,21 | 19,3 |
| | | 5 500 | 1,10 | 8 767 | 1,64 | 10,5 |
| | | 6 000 | 1,01 | 8 444 | 1,70 | 9,3 |
| | | 6 500 | 0,93 | 8 188 | 1,75 | 8,3 |
| 71,60 | 76,10 | 3 000 | 0,92 | 11 753 | 1,22 | 17,4 |
| | | 4 000 | 0,69 | 10 012 | 1,43 | 11,1 |
| | | 4 500 | 0,61 | 9 557 | 1,50 | 9,4 |
| | | 5 000 | 0,55 | 9 220 | 1,56 | 8,2 |
| | | 6 000 | 0,46 | 8 746 | 1,64 | 6,5 |

From Figure 26, it can be seen that the required surface area for the performance of a given heat transfer duty is fairly sensitive to the juice flow velocity. The results in the figure

imply that, in the design of climbing film evaporators, it is not only the overall surface area required which is of importance, but also the actual dimensions of the evaporator. It is better, in terms of minimisation of the installed heat transfer surface area, to utilise many shorter tubes (of 6 to 9 metres in length) in a climbing film evaporator, thereby maintaining the juice flow velocity near its optimal value, than fewer, longer tubes (of over 9 metres in length).

While the figure shows a monotonic decrease in required surface area with decreasing juice flow velocity, this trend cannot continue unabated, as it is obvious that a certain minimum flow of juice is required through the tube to avoid tube dry-out and the region of poor vapour-phase convective heat transfer from occurring. It is expected that an optimal juice flow velocity will exist for each tube size, which results in a minimisation of the surface area required for the performance of a given heat transfer duty.

The optimal juice flow velocity can be seen to decrease with increasing tube diameter. This result is not unexpected in that the larger the tube diameter (and, subsequently, the larger the quantity of liquid within the tube not in close proximity to the tube wall), the longer the residence time required by the juice within the tube for effective evaporation. However, it would appear that tube diameter does not play a major role in the performance of properly designed climbing film evaporators, as the lowest surface area values predicted for each of the three tube diameters appear to be similar.

Most climbing film evaporators in the South African sugar industry use 48,36 mm inner diameter tubes and operate at juice flow velocities of approximately 1 cm/s. Figure 26 justifies this choice of conditions.

## 6.4 CONCLUSIONS

A simplified model of a climbing film evaporator was developed, based on linearisation

of the system of ordinary differential equations making up the original evaporator model. The simplified model was found to be an acceptable approximation of the complex evaporator model under all process conditions tested, and the model was applied to the study of three practical applications in the sugar industry.

In the first application, the model was used to study the effect of feed juice flow rate on evaporator performance. The results obtained were found to corroborate the general trends observed experimentally, although showing quite large discrepancies when compared to the actual numerical results of the experiments. More work, both experimental and theoretical, would be required to evaluate the causes of these discrepancies.

In the second application, the effect of product juice recycling on evaporator performance was evaluated. At recycle fractions of 50% or less, recycling was found to have no significant effect. At higher recycle fractions, a performance benefit was observed, but practical considerations may make the use of such high recycle fractions undesirable.

In the third application, the simplified evaporator model was used to study the effects of tube diameter and numbers of tubes on evaporator performance. The surface area required for the achievement of a specific heat transfer duty was evaluated at three different tube diameters, with varying numbers of tubes. It was found to be better to use many, relatively short tubes than fewer, longer tubes in the design of climbing film evaporators. The results were found to confirm the conventional wisdom of the South African sugar industry with regard to evaporator tube configuration.

# Chapter 7
# Conclusions

Climbing film evaporators are widely used in the South African sugar industry. However, it is generally considered that the performance of these vessels is not optimal and that improvements could be achieved by proper optimisation of the operating parameters. Owing to the complexity of the heat transfer and hydrodynamic interactions in the evaporator tubes, attempts at performance improvement have been hampered by the lack of any theory to explain fully the effects of the operating conditions and physical properties of the feed liquor on the performance of the evaporator. A study was thus carried out to produce a mathematical model of the climbing film evaporator system, which could be used to assess the effects of changing operating conditions on evaporator performance, based on as solid a theoretical base as currently possible.

To describe fully the climbing film evaporator system, it is necessary to obtain information about the pressure, component flow rate and temperature distributions along the length of one of the tubes within the apparatus under steady state conditions. For this purpose, a system of six ordinary differential equations was developed from first principles, making use of mass, enthalpy and momentum balances carried out over one tube of the vessel. Of these six ordinary differential equations, four can be solved analytically, leaving two equations requiring numerical solution.

Numerical solution of ordinary differential equations is fairly routine, provided that all the required boundary conditions for solution are known at one of the boundaries of integration. However, the system under consideration here has known boundary conditions distributed at both boundaries of integration (both ends of the evaporator tube), thus requiring more sophisticated solution techniques. For this study, a shooting method based on the Newton-Raphson technique was used to solve the two-point boundary value

problem, using a fourth order Runge-Kutta method with an automatically adjusted step size to perform the numerical integration of the system of two ordinary differential equations describing the climbing film evaporator.

The climbing film evaporator model was used to develop an evaporator simulation program in the MATLAB programming language. Given a set of inputs describing the physical parameters of an evaporator and its operating conditions, the simulation program produces profiles of various heat transfer and hydrodynamic quantities as they vary along the length of the evaporator tube.

From 1994 to 1997, a pilot plant climbing film evaporator installed at the Felixton sugar mill was used to investigate the effects of both mechanical and operational parameters on evaporator performance (Walthew and Whitelaw, 1996). The raw data from some of these experimental tests were collected and used for validation of the climbing film evaporator model, following the use of a statistical data reconciliation algorithm. Preliminary model verification showed that the model consistently under-predicted the heat transfer actually occurring in the pilot evaporator. Analysis of the heat transfer components of the evaporator model showed that the most probable cause of the erroneous results was the nucleate boiling heat transfer portion of the Chen correlation for flow boiling in vertical tubes. It was felt that the modified Forster-Zuber pool boiling equation was inaccurate.

An attempt was made to replace this outdated, inaccurate correlation with a modern equation of greater accuracy. However, it was found that none of the available correlations could be applied to the conditions normally encountered in the South African sugar industry, due to the extremely low juice flow rates typically used. Following further investigation, it was decided to utilise the Forster-Zuber coefficient, $k_{FZ}$, being the most uncertain parameter in the evaporator model, as the parameter to be optimised in order to improve the accuracy of the model predictions. A least-squares optimisation algorithm was used for this purpose, identifying a new value for $k_{FZ}$ to give a better fit to the experimental data, based on minimisation of an appropriately defined performance index.

In the model identification procedure, it was found that the calculated optimal values of $k_{FZ}$ were several times higher then Chen's original value of 0,00122, ranging from 0,003 to 0,009. Identification of the new values for this coefficient led to a great improvement in model performance, yielding 5% relative error between the model predictions and the experimental measurements.

The original system of ordinary differential equations describing the steady state operation of a climbing film evaporator was strongly coupled and nonlinear. Moreover, this nonlinearity was strengthened by the fact that the mechanism of heat transfer within the tube changes dramatically when moving through the various zones within the tube, such as the non-boiling zone, the subcooled nucleate boiling zone and the saturated nucleate boiling zone. As a result, obtaining an analytical solution to the system of equations was impossible and numerical integration techniques had to be used, requiring extensive computational time. This limited the use of the model for practical application.

A simplified model of the climbing film evaporator system was thus developed, based on linearisation of the original system of ordinary differential equations, which could then be analytically integrated. It was decided to emphasise the discontinuous nature of the heat transfer and hydrodynamic changes occurring along the length of the tube by using piecewise linear representations for the ordinary differential equations, with individual function segments being valid in each of the three heat transfer zones within the tube.

The simplified climbing film evaporator model was verified by comparing the results of several simulations under different operating conditions against the results obtained using the complex model simulation program under the same conditions. While minor differences in the results were observed, it was found that the simplified evaporator model was a reasonably good representation of the more exact, complex model.

The simplified evaporator model was used to develop an evaporator simulation program in the MATLAB programming language. This simulation program was applied to the study

of three important applications in the sugar industry, namely the effect of feed juice flow rate on evaporator performance, the effect of concentrated juice recycling on evaporator performance and the optimisation of the tube configuration in an evaporator to yield the minimum surface area required for the performance of a given heat transfer duty. It was found that the results obtained in these applications corroborated the general trends observed experimentally, reproducing the observed experimental data qualitatively. However, quite large quantitative discrepancies were found when compared to the results of the experiments. More modelling and experimental work would need to be carried out to determine the reasons for these discrepancies.

# Chapter 8

# Nomenclature

| Symbol | Explanation | Units |
|---|---|---|
| a | Constant exponent in the evaporator model of Coulson and Mehta, 1953;<br>Constant in the correlation of Starzak and Peacock, 1997;<br>Constant in the sugar cane juice density correlation of Kadlec *et al.*, 1983 | |
| $a_0$ to $a_3$ | Constants in the sugar cane juice density correlation of Kadlec *et al.*, 1983 | |
| $a_{jk}$ | Coefficients in the linear regression of the complex functions F and G, where j = 1,2 and k = 1,2 | |
| A | Surface area for heat transfer;<br>Constant in the evaporator model of Bourgois and Le Maguer, 1983b;<br>Cross-sectional area for flow within the evaporator tube;<br>Parameter in the Churchill correlation for single phase pressure drop | $m^2$<br><br>$m^2$ |
| **A** | Matrix of $a_{ij}$ coefficients in linear regression analysis | |
| $A_1$ to $A_{11}$ | Constants in the physical properties correlations of Aggarwal, 1989 for pure water | |
| $A_x$ | Cross-sectional area for flow within the evaporator tube | $m^2$ |
| $A_{xL}$ | Cross-sectional area for liquid phase flow within the evaporator tube | $m^2$ |
| $A_{xv}$ | Cross-sectional area for vapour phase flow within the evaporator tube | $m^2$ |
| b | Constant exponent in the evaporator model of Coulson and Mehta, 1953;<br>Constant in the correlation of Starzak and Peacock, 1997;<br>Constant in the sugar cane juice density correlation of Kadlec *et al.*, 1983 | |
| $b_0$ to $a_3$ | Constants in the sugar cane juice density correlation of Kadlec *et al.*, 1983 | |
| $b_{jk}$ | Coefficients in the linear regression of the complex functions F and G, where j = 1,2 and k = 0,1,2 | |
| B | Constant in the evaporator model of Bourgois and Le Maguer, 1983b;<br>Parameter in the Churchill correlation for single phase pressure drop;<br>Constant in the correlation of Starzak and Peacock, 1997 | |

| | | |
|---|---|---|
| **B** | Matrix of $b_{ij}$ coefficients in linear regression analysis | |
| BPE | Boiling point elevation of the boiling fluid within the tube | °C |
| Bx | Dissolved solids content (sucrose and impurities) of sugar cane juice | %(m/m) |
| c | Constant exponent in the evaporator model of Coulson and Mehta, 1953; Constant describing the saturation curve of water in the evaporator model of Bourgois and Le Maguer, 1983a; Constant in the sugar cane juice density correlation of Kadlec *et al.*, 1983 | |
| $c_0$ to $c_3$ | Constants in the sugar cane juice density correlation of Kadlec *et al.*, 1983 | |
| C | Constant in the evaporator model of Bourgois and Le Maguer, 1983b; Constant in the correlation of Starzak and Peacock, 1997 | |
| $C_1$ | Parameter in the slip ratio correlation of Premoli *et al.* , 1970 | |
| $C_2$ | Parameter in the slip ratio correlation of Premoli *et al.* , 1970 | |
| $C_3$ | Parameter in the slip ratio correlation of Premoli *et al.* , 1970 | |
| $C_{nb}$ | Nucleate boiling coefficient in the correlation of Rohsenow, 1952 | |
| $C_p$ | Specific heat capacity of water in the model of Gupta and Holland, 1966a | BTU/lb.°F |
| $C_{p1}$ | Specific heat capacity of the liquid phase within the evaporator tube | kJ/kg.°C |
| $C_{p2}$ | Specific heat capacity of the liquid phase within the evaporator tube | kJ/kg.°C |
| $C_{pi}$ | Specific heat capacity of the liquid at the evaporator inlet conditions | kJ/kg.°C |
| $C_{pk}$ | Specific heat capacity for differential element k within the evaporator tube | kJ/kg.°C |
| $C_{pL}$ | Specific heat capacity of the liquid phase within the evaporator tube | kJ/kg.°C |
| $C_{pLm}$ | Average specific heat capacity of the liquid phase within the non-boiling zone | kJ/kg.°C |
| $C_{pv}$ | Specific heat capacity of the vapour phase within the evaporator tube | kJ/kg.°C |
| $C_{pw}$ | Specific heat capacity of pure water | kJ/kg.°C |
| $C_{sf}$ | Constant in the evaporator model of Piret and Isbin, 1954 | |
| d | Constant exponent in the evaporator model of Coulson and Mehta, 1953; Inner tube diameter in the evaporator model of Coulson and McNelly, 1956; Constant in the sugar cane juice density correlation of Kadlec *et al.*, 1983 | ft |
| $d_0$ to $d_3$ | Constants in the sugar cane juice density correlation of Kadlec *et al.*, 1983 | |
| D | Inner tube diameter | m |

| | | |
|---|---|---|
| $D_1$ | Outer tube diameter | m |
| $D_2$ | Inner tube diameter | m |
| $D_i$ | Inner tube diameter | m |
| $D_o$ | Outer tube diameter | m |
| e | Constant exponent in the evaporator model of Coulson and Mehta, 1953 | |
| E | Parameter in the two phase pressure drop prediction method of Friedel, 1979 | |
| $E_{2\times2}$ | Identity matrix of size 2×2 | |
| $f_L$ | Fanning friction factor for the liquid phase within the tube | |
| $f_v$ | Fanning friction factor for the vapour phase within the tube | |
| F | Frictional force in the opposite direction to fluid flow within the tube;<br>Empirical convective heat transfer enhancement factor in the correlation by Chen, 1966;<br>Parameter in the two phase pressure drop prediction method of Friedel, 1979;<br>Complex function representing the right hand side of the ordinary differential equation describing the overall enthalpy balance in the tube | N |
| $F_0$ | Mass flow rate of cold juice to the preheater | kg/s |
| $F_1$ to $F_3$ | Sub-functions describing the nonlinear function F over the three heat transfer zones within the evaporator tube | |
| $F_{12}$ | Value of the complex F function at $z_{12}$ | |
| $F_{2,12}$ | Value of the sub-function $F_2$ at $z_{12}$ | |
| $F_{2,12}^{Lin}$ | Value of the sub-function $F_2$ at $z_{12}$ as calculated using the linear model | |
| $F_{i,j}^{*}$ | $j^{'}_{th}$ value of the $F_i$ sub-function calculated from the complex evaporator model | |
| $F_i^{Lin}$ | Linearised approximations of the $F_i$ sub-functions, where i = 1...3 | |
| $Fr_{tp}$ | Two phase Froude number | |
| g | Acceleration due to gravity | $m/s^2$ |
| G | Complex function representing the right hand side of the ordinary differential equation describing the momentum balance within the evaporator tube | |
| $G_1$ to $G_3$ | Sub-functions describing the nonlinear function G over the three heat transfer zones within the evaporator tube | |
| $G_{12}$ | Value of the complex G function at $z_{12}$ | |
| $G_{2,12}$ | Value of the sub-function $G_2$ at $z_{12}$ | |

| | | |
|---|---|---|
| $G_{2,12}^{Lin}$ | Value of the sub-function $G_2$ at $z_{12}$ as calculated using the linear model | |
| $G_{i,j}^{*}$ | $j_{th}$ value of the $G_i$ sub-function calculated from the complex evaporator model | |
| $G_i^{Lin}$ | Linearised approximations of the $G_i$ sub-functions, where i = 1...3 | |
| $h_o$ | Local heat transfer coefficient at the outer tube wall | W/m$^2$.°C |
| $h_{av}$ | Average boiling heat transfer coefficient within the evaporator tube | BTU/h.sq ft.°F |
| $h_B$ | Film heat transfer coefficient for the boiling liquid within the evaporator tube | BTU/h.sq ft.°F |
| $h_c^L$ | Specific enthalpy of condensate at position y in the condensate film | J/kg |
| $h_c^V$ | Specific enthalpy of the condensing steam | J/kg |
| $h_{fg}$ | Latent heat of vapourisation of the fluid within the evaporator tube | kJ/kg |
| $h_i$ | Local heat transfer coefficient within the tube | W/m$^2$.°C |
| $h_L$ | Specific enthalpy of the boiling juice | kJ/kg |
| $h_{L1}$ | Specific enthalpy of the hot juice exiting the preheater | J/kg |
| $h_{L2}$ | Specific enthalpy of the flashed juice at the bottom of the evaporator tubes | J/kg |
| $h_{v2}$ | Specific enthalpy of the flash vapour at the bottom of the evaporator tubes | J/kg |
| $h_w$ | Specific enthalpy of saturated water | kJ/kg |
| H | Total enthalpy of liquid and vapour within the evaporator tube;<br>Parameter in the two phase pressure drop prediction method of Friedel, 1979 | J |
| $H^*$ | Arbitrary value of the total enthalpy, H | J |
| $H_0$ | Value of the overall juice and vapour enthalpy at the bottom of the tube | J |
| $H^1$ | Local enthalpy at position z in the non-boiling zone | J |
| $H^2$ | Local enthalpy at position z in the subcooled nucleate boiling zone | J |
| $H^3$ | Local enthalpy at position z in the saturated nucleate boiling zone | J |
| $H_{12}$ | Value of the overall juice and vapour enthalpy at $z_{12}$ | J |
| $H_{23}$ | Value of the overall juice and vapour enthalpy at $z_{23}$ | J |
| $H_c$ | Condensation and subcooling enthalpy flow rate for the condensate film | W/m |
| $H_c^L$ | Enthalpy flow rate of condensate on the outer tube wall per unit perimeter | W/m |
| I | Performance index in the linear regression of the complex functions F and G | |
| $j^*$ | Dimensionless volumetric vapour flux within the evaporator tube | |
| $j_1$ | Volumetric liquid flux within the evaporator tube | m/s |
| $j_2$ | Volumetric vapour flux within the evaporator tube | m/s |

| | | |
|---|---|---|
| $j_1^*$ | Dimensionless volumetric liquid flux within the evaporator tube | |
| $j_2^*$ | Dimensionless volumetric vapour flux within the evaporator tube | |
| Ja | Jakob number for the boiling fluid within the evaporator tube | |
| $k_{FZ}$ | Constant in the heat transfer correlation of Forster and Zuber, 1955 | |
| $k_i$ | Thermal conductivity of the liquid at the evaporator inlet conditions | W/m.°C |
| $k_L$ | Thermal conductivity of the liquid phase within the evaporator tube | W/m.°C |
| $K_{Lw}$ | Thermal conductivity of the liquid phase in the tube at the temperature of the inner tube wall | W/m.°C |
| $k_w$ | Thermal conductivity of the tube wall material | W/m.°C |
| K | Constant in the evaporator model of Coulson and Mehta, 1953 | |
| K' | Constant in the evaporator model of Coulson and Mehta, 1953 | |
| L | Length of the evaporator tube;<br>Mass flow rate of vapour within the evaporator tube | m<br>kg/s |
| $L_0$ | Mass flow rate of vapour entering the bottom of the evaporator tube | kg/s |
| $L_c$ | Physical property parameter in the correlation of Klimenko, 1988 | |
| m | Constant exponent in the correlation of Rohsenow, 1952 | |
| m' | Mass flux of fluid, at position z, flowing through the tube | $kg/m^2.s$ |
| $m_c^0$ | Mass flux of condensation | $kg/m^2.s$ |
| M | Mass flow rate of feed to the evaporator | lb/h |
| n | Constant exponent describing the saturation curve of water in the evaporator model of Bourgois and Le Maguer, 1983a | |
| N | Parameter in the sugar cane juice viscosity correlation of Genotelle, 1978 | |
| $N_F$ | Number of $(H_i, \bar{p}_i)$ points making up the F function | |
| $N_G$ | Number of $(H_i, \bar{p}_i)$ points making up the G function | |
| Nu | Nusselt number for the boiling fluid within the evaporator tube | |
| $Nu_L$ | Nusselt number for the liquid phase within the tube | |
| $Nu_z$ | Local Nusselt number at position z within the evaporator tube | |
| p | Local pressure within the evaporator tube | Pa |
| $\bar{p}$ | Modified pressure term in the climbing film evaporator model | Pa |
| $\bar{p}^*$ | Arbitrary value of the modified pressure term | Pa |
| $\bar{p}_{12}$ | Value of the modified pressure term at $z_{12}$ | Pa |

| | | |
|---|---|---|
| $\bar{p}_{23}$ | Value of the modified pressure term at $z_{23}$ | Pa |
| $p_0$ | Modified pressure term at the bottom of the evaporator tube | Pa |
| $p^1$ | Local modified pressure term at position z in the non-boiling zone | Pa |
| $p^2$ | Local modified pressure term at position z in the subcooled nucleate boiling zone | Pa |
| $p^3$ | Local modified pressure term at position z in the saturated nucleate boiling zone | Pa |
| $p_{top}$ | Vapour space pressure at the top of the evaporator tubes | Pa |
| P | Operating vapour pressure of the climbing film evaporator in the model of Coulson and McNelly, 1956;<br>Local pressure at distance z along the evaporator tube | lbs/sq ft (abs)<br>Pa |
| $P_k$ | Local pressure within differential element k of the evaporator tube | Pa |
| $P_s$ | Pressure of the condensing steam | Pa |
| $P_v$ | Vacuum pressure at the top of the evaporator tube | Pa |
| $Pe_i$ | Peclet number for the evaporator feed, calculated at the inlet conditions | |
| Pr | Prandtl number for the boiling two phase mixture within the evaporator tube | |
| $Pr_L$ | Prandtl number for the liquid phase within the evaporator tube | |
| $q_{condens}$ | Heat flux through the tube wall as a result of condensation heat transfer | $W/m^2$ |
| $q_{conduct}$ | Heat flux transmitted through the tube wall by conduction | $W/m^2$ |
| $q_{conv}$ | Heat flux from the tube wall into the boiling fluid, primarily by convection | $W/m^2$ |
| $q_{crit\ nb}$ | Critical heat flux for the initiation of nucleate boiling | $W/m^2$ |
| Q | Heat flux;<br>Constant in the correlation of Starzak and Peacock, 1997 | $W/m^2$<br>J/mol |
| $Q_T$ | Total heat flux transferred by the evaporator | $W/m^2$ |
| r | Mass fraction impurities in the liquid phase within the evaporator tube | |
| $r_0$ | Mass fraction impurities in the juice entering the bottom of the tubes | |
| $r_p$ | Mass fraction impurities in the juice fed to the preheater | |
| R | Universal gas constant, R = 8314,5 J/kmol.K | J/kmol.K |
| $R_{fi}$ | Inner tube wall fouling resistance | $m^2.°C/W$ |
| $R_{fo}$ | Outer tube wall fouling resistance | $m^2.°C/W$ |
| Re | Reynolds number for the boiling two phase mixture in the evaporator tube | |

| | | |
|---|---|---|
| $Re_k$ | Modified Reynolds number in the correlation of Klimenko, 1988 | |
| $Re_L$ | Reynolds number for the liquid phase within the evaporator tube | |
| $Re_{tp}$ | Two phase Reynolds number | |
| $Re_v$ | Reynolds number for the vapour phase within the evaporator tube | |
| s | Mass fraction sucrose in the liquid phase within the evaporator tube | |
| $s_0$ | Mass fraction sucrose in the juice entering the bottom of the tubes | |
| $s_p$ | Mass fraction sucrose in the juice fed to the preheater | |
| S | Slip ratio within the evaporator tube;<br>Empirical nucleate boiling suppression factor in the correlation of Chen, 1966 | |
| $t_c$ | Temperature of condensate | K |
| $t_v$ | Temperature of water vapour | K |
| $t_w$ | Temperature of condensate | K |
| T | Temperature | °C |
| $T^*$ | Dimensionless temperature term in the evaporator model of Bourgois and Le Maguer, 1983a;<br>Critical wall temperature for nucleation | °C |
| $T_0$ | Boiling point temperature of water | °C |
| $T_b$ | Boiling point of water | °F |
| $T_{bp}$ | Local boiling point temperature of the liquid within the evaporator tube | °C |
| $T^v_{bp}$ | Boiling point temperature of the liquid at the vapour pressure prevailing at the top of the evaporator tube | °C |
| $T_c$ | Temperature of condensate | °C |
| $T_e$ | Temperature of the fluid exiting the evaporator | °C |
| $T_i$ | Feed inlet temperature | °C |
| $T_k$ | Temperature in differential element k of the evaporator tube | °C |
| $T_L$ | Temperature of the liquid phase within the evaporator tube | °C |
| $T^*_L$ | Critical bulk juice temperature at which nucleation begins | °C |
| $T_{L0}$ | Temperature of the hot juice entering the bottom of the evaporator | °C |
| $T^1_L$ | Local temperature of the juice at position z in the non-boiling zone | °C |
| $T^2_L$ | Local temperature of the juice at position z in the subcooled nucleate boiling zone | °C |

| | | |
|---|---|---|
| $T^3_L$ | Local temperature of the juice at position z in the saturated nucleate boiling zone | °C |
| $T_s$ | Temperature of the condensing steam | °C |
| $T_v$ | Temperature of the vapour phase within the evaporator tube | °C |
| $T_{vt}$ | Temperature of the vapour exiting the top of the evaporator tube | °C |
| $T_{w1}$ | Outer tube wall temperature | °C |
| $T_{w2}$ | Inner tube wall temperature | °C |
| $T_x$ | The difference between the heating surface temperature and the boiling fluid saturation temperature | °C |
| u | Velocity of the condensate film flowing down the outer tube wall;<br>Average velocity of the fluid flowing through the tube, at position z | m/s<br>m/s |
| $u_m$ | Logarithmic mean liquid-vapour velocity in the evaporator tube, as defined by Piret and Isbin, 1954 | ft/s |
| $u_L$ | Mean velocity of the liquid phase within the tube | m/s |
| $u_r$ | Slip ratio | |
| $u_v$ | Mean velocity of the vapour phase within the tube | m/s |
| U | Overall boiling heat transfer coefficient for the evaporator | W/m².°C |
| $U_k$ | Overall heat transfer coefficient for differential element k of the tube | W/m².°C |
| $U_z$ | Local boiling heat transfer coefficient at position z within the evaporator tube | W/m².°C |
| $var_j$ | Variance of experimental variable j | |
| V | Mass flow rate of vapour within the evaporator tube | kg/s |
| $V_0$ | Mass flow rate of vapour entering the bottom of the evaporator tube | kg/s |
| $V_1$ | Liquid phase velocity within the evaporator tube | m/s |
| $V_2$ | Vapour phase velocity within the evaporator tube | m/s |
| $V_e$ | Vapour phase flow rate exiting the evaporator tube | kg/s |
| $V_r$ | Ratio of volumetric vapour flow rate to volumetric liquid flow rate in the tube | |
| W | Mass flow rate of feed to the evaporator | kg/s |
| $W_1$ | Mass flow rate of liquid within the evaporator tube | kg/s |
| $W_2$ | Mass flow rate of vapour within the evaporator tube | kg/s |
| $W_{2e}$ | Mass flow rate of vapour exiting the evaporator tube | kg/s |
| $W_f$ | Mass flow rate of feed to the evaporator | lbs/h |

| | | |
|---|---|---|
| $We_L$ | Weber number calculated assuming all the flow within the tube to be in the liquid phase | |
| $We_{tp}$ | Two phase Weber number | |
| x | Mass fraction vapour within the evaporator tube | |
| $x_j$ | Optimised value of experimental variable j | |
| $x_k$ | Mass fraction vapour in differential step k within the evaporator tube | |
| $x_s$ | Mass fraction sucrose in the liquid phase within the evaporator tube | |
| $x_v$ | Mass fraction vapour within the evaporator tube | |
| $X_{tt}$ | Martinelli factor | |
| y | Position within the condensate film on the outer tube wall, as measured in the direction perpendicular to the axis of the tube | m |
| z | Position along the length of the tube, measured from the bottom | m |
| $z_{12}$ | Position along the tube of the transition between the non-boiling and subcooled nucleate boiling heat transfer zones | m |
| $z_{23}$ | Position along the tube of the transition between the subcooled nucleate boiling and saturated nucleate boiling heat transfer zones | m |
| Z | Total length of the evaporator tube | m |
| $Z^*$ | Dimensionless distance along the evaporator tube, as defined by Bourgois and Le Maguer, 1983a | |
| $Z^*_b$ | Dimensionless position within the tube at which boiling starts | |
| $\alpha$ | Volumetric mass fraction vapour within the evaporator tube<br>Heat transfer coefficient within the evaporator tube | <br>$W/m^2.°C$ |
| $\alpha_F$ | Film boiling heat transfer coefficient within the evaporator tube | $W/m^2.°C$ |
| $\alpha_L$ | Single phase liquid convective heat transfer coefficient in the tube | $W/m^2.°C$ |
| $\alpha_{nb}$ | Nucleate boiling heat transfer coefficient within the evaporator tube | $W/m^2.°C$ |
| $\delta(z)$ | Thickness of the condensate film on the outer tube wall at position z | m |
| $\Delta A_k$ | Differential surface area element corresponding to the differential element k of the evaporator tube | $m^2$ |
| $\Delta H_k$ | Change in enthalpy across integration step k | J |
| $\Delta p$ | Difference in vapour pressures for the boiling fluid, corresponding to the temperature difference between the inner tube wall and the boiling fluid | Pa |

| | | |
|---|---|---|
| $\Delta Q_k$ | Heat flux for the differential element k along the evaporator tube | $W/m^2$ |
| $\Delta t$ | Temperature difference across the boiling film of liquid against the tube wall | °C |
| $\Delta T$ | Temperature difference between the condensing steam and the boiling fluid | °C |
| $\Delta T_k$ | Temperature difference for differential element k of the evaporator tube | °C |
| $\Delta z_k$ | Differential tube length element corresponding to the differential element k of the evaporator tube | m |
| $\varepsilon$ | Absolute roughness of the tube surface | m |
| $\varepsilon_v$ | Volumetric void fraction of vapour within the evaporator tube | |
| $\Gamma$ | Mass flow rate of condensate per unit length of tube perimeter | kg/m.s |
| $\Gamma_0$ | Mass flow rate of condensate per unit length of tube perimeter at the top of the evaporator tubes | kg/m.s |
| $\lambda$ | Latent heat of vapourisation of the fluid within the evaporator tube | kJ/kg |
| $\lambda_c$ | Latent heat of condensation of the condensing steam | kJ/kg |
| $\Psi$ | Empirical term in the evaporator model of Gupta and Holland, 1996a, determined graphically asa function of $\Delta T$;<br>Parameter in the saturation pressure correlation of Wagner, 1973 for water | |
| $\phi^2_{lo}$ | Two phase pressure drop enhancement factor | |
| $\Phi$ | Klimenko parameter for fully developed film boiling | |
| $\rho$ | Density of the two phase mixture within the evaporator tube<br>Density of the condensate film on the outer tube wall | $kg/m^3$<br>$kg/m^3$ |
| $\rho_1$ | Density of the liquid phase within the evaporator tube | $kg/m^3$ |
| $\rho_2$ | Density of the vapour phase within the evaporator tube | $kg/m^3$ |
| $\rho_L$ | Density of the liquid phase within the evaporator tube | $kg/m^3$ |
| $\rho_m$ | Average density of the fluid flowing within the tube, at position z | $kg/m^3$ |
| $\rho_{tp}$ | Two phase density of the fluid within the evaporator tube | $kg/m^3$ |
| $\rho_v$ | Density of the vapour phase within the evaporator tube | $kg/m^3$ |
| $\sigma$ | Surface tension of the fluid within the evaporator tube | N/m |
| $\sigma_w$ | Surface tension of water at its normal boiling point | N/m |
| $\mu_L$ | Viscosity of the liquid phase within the evaporator tube | Pa.s |
| $\mu_{Lw}$ | Viscosity of the liquid phase in the tube at the inner tube wall temperature | Pa.s |
| $\mu_v$ | Viscosity of the vapour phase within the evaporator tube | Pa.s |

| | | |
|---|---|---|
| $\mu_w$ | Viscosity of water | Pa.s |
| $v$ | Specific volume of the fluid at position z within the evaporator tube | $m^3/kg$ |
| $v_c$ | Specific volume of saturated water | $dm^3/kg$ |
| $\chi_j$ | Experimentally measured value of variable j | |

# Chapter 9

# References


Aggarwal, M.C. (1989), "Computerized formulation for the thermodynamic properties of saturated water based on the IAPS formulation 1984", *Heat Transfer Division of the American Society of Mechanical Engineers*, **116** (Convective heat transfer and transport processes), 21-26.

Bourgois, J. & Le Maguer, M. (1983a), "Modelling of heat transfer in a climbing-film evaporator: Part I", *Journal of Food Engineering*, **2**, 63-75.

Bourgois, J. & Le Maguer, M. (1983b), "Modelling of heat transfer in a climbing-film evaporator: Part II", *Journal of Food Engineering*, **2**, 225-237.

Bourgois, J. & Le Maguer, M. (1984), "Modelling of heat transfer in a climbing-film evaporator: Part III. Application to an industrial evaporator", *Journal of Food Engineering*, **3**, 39-50.

Bourgois, J. & Le Maguer, M. (1987), "Heat-transfer correlation for upward liquid film heat transfer with phase change: Application in the optimization and design of evaporators", *Journal of Food Engineering*, **6**, 291-300.

Chen, J.C. (1966), "Correlation for boiling heat transfer to saturated liquids in convective flow", *Industrial and Engineering Chemistry Process Design and Development*, **5**, 322-329.

Churchill, S.W. (1977), *Chemical Engineering*, **84**, 7 November, 91-92.

Collier, J.G. (1980), *Convective Boiling and Condensation*, Second Edition, London : McGraw-Hill.

Cooper, M.G. (1989), "Flow boiling - the 'apparently nucleate' regime", *International Journal of Heat and Mass Transfer*, **32**, 459-464.

Coulson, J.M. & McNelly, M.J. (1956), "Heat transfer in a climbing film evaporator. Part II.", *Transactions of the Institution of Chemical Engineers*, **34**, 247-257.

Coulson, J.M. & Mehta, R.R. (1953), "Heat transfer coefficients in a climbing film evaporator", *Transactions of the Institution of Chemical Engineers*, **31**, 208-228.

Davis, M.E. (1984), *Numerical methods and modelling for chemical engineers*, New York: Wiley House Publishers, 258 pp.

Dhir, V.K. (1991), "Nucleate and transition boiling heat transfer under pool and external flow conditions", *International Journal of Heat and Fluid Flow*, **12**, 290-314.

Engineering Sciences Data Unit (1967), "Forced convection heat transfer in circular tubes. Part 1: Correlations for fully developed turbulent flow - their scope and limitations", *Engineering Sciences Data*, Item **67016**.

Engineering Sciences Data Unit (1968), "Forced convection heat transfer in circular tubes. Part 2: Data for laminar and transitional flows including free-convection effects", *Engineering Sciences Data*, Item **68006**.

Foster, H.K. & Zuber, N. (1955), "Dynamics of vapour bubbles and boiling heat transfer", *American Institution of Chemical Engineers Journal*, **1**, 531-535.

Friedel, L. (1979), "Improved friction pressure drop correlation for horizontal and vertical two-phase pipe flow", *Paper 2 - European Two-Phase Group Meeting*, Ispra, Italy.

Genotelle, J. (1978), "Expressing the viscosity of sugar solutions", *Industries Alimentaires et Agricoles*, **95**, 747-755.

Gorenflo, D. (1994), "Behältersieden" in *VDI Wärmeatlas*, Section Ha, Seventh edition, Berlin: VDI-Verlag.

Gundmundson, C. & Olauson, L. (1971), "Harmful Pulsation Phenomena in a Climbing Film Evaporator With Superheated Feed", *Svensk Papperstidning*, **74**(7-15), 197-200.

Gungor, K.E. & Winterton, R.H.S. (1986), "A general correlation for flow boiling in tubes and annuli", *International Journal of Heat and Mass Transfer*, **29**, 351-358.

Gupta, A.S. & Holland, F.A. (1966a), "Heat Transfer Studies in a Climbing Film Evaporator. Part I: Heat Transfer from Condensing Steam to Boiling Water", *Canadian Journal of Chemical Engineering*, **44**, 77-81.

Gupta, A.S. & Holland, F.A. (1966b), "Heat Transfer Studies in a Climbing Film Evaporator. Part II: Heat Transfer Regions", *Canadian Journal of Chemical Engineering*, **44**, 326-329.

Hetsroni, G. [ed] (1982), *Handbook of Multiphase Systems*, New York: Hemisphere Publishing Corporation.

Holland, F.A. & Bragg, R. (1995). *Fluid Flow for Chemical Engineers*, London: Edward Arnold, Chapter 7.

Hughmark, G.A. (1969), "Designing thermosiphon reboilers", *Chemical Engineering Progress*, **65**(7), 67-70.

Kadlec, P., Bretschneider, R. & Bubnik, Z. (1983), *Chemical Engineering Communications*, **21**, 183-190.

Kenning, D.B.R. & Cooper, M.G. (1989), "Saturated flow boiling of water in vertical tubes", *International Journal of Heat and Mass Transfer*, **32**, 445-458.

Klimenko, V.V. (1988), "A generalised correlation for two phase forced flow heat transfer", *International Journal of Heat and Mass Transfer*, **31**, 541-552.

Levenberg, K. (1944), "A method for the solution of certain problems in least squares", *Quarterly of Applied Mathematics*, **2**, 164-168.

Linden, C.M. & Montillon, G.H. (1930), *Industrial and Engineering Chemistry*, **22**, 708-713.

Lockhart, R.W. & Martinelli, R.C. (1949), "Proposed correlation of data for isothermal two phase, two component flow in pipes", *Chemical Engineering Progress*, **45**(1), 39-48.

Lyle, O. (1950), *Technology for Sugar Refinery Workers*, London: Chapman and Hall Limited, Second Edition, p 472.

Marquardt, D.W. (1963), "An algorithm for least squares estimation of nonlinear parameters", *Journal SIAM*, **11**, 431-441.

Mayinger, F. & Schult, M. (1981), "Dynamic behaviour of double phase-change heat exchangers", *Heat Exchangers: Thermal-Hydraulic Fundamentals and Design*, Washington: Hemisphere Publishing Corporation, 955-979.

McNelly, M.J. (1953), *Journal of the Imperial College Chemical Engineering Society*, 7, 18.

Mills, A.F. (1992), *Heat Transfer*, Boston: Irwin, Chapter 7: "Condensation, evaporation and boiling".

Monrad, C.C. & Badger, W.L. (1930), "The condensation of vapours", *Transactions of the American Institution of Chemical Engineers*, **24**, 84.

Müller-Steinhagen, H. (1995), Personal communication, Department of Chemical and Process Engineering, University of Surrey, Guildford, Surrey, GU2 5XH, United Kingdom.

Na, T.Y. (1979), *Computational methods in engineering boundary value problems*, New York: Academic Press, 309 pp.

Peacock, S.D. (1995a), "Selected physical properties of sugar factory process streams", *Sugar Milling Research Institute Technical Report*, **1714**, 46 pp.

Peacock, S.D. (1995b), "Predicting physical properties of factory juices and syrups", *International Sugar Journal*, **97**(1162), 571-577.

Peacock, S.D. (1995c), "Data reconciliation as applied to the first effect factorial experiment data from the Felixton pilot plant evaporator", *Sugar Milling Research Institute Technical Note*, **47/95**, 5 pp.

Peacock, S.D. (1996), "The optimisation of feed juice temperature for climbing film evaporators - A preliminary study", *Sugar Milling Research Institute Technical Note*, **49/96**, 7pp.

Peacock, S.D. (1998), "Tools for the study of clear juice heating and its effect on climbing film evaporator operation", *Sugar Milling Research Institute Technical Report*, **1773**, 9 pp.

Piret, E.L. & Isbin, H.S. (1954), "Natural Circulation Evaporation: Two Phase Heat Transfer", *Chemical Engineering Progress*, **50**(6), 305-311.

Premoli, A., Francesco, D. & Prima (1970), "An empirical correlation for evaluating two-phase mixture density under adiabatic conditions", *European Two-Phase Flow Group Meeting*, Milan, 8-10 June 1970.

Rein, P.W. & Love, D.J. (1995), "Experiences With Long Tube Climbing Film Evaporators", *Proceedings of the International Society of Sugar Cane Technologists' Conference*, **22**, Volume 1, 251-259.

Riedel, L. (1949), "Heat conductivity measurements in sugar solutions, fruit juices and milk", *Chem. Ing. Technik*, **21**, 340-341.

Rohsenow, W.M. (1953), *Heat Transfer: A Symposium*, Chapter 4, Ann Arbor: University of Michigan Press.

Rohsenow, W.M. (1983), "Needed Research in Boiling Heat Transfer", *Heat Transfer in Energy Problems*, Washington : Hemisphere Publishing Corporation, 51-58.

Shah, M.M. (1982), "Chart correlation for saturated boiling heat transfer", *ASHRAE Transactions*, **88**, 185-196.

Smith, R.A. (1983), "Evaporators" in *Heat exchanger design handbook*, New York: Hemisphere Publishing Corporation, pp 3.5.2-3.5.5.

Smith, R.A. (1986), *Vaporisers: selection, design and operation*, New York: Longman.

Starzak, M. & Peacock, S.D. (1997), "Water activity coefficient in aqueous solutions of sucrose - A comprehensive data analysis", *Zuckerindustrie*, **122**(5), 380-387.

Starzak, M. & Peacock, S.D. (1998), "Boiling point elevation for aqueous solutions of sucrose - A comparison of different prediction methods", *Zuckerindustrie*, **123**(6), 433-441.

Steiner, D. (1995), Personal communication, Universität Karlsruhe, Postfach 6980, Kaiserstraße 12, D-76128, Karlsruhe, Germany.

Steiner, D. & Taborek, J. (1992), "Flow boiling heat transfer in vertical tubes correlated by an asymptotic method", *Heat Transfer Engineering*, **13**, 43-69.

Stephan, K. (1995), Personal communication, Institut für Technische Thermodynamik und Thermische Verfahrenstechnik, Universität Stuttgart, 70550, Stuttgart, Germany.

Tang, C.L. (1980), "Two phase flow in a climbing film evaporator", *Canadian Journal of Chemical Engineering*, **58**, 425-430.

Turner, J.M. (1966), "Annular two-phase flow", PhD Thesis, Darmouth College, Hanover, New Hampshire, USA.

Wagner, W. (1973), *Cryogenics*, **13**, 470.

Wallis, G.B. (1969), *One-dimensional two-phase flow*, New York: McGraw Hill Book Company.

Walthew, D.C. & Whitelaw, R.W. (1996), "Factors affecting the performance of long tube climbing film evaporators", *Proceedings of the South African Sugar Technologists' Association*, **70**, 221-224.

Walthew, D.C., Whitelaw, R.W. & Peacock, S.D. (1995), "Preliminary results from a long tube climbing film pilot evaporator", *Proceedings of the South African Sugar Technologists' Association*, **69**, 132-137.

Watson, L.J. (1989), "Heat transfer performance in evaporators. Part 1: Theory and mechanisms", *Sugar Research Institute Technical Report*, **191**.

Webb, R.L. & Gupte, N.S. (1992), "A critical review of correlations for convective vaporization in tubes and tube banks", *Heat Transfer Engineering*, **13**, 58-81.

Winterton, R.H.S. (1981), *Thermal Design of Nuclear Reactors*, Oxford : Pergamon Press, Chapter 5 : "Boiling Heat Transfer", 67-83.

Winterton, R.H.S. (1995), Personal communication, School of Manufacturing and Mechanical Engineering, Birmingham University, Birmingham, BI5 2TT, United Kingdom.

Zinemanas, D. (1983), "Simulation of heat transfer systems with phase change", *Msc Thesis*, Technion - Israel Institute of Technology.

Zinemanas, D., Hasson, D. & Kehat, E. (1984), "Simulation of heat exchangers with change of phase", *Computers and Chemical Engineering*, **8**(6), 367-375.

# Appendix A

# Statistical Data Reconciliation

# SUGAR MILLING RESEARCH INSTITUTE

Technical Note 47/95

| | | |
|---|---|---|
| Title | : | DATA RECONCILIATION AS APPLIED TO THE FIRST EFFECT FACTORIAL EXPERIMENT DATA FROM THE FELIXTON PILOT PLANT EVAPORATOR |
| To | : | DC Walthew, SMRI<br>GRE Lionnet, SMRI<br>M Starzak, UND |
| From | : | SD Peacock |
| Date | : | 11 December 1995 |

## 1. Introduction

In order to increase the accuracy of the climbing film evaporator model[1], the model was *calibrated* against the experimental data from the Felixton pilot plant. The data used for this model optimisation were those from the first effect factorial experiment. Great difficulties were experienced in matching the model to the experimental data, as the data were found to be inconsistent - the overall mass, heat and brix balances were not satisfied. While the errors in the mass and brix balances were evenly distributed about zero, the error in the heat balance was found to be consistently positive (i.e. more steam was condensed in the calandria than was accounted for by the observed evaporation/heat transfer). It was thus decided to reconcile the experimental data so as to satisfy the mass, heat and brix balances - to yield data more amenable to use in calibrating the evaporator model.

## 2. Data Reconciliation

Data reconciliation involves the manipulation of the experimentally measured variables so as to satisfy the mass, brix and heat balances, while changing the experimental data as little as possible. For the purposes of data reconciliation, each experimentally measured variable was assigned a *variance*, representing the range of experimental error expected for that variable. An optimisation *index* was defined as follows:

---

[1] Peacock, SD; "*Mathematical Modelling and Experimental Study of Climbing Film Evaporators*"; SMRI Technical Report No. 1698; 8 November 1994.

$$INDEX = \sum_{j=1}^{n} \frac{(x_j - \bar{x}_j)}{var_j}$$

where

| | | |
|---|---|---|
| $x_j$ | = | the changed (or *optimised*) value of variable j |
| $\bar{x}_j$ | = | the experimentally measured value of variable j |
| $var_j$ | = | the variance of variable j |

The reconciliation algorithm satisfies the mass, brix and heat balances while minimising the optimisation index (i.e. the effect on the experimental data). Thus the experimental data are *weighted* by their variances - the more accurately measured variables will be changed less during the reconciliation procedure than those with higher variances.

# 3. Results

The data reconciliation algorithm was implemented by means of a MATLAB computer program. The data from seven of the original 27 experiments were discarded, due to huge errors. The results of the data reconciliation are displayed in Figures 1 and 2. Figure 1 shows the modified data (x-axis) plotted against the original experimental data (y-axis). Figure 2 shows the modified data (circles) and the original data (lines) plotted on the y-axis, against the experiment number on the x-axis (with no specific ordering). The original and modified experimental data are displayed in Table 1.

S D PEACOCK

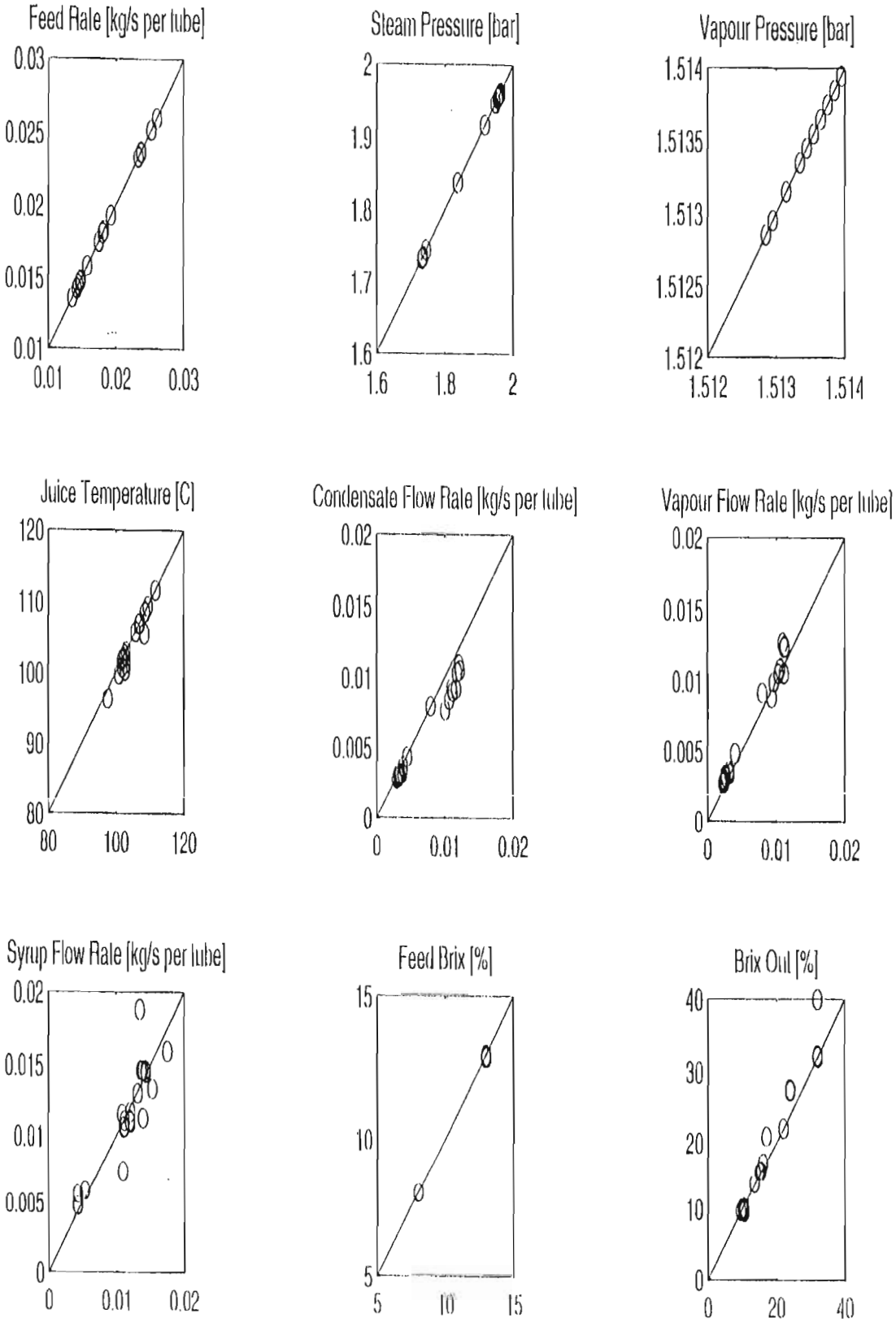


**Figure 1: Results of Data Reconciliation**

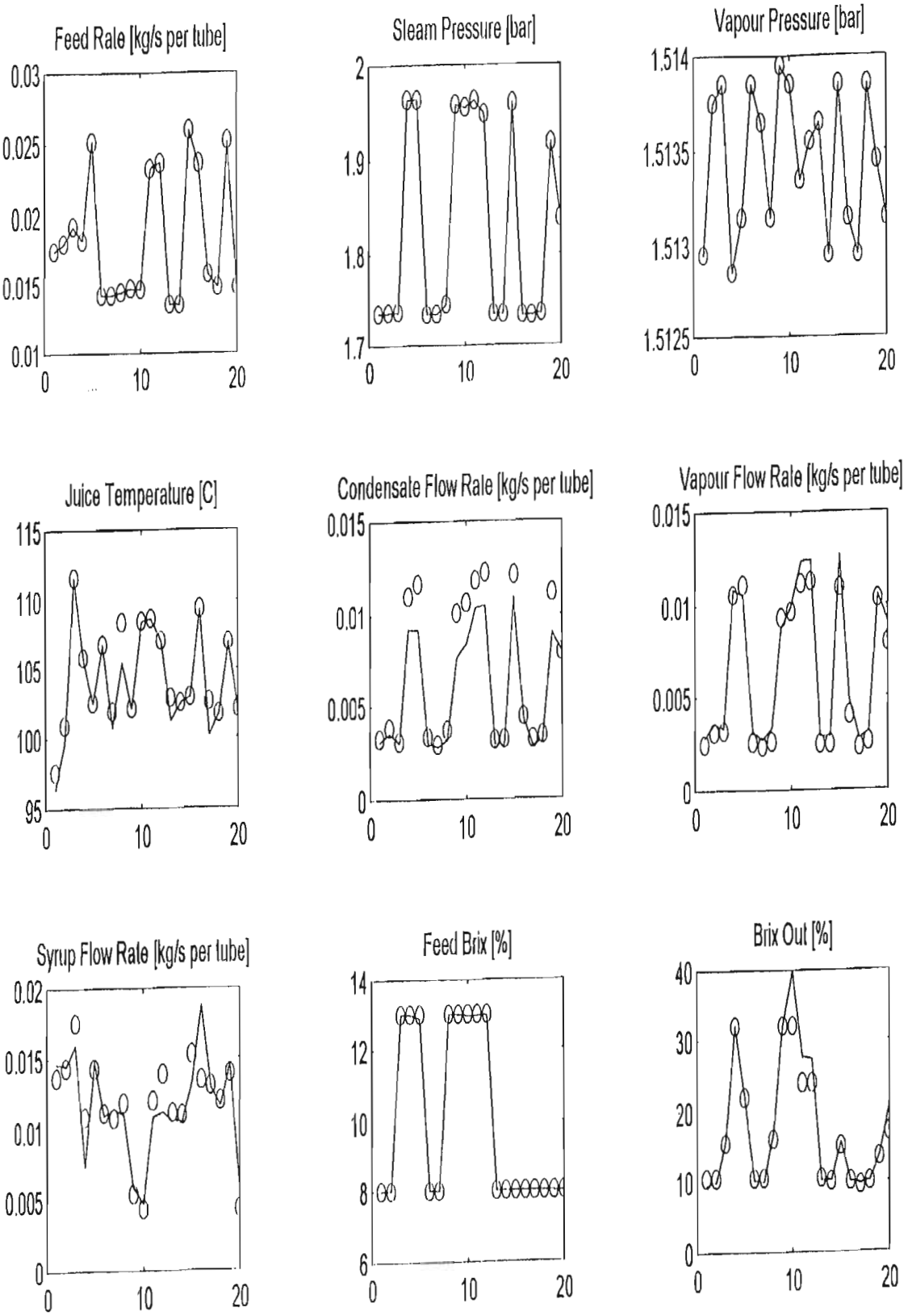


**Figure 2: Results of Data Reconciliation**